



**VASCO FIGUEIREDO  
BATISTA**

**BIOCATÁLISE NA SÍNTESE DE ALCALOIDES  
TETRA-HIDROISOQUINOLINA**

**BIOCATALYSIS IN THE SYNTHESIS OF  
TETRAHYDROISOQUINOLINE ALKALOIDS**





**VASCO FIGUEIREDO  
BATISTA**

**BIOCATÁLISE NA SÍNTESE DE ALCALOIDES  
TETRA-HIDROISOQUINOLINA**

**BIOCATALYSIS IN THE SYNTHESIS OF  
TETRAHYDROISOQUINOLINE ALKALOIDS**

Tese apresentada à Universidade de Aveiro para cumprimento dos requisitos necessários à obtenção do grau de Mestre em Química, realizada sob a orientação científica da Doutora Diana Cláudia Gouveia Alves Pinto, Professora Auxiliar do Departamento de Química da Universidade de Aveiro, e do Professor Doutor Nicholas J. Turner, Professor do Manchester Institute of Biotechnology, University of Manchester, UK.



universidade  
de aveiro





## **o júri**

Presidente

Professor Doutor Artur Manuel Soares Silva

Professor Catedrático do Departamento de Química da Universidade de Aveiro

Doutora Diana Cláudia Gouveia Alves Pinto

Professora Auxiliar do Departamento de Química da Universidade de Aveiro

Doutora Maria Emília da Silva Pereira de Sousa

Professora Auxiliar da Faculdade de Farmácia da Universidade do Porto



## Agradecimentos

This has truly been a year-long wild ride. With ups and downs, an amazing progress that is almost over. More than just a dissertation and a research project, the opportunity to learn and experience a new field of expertise, go out of my comfort zone and see the world! I cannot thank enough for the opportunity to do an Erasmus at the best biotechnology institute in Europe and, for that, I have to thank both my supervisors. To Dr. Diana Pinto, for all the guidance during my “adventure” in Organic Chemistry, all the advices and support, and for allowing me the opportunity to go to Manchester. And to Prof. Nicholas Turner, for accepting me at the institute and giving me all the support and guidance I needed when facing such an unknown challenge. Also, my sincerest appreciations to Prof. Artur Silva for all his help in the last five years.

Next, to all those that made me feel at home in Manchester, helped me experience the local gastronomy (beer) but also went out of their way to help me with my work: Fabio, Iustina, Syed, Ulrich, and many more. Always not forgetting the company of the amazing Tori and Isis. A very special thanks to James Galman, for being my mentor and having a huge patient in teaching me the basics of biology and genetics. Also, my sincerest gratitude to Janes Kwok for providing the additional MAO-N variants used in this work and to Rachel Heath for providing the HDNO enzyme.

Then, to the QOPNA research group, the University of Aveiro and the Manchester Institute of Biotechnology for hosting me and providing all the conditions I needed to grow up as a student, professional and person. And a tremendous thank you to all the people I’ve met along the way, each one fantastic in their own way, and all great friends. Also, I cannot forget the annoying guys from the lab, Carlos, Emanuel, João and Sara: my years at the UA would have been much easier without you!

Most importantly, I have to thank the most amazing person in the world, without whom I couldn’t possibly have been so happy these last few years. Raquel, you’re a source of inspiration and the person I want to be with at all times. Without you, the UK wouldn’t have been half as colourful. To me, you are everything.

Por ultimo, um grande abraço para toda a minha família e, em particular, para os meus pais, por procurarem dar-me a melhor educação possível, nunca questionarem as minhas ambições e, acima de tudo, por serem quem são: perfeitos.





## Palavras-chave

1,2,3,4-Tetra-hidroisoquinolina; química verde; biocatálise; evolução dirigida; ácido 1,2,3,4-tetra-hidroisoquinolina-1-carboxílico; aminoácido não-natural.

## Resumo

A biocatálise, e em particular a evolução dirigida de enzimas e posterior expressão em bactérias, permitiu aos químicos obter moléculas complexas com elevada estereo- e regioselectividade e baixo impacto ambiental. A Monoamina oxidase de *Aspergillus niger* (MAO-N) é uma oxidase, dependente de FAD e oxigénio, que catalisa a desaminação de aminas primárias. No *Manchester Institute of Biotechnology* foram efetuadas rondas sucessivas de evolução dirigida desta enzima, que permitiram a oxidação e resolução de aminas secundárias e terciárias. Contudo, não se encontra descrita na literatura a oxidação de compostos dimetoxilados com MAO-N.

O uso de tetra-hidroisoquinolinas (THIQs) quirais na indústria farmacêutica é cada vez mais comum devido às suas importantes propriedades antimicrobianas, antibióticas, anti tumorais ou antimuscarínicas. Assim, é cada vez mais necessário o desenvolvimento de métodos de síntese assimétrica destes compostos.

Neste trabalho procurámos funcionalizar THIQs através de métodos biocatalíticos. Para tal, estudámos a atividade várias variantes da MAO-N com derivados da THIQ. Os dados obtidos foram usados para a construção de uma nova variante capaz de oxidar a (S)-6,7-dimetoxi-1,2,3,4-tetra-hidroisoquinolina com um rendimento de 60%. Foi também efetuada a resolução de várias THIQs com as variantes de MAO-N disponíveis.

Por fim, neste trabalho foi desenvolvida uma cascata enzimática com três passos sem purificação intermédia para a síntese de ácidos 1,2,3,4-tetra-hidroisoquinolina-1-carboxílicos. Foram obtidas 1-cianotetra-hidroisoquinolinas com rendimentos superiores a 50% e o ácido tetra-hidroisoquinolina-1-carboxílico com um rendimento de 13% (e.e. 88%).



## Keywords

1,2,3,4-Tetrahydroisoquinoline; green chemistry; biocatalysis; directed evolution; substrate scope; 1,2,3,4-tetrahydroisoquinoline-1-carboxylic acid; unnatural amino acids.

## Abstract

Biocatalysis, and particularly the directed evolution of enzymes and further expression in bacterium, has allowed chemists to obtain complex molecules with improved stereo and regio-selectivity, at high reaction rates and with a low environmental impact. Monoamine oxidase from *Aspergillus niger* (MAO-N) is a FAD and oxygen dependent oxidase that catalyses the deamination of primary amines. Successive rounds of directed evolution at the Manchester Institute of Biotechnology have allowed the oxidation and deracemisation of secondary and tertiary amines with MAO-N variants. Nevertheless, significant activity of these mutants with dimethoxylated substrates is yet to be reported.

Chiral tetrahydroisoquinoline (THIQ) derivatives are increasingly common in the pharmaceutical industry due to their antimicrobial, antibiotic, antitumor or antimuscarinic properties, demanding for easy and highly selective methods for their synthesis.

In this work, we used biocatalytic methods to functionalize THIQs. First, we studied the substrate scope of MAO-N variants with several THIQs, and used the data obtained to construct a new mutant capable of oxidizing (*S*)-6,7-dimethoxy-1-methyltetrahydroisoquinoline with approximately 60% yield. Moreover, the deracemisation of several THIQs with MAO-N variants was performed with success.

Finally, a one pot three step cascade using two distinct enzymes was developed for the selective synthesis of tetrahydroisoquinoline-1-carboxylic acids from simple tetrahydroisoquinolines, at low temperatures and in water. 1-Cyanotetrahydroisoquinolines were obtained with good yields (>50%), and tetrahydroisoquinoline-1-carboxylic acid was obtained with 13% yield and 88% e.e..



# CONTENTS

<b>FIGURE INDEX</b> .....	<b>V</b>
<b>SCHEME INDEX</b> .....	<b>VII</b>
<b>TABLE INDEX</b> .....	<b>VIII</b>
<b>ABBREVIATIONS AND ACRONYMS</b> .....	<b>IX</b>
<b>CHAPTER 1. INTRODUCTION</b> .....	<b>1</b>
1.1 ALPHA-CHIRAL AMINES AND THEIR IMPORTANCE IN THE CHEMICAL INDUSTRY .....	3
1.1.1 Overview .....	3
1.1.2 Synthetic routes to single-enantiomer $\alpha$ -chiral amines .....	4
1.1.3 Tetrahydroisoquinoline as an important building block in the chemical industry .....	9
1.1.4 Asymmetric synthesis of C1 substituted tetrahydroisoquinolines .....	11
1.2 BIOCATALYSIS: A GREEN PATH IN CHIRAL AMINE SYNTHESIS .....	14
1.2.1 Overview .....	14
1.2.2 Development of an enzymatic synthesis: main steps .....	15
1.2.3 Enzymes employed in chiral amine synthesis .....	21
1.2.4 Monoamine oxidase from <i>Aspergillus niger</i> .....	26
1.3 SCOPE OF THIS WORK .....	35
<b>CHAPTER 2. EXPERIMENTAL SECTION</b> .....	<b>37</b>
GENERAL INFORMATION .....	39
2.1 PLASMID SELECTION .....	39
2.1.1 pET16b ( <i>E. coli</i> ) .....	39
2.1.2 pPicZ $\alpha$ C ( <i>P. pastoris</i> ) .....	40
2.2 TRANSFORMATION PROTOCOLS .....	41
2.2.1 <i>E. coli</i> BL21 (DE3) .....	41
2.2.2 <i>E. coli</i> NEB <sup>®</sup> 5-alpha .....	41
2.2.3 <i>E. coli</i> Rosetta <sup>™</sup> (DE3) .....	41
2.2.4 <i>P. pastoris</i> GS115 .....	42

2.2.5	<i>P. pastoris</i> X-33 .....	43
2.3	GROWTH OF MAO-N IN <i>E. COLI</i> .....	43
2.4	PURIFICATION OF MAO-N .....	44
2.5	SDS-PAGE .....	44
2.6	PROTEIN QUANTIFICATION: BRADFORD PROTEIN ASSAY .....	44
2.7	SPECIFIC ACTIVITY ASSAYS .....	45
2.8	DNA PROTOCOLS .....	45
2.8.1	Preparation of plasmid DNA from <i>E. coli</i> .....	45
2.8.2	Determination of DNA concentration .....	46
2.8.3	Agarose gel electrophoresis .....	46
2.8.4	Ligation independent cloning: insertion of MAO-N D9 gene into pPicZ $\alpha$ C empty vector.....	46
2.8.5	Site-directed mutagenesis.....	48
2.9	BIOTRANSFORMATIONS .....	50
2.9.1	Amine deracemisations with MAO-N D5/D9/D11 or HDNO.....	50
2.9.2	MAO-N D9/D11 or HDNO imine formation reactions .....	50
2.9.3	HPLC analysis: determination of the relative response factor .....	51
2.9.4	Nitrilase catalysed hydrolysis.....	52
2.10	CHEMICAL REACTIONS .....	52
2.10.1	Cyanation of 3,4-dihydroisoquinolines .....	52
<b>CHAPTER 3. RESULTS AND DISCUSSION.....</b>		<b>53</b>
3.1	PROTEIN EXPRESSION .....	55
3.1.1	Protein expression in <i>E. coli</i> .....	55
3.1.2	Protein expression in <i>P. pastoris</i> .....	56
3.2	SUBSTRATE SCOPE OF MAO-N IN THE OXIDATION OF TETRAHYDROISOQUINOLINES .....	58
3.2.1	Overview .....	58
3.2.2	Specific activity assays.....	59
3.2.3	Final discussion .....	63

3.3 DIRECTED EVOLUTION OF MAO-N D9 BY SITE-DIRECTED MUTAGENESIS .....	65
3.3.1 Overview .....	65
3.3.2 Oxidation and deracemization of salsolidine.....	66
3.4 DYNAMIC KINETIC RESOLUTION OF CHIRAL TETRAHYDROISOQUINOLINES.....	68
3.4.1 Overview .....	68
3.4.2 Resolution of chiral amines .....	68
3.5 ONE POT THREE STEP CASCADE FOR THE C1 FUNCTIONALIZATION OF TETRAHYDROISOQUINOLINES.....	73
3.5.1 Overview .....	73
3.5.2 Synthesis of 3,4-dihydroisoquinolines .....	74
3.5.3 Synthesis of 1-cyanotetrahydroisoquinolines .....	80
3.5.4 Nitrilase in the enantioselective hydrolysis of 1-cyanotetrahydroisoquinoline.....	86
3.5.5 General discussion.....	88
<b>CHAPTER 4. CONCLUSIONS AND FUTURE PROSPECTS .....</b>	<b>91</b>
<b>CHAPTER 5. REFERENCES .....</b>	<b>95</b>
<b>ANNEX 1. CALIBRATION CURVES.....</b>	<b>A1</b>
<b>ANNEX 2. SPECIFIC ACTIVITY ASSAYS.....</b>	<b>A2</b>
<b>ANNEX 3. RESPONSE FACTORS.....</b>	<b>A3</b>
<b>ANNEX 4. NMR SPECTRA.....</b>	<b>A4</b>





## FIGURE INDEX

<b>Figure 1.</b> Both enantiomers of thalidomide .....	3
<b>Figure 2.</b> Examples of $\alpha$ -chiral amine-based drugs currently marketed.....	4
<b>Figure 3.</b> Visual comparison between chemical and enzymatic DKR. ....	8
<b>Figure 4.</b> Structure of THIQ and atom number nomenclature adopted in this work.....	10
<b>Figure 5.</b> Structure of THIQs associated with brain disorders. ....	10
<b>Figure 6.</b> Examples of THIQ compounds in three major sub-classes with important biological activities. ....	11
<b>Figure 7.</b> Metagenomics in gene discovery .....	16
<b>Figure 8.</b> Simulated fitness landscape in directed evolution. ....	18
<b>Figure 9.</b> Example of an enzyme engineering experiment. ....	20
<b>Figure 10.</b> Enzymes used in the synthesis of chiral amines: examples .....	21
<b>Figure 11.</b> Deracemisation of tetrahydroisoquinoline and tryptoline derivatives with the E350L/E352D HDNO mutant.....	25
<b>Figure 12.</b> Common MAO A and MAO B natural substrates .....	26
<b>Figure 13.</b> Proposed hydrophobic cavity in MAO-N D5. ....	28
<b>Figure 14.</b> Structure of mexiletine.....	30
<b>Figure 15.</b> Summary of the solid phase screening of MAO-N mutants .....	33
<b>Figure 16.</b> Tetrahydroisoquinoline substrates used within the scope of this work.....	35
<b>Figure 17.</b> Scheme of an empty pET16b plasmid.. ....	40
<b>Figure 18.</b> Scheme of an empty pPicZ $\alpha$ C plasmid.....	41
<b>Figure 19.</b> Ligation independent cloning for the insertion of MAO-N D9 gene into a pPicZ $\alpha$ C empty vector.....	47
<b>Figure 20.</b> Normal phase HPLC trace of a 10 mm standard solution of either 6,7-dimethoxy-1-methyl-3,4-dihydroisoquinoline (top) or 6,7-dimethoxy-1-methyltetrahydroisoquinoline (bottom). ....	51
<b>Figure 21.</b> SDS-PAGE gel of MAO-N variant's purification. ....	55
<b>Figure 22.</b> Protein concentration of MAO-N variants calculated by the Bradford assay .....	56
<b>Figure 23.</b> Agarose gel electrophoresis of MAO-N D9 in pPicZ $\alpha$ C after action of the restriction enzymes XhoI and BamHI. ....	57
<b>Figure 24.</b> Agarose gel electrophoresis of the results from the Touchdown PCRs for the amplification of MAO-N D9 gene in <i>P. pastoris</i> ' genome.. ....	58
<b>Figure 25.</b> Specific activity of MAO-N variants with racemic $\alpha$ -AMBA – in blue – and THIQ – in grey.....	60
<b>Figure 26.</b> Specific activity of MAO-N variants with 1-MTQ.....	60

<b>Figure 27.</b> Specific activity of MAO-N variants with 3-MTQ – in blue – and 4-MTQ – in grey...	61
<b>Figure 28.</b> Specific activity of MAO-N variants with 5-MTQ, in blue, 6-MTQ, in grey, and 8-MTQ, in orange.....	62
<b>Figure 29.</b> Specific activity of some MAO-N variants with DMTHIQ, in blue, and 1-M-DMTHIQ, in grey.....	63
<b>Figure 30.</b> Summary of the activity of MAO-N variants with methyl substituted THIQs .....	64
<b>Figure 31.</b> Summary of the mutants with best activity towards each one of the substrates tested. The values presented are relative to the best activity determined for $\alpha$ -AMBA (MAO-N D9) .....	65
<b>Figure 32.</b> Normal phase HPLC trace of three biotransformations: oxidation of <b>(92)</b> with MAO-N D9 (top), oxidation of <b>(92)</b> with MAO-N D13 (middle) and deracemisation of <b>(92)</b> with MAO-N D13 (bottom).....	67
<b>Figure 33.</b> Normal phase HPLC trace of the deracemisation of $\alpha$ -AMBA with HDNO (top) or MAO-N D5 (bottom).....	69
<b>Figure 34.</b> Normal phase HPLC trace of the deracemisation of 1-MTQ with HDNO (top) or MAO-N D9 (bottom).....	70
<b>Figure 35.</b> Normal phase HPLC trace of the deracemisation of Crispine A with HDNO (top) or MAO-N D11 (bottom).....	72
<b>Figure 36.</b> <sup>1</sup> H NMR spectrum of 5-methyl-3,4-dihydroisoquinoline as a direct result of an oxidation by MAO-N D9 .....	75
<b>Figure 37.</b> Normal phase HPLC trace of the oxidation of <b>(103a)</b> with HDNO (top) and MAO-N D9 (bottom).....	76
<b>Figure 38.</b> Normal phase HPLC trace of the oxidation of <b>(103e)</b> with HDNO (top) and MAO-N D9 (bottom).....	77
<b>Figure 39.</b> Normal phase HPLC trace of the oxidation of <b>(103b)</b> with HDNO (top) and MAO-N D9 (bottom).....	78
<b>Figure 40.</b> Normal phase HPLC trace of the oxidation of <b>(103c)</b> with HDNO (top) and MAO-N D9 (bottom).....	79
<b>Figure 41.</b> Normal phase HPLC trace of the oxidation of <b>(103d)</b> with HDNO (top) and MAO-N D12 (G) (bottom).....	80
<b>Figure 42.</b> <sup>1</sup> H NMR of the product from the cyanation of 3,4-dihydroisoquinoline .....	82
<b>Figure 43.</b> <sup>13</sup> C NMR of the product from the cyanation of 3,4-dihydroisoquinoline .....	83
<b>Figure 44.</b> Reverse phase HPLC trace of the biotransformation of unpurified <b>(105a)</b> with nitrilase N006.....	86
<b>Figure 45.</b> Reverse-phase chiral HPLC trace of a tetrahydroisoquinoline-1-carboxylic acid 10mm standard (top) and the biotransformation of <b>(105a)</b> with nitrilase N006 (bottom).....	87

## SCHEME INDEX

<b>Scheme 1.</b> Final step in the industrial synthesis of sitagliptin by Merck & Co. ....	5
<b>Scheme 2.</b> Synthesis of tryptolines from chiral tryptophan derivatives. ....	6
<b>Scheme 3.</b> Diastereomer crystallization for the synthesis of ( <i>R</i> )-PZQ .....	7
<b>Scheme 4.</b> Synthesis of enantiopure amino acids by the DKR of racemic $\alpha$ -amino nitriles. ....	9
<b>Scheme 5.</b> Main routes towards the asymmetric synthesis of 1-substituted THIQ's.....	12
<b>Scheme 6.</b> Cascade enzymatic synthesis of magnoflorine from simple and available substrates. <sup>47</sup>	13
<b>Scheme 7.</b> TA catalysed amination in the synthesis of sitagliptin.....	14
<b>Scheme 8.</b> PAL in the synthesis of amino acids. ....	22
<b>Scheme 9.</b> Asymmetric amination of 4-phenyl-2-butanone by a PheDH triple mutant .....	22
<b>Scheme 10.</b> One pot CAR-ATA-IREN cascade for the asymmetric synthesis of piperidines .....	23
<b>Scheme 11.</b> Asymmetric synthesis of tetrahydroisoquinolines with an ( <i>R</i> )-IREN.....	23
<b>Scheme 12.</b> Chemoenzymatic synthesis of nersertraline ( <b>57</b> ). ....	24
<b>Scheme 13.</b> Modified polar mechanism for amine oxidation .....	27
<b>Scheme 14.</b> Dynamic kinetic resolution of AMBA.....	29
<b>Scheme 15.</b> DKR in the deracemisation of 1-MTQ.....	29
<b>Scheme 16.</b> Chemoenzymatic route for the synthesis of ( <i>R</i> )-2-phenylpyrrolidine.....	30
<b>Scheme 17.</b> Deracemisation of Crispine A with MAO-N D9 C.....	31
<b>Scheme 18.</b> Enzymatic synthesis of enantiopure chiral amines with MAO-N D5 or D9 variants ..	31
<b>Scheme 19.</b> MAO-N D11 catalysed synthesis of enantiopure 1-benzyltetrahydroisoquinoline derivatives. ....	32
<b>Scheme 20.</b> Oxidative coupling of TBHBA and 4-AAP .....	59
<b>Scheme 21.</b> Oxidation of 1-M-DMTHIQ with MAO-N variants .....	66
<b>Scheme 22.</b> Deracemisation of $\alpha$ -AMBA with MAO-N D5 and HDNO .....	69
<b>Scheme 23.</b> Deracemisation of 1-MTQ with MAO-N D9 and HDNO .....	70
<b>Scheme 24.</b> Deracemisation of Crispine A with MAO-N D11 and HDNO .....	71
<b>Scheme 25.</b> Cascade reaction for the stereoselective synthesis of tetrahydroisoquinoline-1-carboxylic acid....	73
<b>Scheme 26.</b> Mechanism for the cyanation of 3,4-dihydroisoquinoline with cyanide.....	80
<b>Scheme 27.</b> Stereoselective hydrolysis of ( <b>105a</b> ) with nitrilases for the synthesis of tetrahydroisoquinoline-1-carboxylic acid.....	86

## TABLE INDEX

<b>Table 1.</b> MAO-N variants used in the specific activity assays.....	36
<b>Table 2.</b> Experiment parameters for MAO-N D9 expression in <i>E. coli</i> .....	43
<b>Table 3.</b> List of the primers used in the ligation independent cloning.....	47
<b>Table 4.</b> Phusion® PCR mix.....	48
<b>Table 5.</b> Phusion® PCR cycle program.....	48
<b>Table 6.</b> List of mutagenic primers used in the double mutation.....	49
<b>Table 7.</b> Site-directed mutagenesis PCR reaction mix .....	49
<b>Table 8.</b> Site-directed mutagenesis PCR cycle program.....	49
<b>Table 9.</b> Summary table for the results described in section 3.5. ....	88

## ABBREVIATIONS AND ACRONYMS

1-M-DMTHIQ	6,7-dimethoxy-1-methyl-1,2,3,4-tetrahydroisoquinoline
4-AAP	4-Aminoantipyrine
ACE	Angiotensin-converting-enzyme
ACL	$\alpha$ -Amino- $\epsilon$ -caprolactam
ADHD	Attention deficit/hyperactivity disorder
AL	Ammonia lyase
AMBA	$\alpha$ -Methylbenzylamine
AmDH	Amine dehydrogenase
AO	Amine oxidase
AOX	Alcohol oxidase
API	Active principle
ATHase	Artificial transfer-hydrogenase
BBE	Berberine bridge enzyme
bp	Base pair
BSA	Bovine serum albumin
CAL-B	<i>Candida antarctica</i> lipase B
CAR	Carboxylic acid reductase
COD	1,5-Cyclooctadiene
CYP	Cytochrome P450
DCM	Dichloromethane
DKR	Dynamic Kinetic Resolution
DMSO	Dimethyl sulfoxide
DMTHIQ	6,7-dimethoxy-1,2,3,4-tetrahydroisoquinoline
DNA	Deoxyribonucleic acid
dNTP	Deoxynucleotide triphosphates
<i>E. coli</i>	<i>Escherichia coli</i>
epPCR	Error-prone polymerase chain reaction
FAD	Flavin adenine dinucleotide
FDA	Federal Drug Administration
FT	Flow-through
GDH	Glucose dehydrogenase

HDNO	6-hydroxy-D-nicotine oxidase
HF	High-fidelity
HIV	Human immunodeficiency virus
HPLC	High performance liquid chromatography
HRP	Horseradish peroxidase
IPTG	Isopropyl $\beta$ -D-1-thiogalactopyranoside
IRED	Imine reductase
kb	Kilobase
LB	Lysogeny broth
LDH	Lactate dehydrogenase
MAL	Methylaspartate ammonia lyase
MAO	Monoamine oxidase
MAO-N	Monoamine oxidase from <i>Aspergillus niger</i>
MT	Methyltransferase
MTQ	Methyl-1,2,3,4-tetrahydroisoquinoline
NAD	Nicotinamide adenine dinucleotide
NADP	Nicotinamide adenine dinucleotide phosphate
NCS	Norcoclaurine synthase
NMR	Nuclear magnetic resonance
OD	Optical density
<i>P. pastoris</i>	<i>Pichia pastoris</i>
PAGE	Polyacrylamide gel electrophoresis
PAL	Phenylalanine ammonia lyase
PCR	Polymerase chain reaction
PheDH	Phenylalanine dehydrogenase
PLP	Pyridoxal phosphate
PZQ	Praziquantel
RNA	Ribonucleic acid
RRF	Relative response factor
RT	Retention time
SDM	Site-directed mutagenesis
SDS	Sodium dodecyl sulfate

SOC	Super optimal broth with catabolite repression
TA	Transaminase
TAE	Tris-acetate-EDTA
TB	Terrific broth
TBHBA	2,4,6-tribromo-3-hydroxybenzoic acid
THIQ	1,2,3,4-Tetrahydroisoquinoline
TIC	1,2,3,4-Tetrahydroisoquinoline-3-carboxylic acid
tRNA	Transfer ribonucleic acid
wt	Wild type
WT	Wash-through
XDH	Xanthine dehydrogenase
YPD	Yeast extract peptone dextrose





# CHAPTER 1. INTRODUCTION



## 1.1 $\alpha$ -CHIRAL AMINES AND THEIR IMPORTANCE IN THE CHEMICAL INDUSTRY

### 1.1.1 Overview

Since the discovery of chirality by Louis Pasteur more than a century ago, its importance has spread to all areas of industrial and pharmaceutical chemistry.<sup>1</sup> In fact, more than half of currently marketed drugs present a chiral centre and an increase in these values, driven by the rise in drug complexity, is expected.<sup>2</sup> These compounds are usually administered in their cheaper racemic form, an equimolar mixture of both enantiomers, but history has shown that possible health hazards can mandate the use of an enantiopure drug. A common example can be found in Contergan<sup>®</sup>, an over-the-counter drug from the mid-20<sup>th</sup> century. This medicine contained the active ingredient thalidomide as a racemate and was widely advertised for the relief of morning-sickness in pregnant women. However, while (*R*)-thalidomide (**2**) was an effective sedative with great pharmaceutical properties, the (*S*) enantiomer (**1**) was teratogenic to foetus (**Figure 1**), causing severe malformations in over 10,000 children.<sup>3</sup> An additional boost in the search for enhanced enantiopure drugs arose with FDA's "chiral switch" program, fastening the approval procedure for single-enantiomer drugs from previously used racemic active principles (APIs).<sup>4</sup>

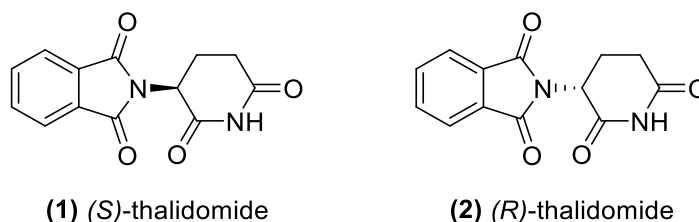


**Figure 1.** Both enantiomers of thalidomide

Chiral amines, particularly ones with an asymmetric carbon in  $\alpha$ -position, represent a significant part of chiral drugs, as seen in the examples with relevant pharmacological application in **Figure 2**. Their potential extends to other chemical areas, providing useful scaffolds for chiral catalysts<sup>5</sup>, resolving agents<sup>6</sup> and ligands in metal complexes<sup>7</sup> for diverse applications.

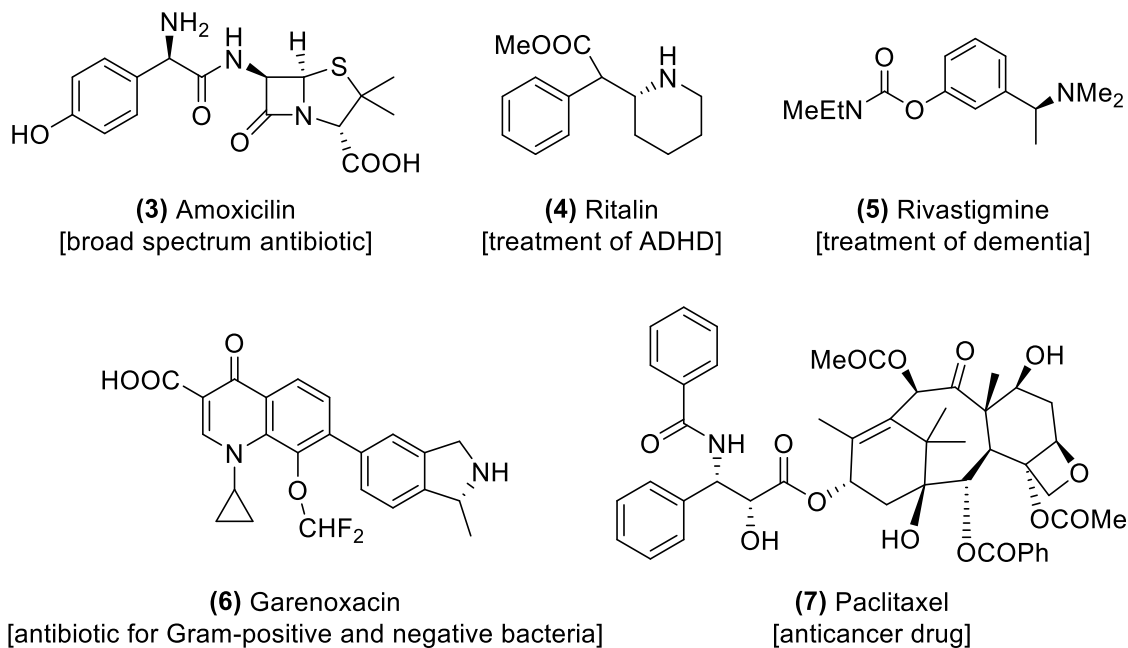


**Figure 2.** Examples of  $\alpha$ -chiral amine-based drugs currently marketed

### 1.1.2 Synthetic routes to single-enantiomer $\alpha$ -chiral amines

Various reliable routes for the synthesis of substituted amines have been developed and are extensively reported elsewhere.<sup>8,9</sup> Similarly, several techniques have been reported in the search for their pure chiral analogues, by either chiral synthesis or posterior resolution.<sup>10</sup> Unfortunately, these methods still pose concerns, either by their low versatility, long multi-step procedures, low yields or selectivity or high environmental impact. Besides, even optimal laboratory procedures may not be adequate for industrial application due to complicated separation methods. The most common methods for the synthesis of enantiopure chiral amines are concisely explained in the following topics.

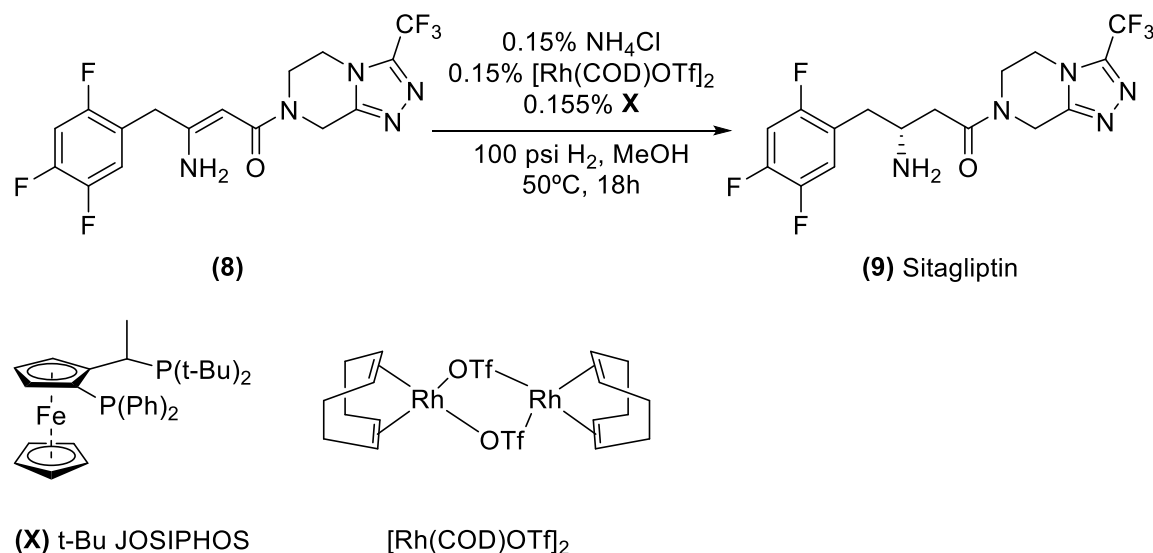
#### 1.1.2.1 Asymmetric synthesis

Asymmetric synthesis encompasses the creation of a chiral centre from a prochiral compound, using either a chiral auxiliary or a chiral catalyst. In the first approach, a stoichiometric amount of a suitable compound is introduced and covalently binds to a prochiral molecule to form an asymmetric centre with a particular configuration. Cleavage of the auxiliary leads to a pure chiral product. Instead, a chiral catalyst can be used in small amounts to increase the selectivity of a reaction involving a stereogenic centre, for example, by coordinating with the substrate. In both cases the cost of the chiral compound and its

separation process from the reaction product, as well as its recyclability, can be a major factor in the scale up of such processes.<sup>11</sup>

Several synthetic routes have been developed according to these criteria. The asymmetric reduction of imines or enamides, either aliphatic or aromatic, with chiral Lewis bases<sup>12</sup>, metal complexes<sup>13</sup> or organocatalysts<sup>14</sup> can be considered the preferential route in large-scale synthesis. Nevertheless, selective amination from aldehydes (reductive amination) or alkenes (hydroamination) along with some more complex approaches can also be used.<sup>10,15</sup>

An example is found in the 2009 synthesis of sitagliptin (**9**), the API in the antihyperglycemic Januvia<sup>®</sup> (**Scheme 1**). The use of a rhodium catalyst for the enantioselective hydrogenation of the enamine (**8**) allowed, at the time, for a new one-pot route with high yield and purity (>95% e.e.), combined with a large reduction in waste production.<sup>16</sup>

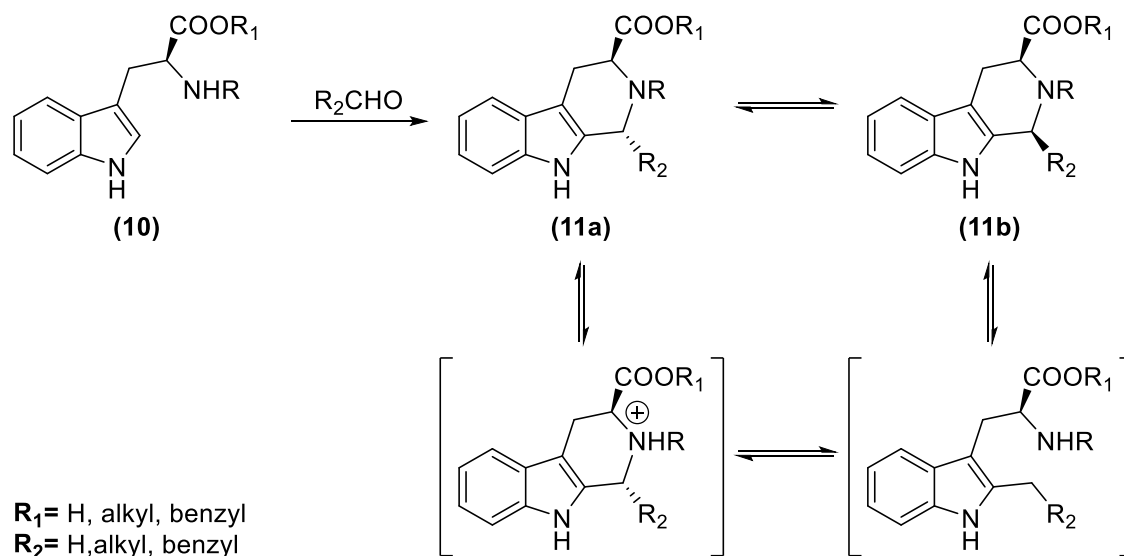


**Scheme 1.** Final step in the industrial synthesis of Sitagliptin by Merck & Co, Inc.

### 1.1.2.2 Chiral pool synthesis

“Chiral pool” is a synthetic strategy that uses cheap and easily obtainable enantiopure substrates as the starting point in the synthesis of complex chiral compounds, therefore eliminating the need for final resolution steps. This approach has some limitations as common chiral substrates are limited to some amino acids, hydroxy acids, sugars and other alkaloids. Still, techniques have been reported that allow inversion in the configuration of the enantiopure substrate, increasing the scope of this strategy.<sup>17</sup> An example of a chiral pool

approach can be seen in the synthesis of tryptoline derivatives (**11**) from chiral tryptophan derivatives (**10**) (**Scheme 2**).<sup>18</sup>

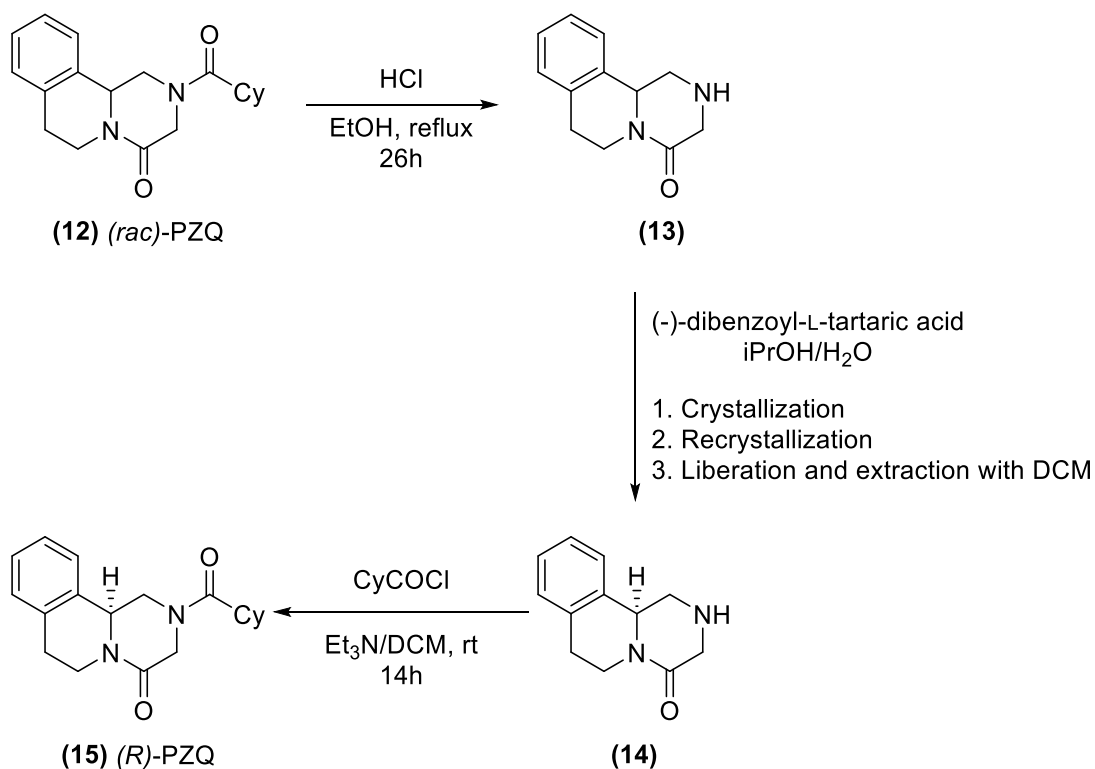


**Scheme 2.** Synthesis of tryptolines from chiral tryptophan derivatives.

### 1.1.2.3 Crystallization

Preferential crystallization stands as one of the first routes to obtain enantiopure compounds. It consists in the chemical property, first defined by Louis Pasteur, that some racemates tend to crystallize in mixtures of enantiopure crystals, that is, an enantiomer has a greater affinity to crystallize in a crystal of the same isomer.<sup>19</sup> Unfortunately, only a small fraction of racemic compounds can be resolved by this technique. A particular downside is that even full recovery of the wanted isomer achieves only 50% yield.<sup>1</sup>

An alternative technique with limited applicability was also found by Pasteur in 1853.<sup>20</sup> Diastereomer crystallization comprises the separation of an enantiomer by selective crystallization of the salt formed with a readily available enantiopure compound, alias, resolving agent. Praziquantel (PZQ) (**12**), to this moment the main API used in the treatment of schistosomiasis, is presented as an example. Besides not having any therapeutic effect, (*S*)-PZQ is extremely bitter and therefore undesirable in the formulation. Unfortunately, the presence of an amide bond has hindered the development of an asymmetric synthesis. Nevertheless, the diastereomeric crystallization of (**13**) with (-)-dibenzoyl-L-tartaric acid, followed by recrystallization, neutralization, extraction with dichloromethane (DCM) and acylation, to form (*R*)-Praziquantel (**15**) has recently been reported with 33% yield and 97% e.e. (**Scheme 3**). Moreover, the resolving agent could be recycled with 89% yield.<sup>21</sup>



**Scheme 3.** Diastereomer crystallization for the synthesis of (*R*)-PZQ

#### 1.1.2.4 Kinetic resolution

Kinetic resolution explores the different reactivity of the enantiomers in a racemic mixture with a given compound, allowing a simple separation of the reacted and unreacted species. The final purpose of this technique is the selective full conversion of only one enantiomer, allowing a theoretical maximum yield of 50%.<sup>22</sup>

A different and more appealing variant to this resolution method is the dynamic kinetic resolution (DKR). This approach allows a yield above 50% by assuming that both isomers are interchangeable during the reaction, sometimes using a catalyst to drive the process.<sup>23</sup> Recently, a different DKR methodology has been applied where a non-chiral reaction product, formed by a selective reaction with one isomer, is converted back to the reagent, with a non-selective catalyst, in a racemic manner. After several cycles, it is theoretically possible to obtain an enantiopure compound.

In fact, DKR is experiencing an exponential growth driven by the recent boom in biocatalysis and genetic engineering. Enzymes are great catalysts due to their high selectivity, low cost and mild reaction conditions but, until now, the need to use reagents close to the enzyme's

natural substrate has hindered further investigation. However, the consistent drop in the price of gene sequencing and synthesis and the large investment in the development of this area have supported the discovery of a broad range of enzymes and further appearance of several engineered enzymes with a wide substrate scope. The advantages and disadvantages of enzymatic dynamic kinetic resolution in current organic synthesis, by comparison with its chemical counterpart, are briefly presented in **Figure 3**.<sup>23</sup>

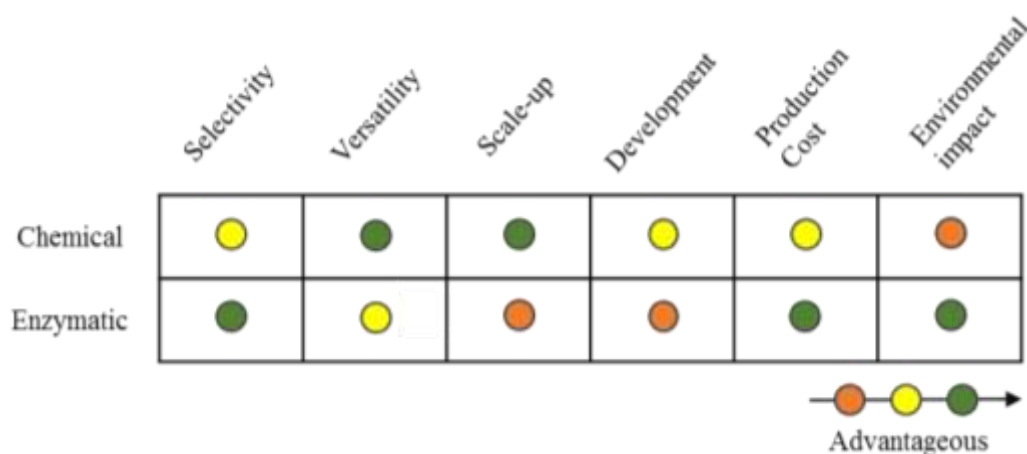
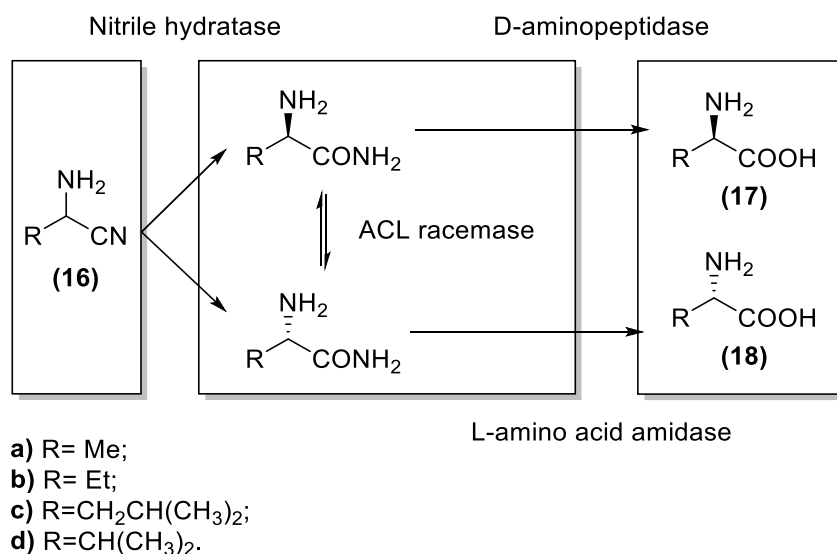


**Figure 3.** Visual comparison between chemical and enzymatic DKR.

One example of an enzymatic DKR is found in an article by Yasukawa *et al.*, where both (*R*) (**17**) and (*S*) (**18**) enantiomers of simple amino acids could be obtained from their nitrile analogue (**16**) by a cascade reaction with a non-selective nitrile hydratase from *Rhodococcus opacus* and either a D-aminopeptidase from *Ochrobactrum anthropic* or a L-amino acid amidase from *Brevundimonas diminuta* (**Scheme 4**). Remarkably,  $\alpha$ -amino- $\epsilon$ -caprolactam (ACL) racemase from *Achromobacter obae* was used in the interconversion of both amide enantiomers.<sup>24</sup>





**Scheme 4.** Synthesis of enantiopure amino acids by the DKR of racemic  $\alpha$ -amino nitriles.

### 1.1.3 Tetrahydroisoquinoline as an important building block in the chemical industry

#### 1.1.3.1 Overview

The large family of isoquinolines alkaloids is ubiquitous in chemical research, with broad occurrence in nature and extensive application in all areas of industrial chemistry. Among them, the 1,2,3,4-tetrahydroisoquinoline (THIQ) scaffold (**19**) (**Figure 4**) has been extensively studied for its natural incidence in plants and humans.<sup>25</sup> The interest in these particular compounds began with allegations of their relationship with chronic alcoholism and role in behavioural disorders. Studies in the expression of THIQ and its relation with blood alcohol levels in the brain began as early as 1934, but only in 1970 was any definitive evidence presented. It was shown that ethanol is oxidised to acetaldehyde by alcohol dehydrogenases in the brain, which then readily reacts with neurotransmitters to form THIQ's such as salsolinol (**21**) (**Figure 5**).<sup>26</sup> Studies have shown that some THIQs can be partially responsible for chronic alcoholism, greatly stimulating alcohol consumption. Nevertheless, several theories in the mechanism through which these heterocyclic compounds are synthesized remain unopposed.<sup>27</sup>

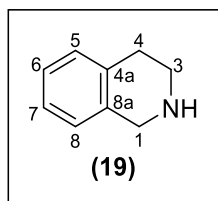


**Figure 4.** Structure of THIQ and atom number nomenclature adopted in this work

Further research has determined that dopamine (**20**) derived THIQs such as salsolinol (**21**) and norsalsolinol (**22**) (**Figure 5**) actively modulate neurotransmission, catecholamine biosynthesis and mitochondrial activity<sup>28</sup>, particularly by its interaction with monoamine oxidase (MAO)<sup>29</sup>. Although no unequivocal proof has been reported, THIQ's have also been greatly associated with Parkinson disease and attention-deficit/hyperactivity disorder (ADHD)<sup>30</sup>. It is reported that research in this area can potentially lead to new treatments based on THIQ's.

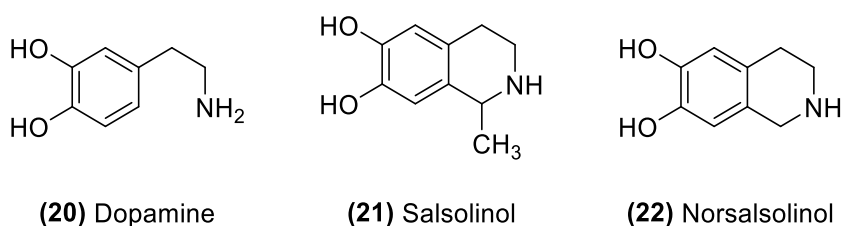


**Figure 5.** Structure of THIQ's associated with brain disorders.

### 1.1.3.2 Current applications

The presence of a wide range of natural THIQ alkaloids and the previously mentioned studies of their impact in the human body lead to the development of derivatives with a wide range of biological activities. Indeed, these compounds have shown antidiuretic activity through the selective inhibition of M3 muscarinic receptors<sup>31</sup>, sleep-promoting activity by the inhibition of orexin receptors 1 and 2<sup>32</sup>, anti-HIV (human immunodeficiency virus) activity by the inhibition of HIV-1 reverse transcriptase<sup>33</sup> and high anticancer activity against breast cancer cells<sup>34</sup>. Moreover, some derivatives have proven to be good inhibitors of P-glycoproteins, transporter proteins associated to drug resistance and brain diseases such as Parkinson and Alzheimer.<sup>35</sup>

Three sub-classes of THIQ's with distinctive structures are presented in **Figure 6**. First, tetrahydroisoquinoline-3-carboxylic acid (TIC) derivatives (**23**) are constrained analogues of phenylalanine and its use in peptide-based drugs<sup>36</sup> has shown remarkable potential for the

treatment of atherosclerosis, opioid-dependence, hepatitis C, among others. Quinapril (Accupril®: Pfizer) is, at the moment, the most important TIC derivative, acting as an angiotensin-converting-enzyme (ACE) inhibitor for the treatment of hypertension. Second, norcoclaurine (**24**), a 1-benzyltetrahydroisoquinoline found in high concentration in the fruits of *Nandina domestica*, is used as fat-burner and a mild anti-asthmatic.<sup>37</sup> Derivatives of this scaffold include morphine and codeine, analgesics, aporphine, an antipsychotic, and tubocurarine, a muscle relaxant. Finally, protoberberine alkaloids such as berberine (**25**) are extensively marketed as food supplements for diabetics<sup>38</sup> but have shown relevant cardiovascular, anti-cancer, anti-depressive and anti-inflammatory activities.<sup>39</sup>

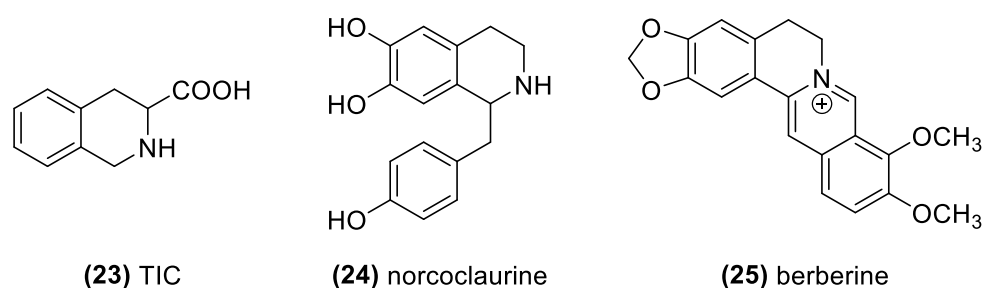
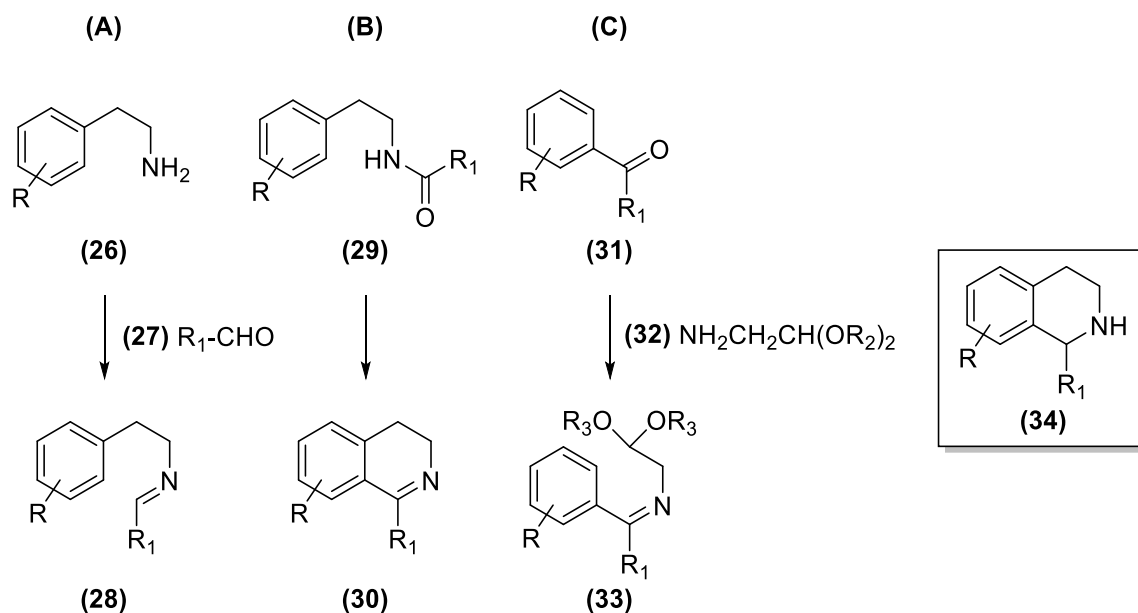


**Figure 6.** Examples of THIQ compounds in three major sub-classes with important biological activities.

#### 1.1.4 Asymmetric synthesis of C1 substituted tetrahydroisoquinolines

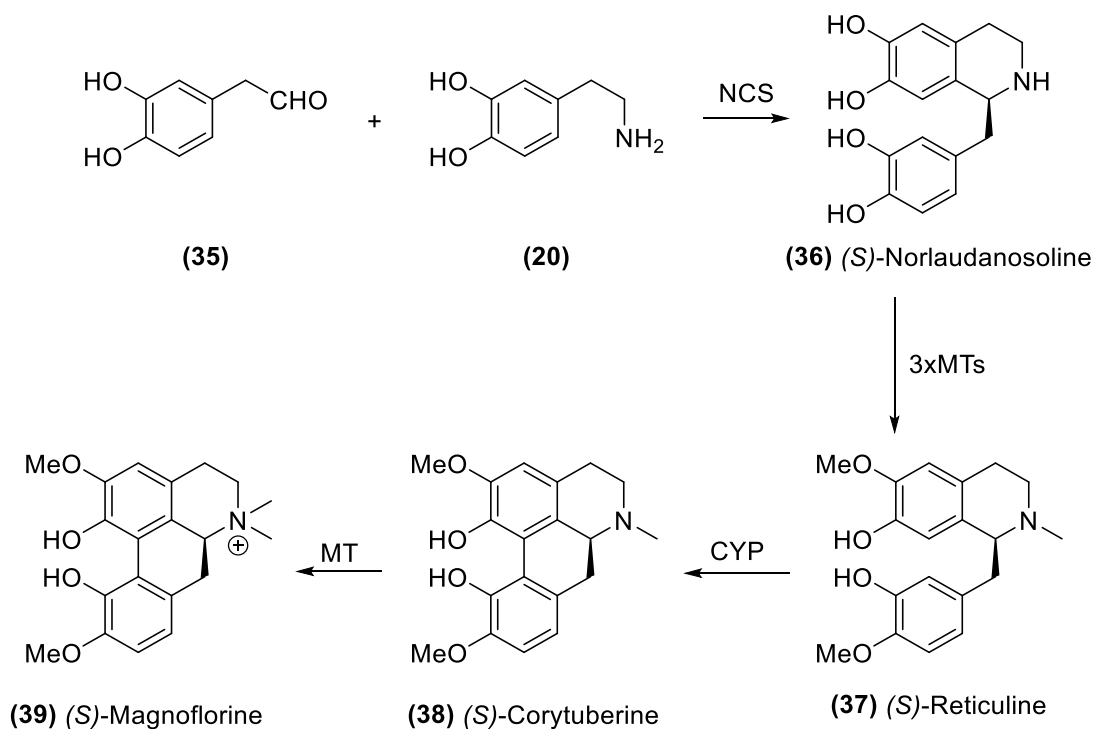
To this day numerous methods have been reported for the synthesis of THIQs. In fact, the challenge presented in the stereo centre in C1 has also encouraged scientists to develop asymmetric routes to these compounds. Three common approaches towards C1 substituted THIQ's - the Pictet-Spengler (**A**), Bischler-Napieralski (**B**) and Pomeranz-Fritsch-Bobbitt (**C**) reactions - are presented in this work, as seen in **Scheme 5**. Nevertheless, today's scientists still struggle with its synthesis, as no method reported is without flaw.



**Scheme 5.** Main routes towards the asymmetric synthesis of 1-substituted THIQ's.

The Pictet-Spengler reaction was discovered more than 100 years ago, in 1911, for the synthesis of THIQ and it is now one of the most important reactions in the synthesis of heterocyclic compounds.<sup>40</sup> Over the last 25 years, the remarkable progress in the asymmetric form of this synthesis has spurred a new area of investigation. Chemically, it is generally performed in aprotic solvents with acid catalysis and comprises the condensation of a phenylethylamine derivative (**26**) with an aldehyde (**27**) to form an iminium intermediate (**28**). This species is promptly attacked by the aromatic ring's  $\pi$  system and restores aromaticity to form a THIQ (**34**) (**Scheme 5**).<sup>41</sup> Several catalysts have been explored towards this synthesis, including chiral auxiliary groups<sup>42</sup>, Lewis and Brønsted acids<sup>43</sup>, organocatalysts<sup>44</sup>, among others.

Notably, an enzymatic Pictet-Spengler synthesis of THIQs has also been developed through the use of norcoclaurine synthase (NCS), responsible in nature for the synthesis of (*S*)-norcoclaurine.<sup>45</sup> Although wide applicability of this enzyme for 1-benzyltetrahydroisoquinolines is still to be reported due to its very limited substrate scope (it required a 7-OH aromatic substituent<sup>46</sup>), a remarkable bioengineering experiment allowed the expression of the THIQ alkaloid magnoflorine (**39**) using a combination of NCS, methyltransferases (MTs) and cytochrome P450 (CYP).<sup>47</sup> A summary of the metabolic pathway can be seen in **Scheme 6**.



**Scheme 6.** Cascade enzymatic synthesis of magnoflorine from simple and available substrates.<sup>47</sup>

The Bischler-Napieralski reaction, followed by hydrogenation, can also be used in the asymmetric synthesis of THIQ's. An acylated dopamine derivative (**29**) reacts with appropriate catalyst, usually  $\text{POCl}_3$ ,  $\text{P}_2\text{O}_5$  or  $\text{ZnCl}_2$ , to form an iminium intermediate that promptly cyclizes into a 3,4-dihydroisoquinoline (**30**). This compound can then be asymmetrically reduced by a variety of methods to form the desired THIQ's (**34**) (**Scheme 5**).<sup>48</sup>

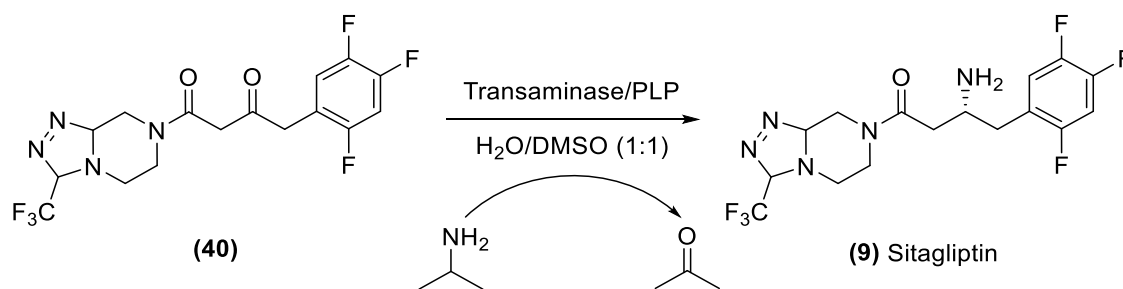
Finally, the Bobbitt modification to the Pomeranz and Fritsch synthesis of quinolines allows for a rather complex synthesis of THIQ's. In fact, this route requires two reductions to reach the target molecule or a reaction of the imine group prior to the final cyclization-hydrogenation step. First, a *N*-benzyliminoacetaldehyde diethyl acetal compound (**33**) is formed by reaction of the free benzylaldehyde derivatives (**31**) with (**32**) (**Scheme 5**). The imine group is either reacted or reduced to its amine analogue and this intermediate is reductively cyclized to afford the desired core (**34**).<sup>49</sup> Although not common in THIQ synthesis, this method has been successfully applied towards the synthesis of protoberberines, for example by Grajewska *et al.*<sup>50</sup>, where the presence of the imine intermediate proved advantageous as a reactive site for further functionalization.

## 1.2 BIOCATALYSIS: A GREEN PATH IN CHIRAL AMINE SYNTHESIS

### 1.2.1 Overview

The chemical synthesis of enantiopure chiral compounds often requires a compromise between yield and enantiomeric purity. Existing industrial procedures usually require additional resolution steps, greatly reducing the final yield and increasing the E-factor.<sup>51</sup> In fact, by 2007, the pharmaceutical industry presented the highest E-factor, ranging from 25 to 100<sup>52</sup>, due to rather complex chiral targets. Therefore, it has shown a particular interest in the development of cost-effective, sustainable alternatives to these resolution methods.<sup>53</sup>

Nowadays, the development of biocatalytic synthetic methods can be highly appealing in synthetic chemistry due to the use of cheap, non-toxic and renewable catalysts that can achieve extremely high selectivity at mild pH, temperature and pressure conditions and with low waste production.<sup>54,55</sup> Still, the use of water as a non-toxic solvent can limit the concentration of non-polar substrates and demand a final extraction step, leading to higher production costs.<sup>56</sup> One acclaimed use of enzyme catalysis in industrial amine synthesis is the transaminase (TA)/pyridoxal phosphate (PLP) selective reductive amination of a diketone sitagliptin intermediate (**40**) (Scheme 7), substituting the previously mentioned chemical method (Scheme 1).<sup>57</sup>



**Scheme 7.** TA catalysed amination in the synthesis of sitagliptin

Biocatalysis can be defined, as said by Bornscheuer *et al.*, as “the application of enzymes and microbes in synthetic chemistry, [using] nature’s catalysts for new purposes (...)”.<sup>58</sup> Its first applications in chemical synthesis consisted in the direct use of cell extracts to convert a given substrate into a desired molecule. Since then, it has evolved to increase enzyme activity towards unnatural molecules, for example, through the use of evolution and heterologous expression techniques. Today’s research in biocatalysis focuses on two main challenges: the discovery and engineering of enzymes with broad substrate scope for the

production of complex chiral molecules, and the scale-up of these catalytic systems to industrial applications, increasing enzyme stability and maximum substrate concentration. In the following topic, the various steps required in a full biocatalytic research are described.

## **1.2.2 Development of an enzymatic synthesis: main steps**

### **1.2.2.1 Enzyme discovery**

Enzyme discovery stands as the basis for all biocatalytic development. Traditionally, new enzymes were discovered by the culture of environmental samples with media enriched with a suitable substrate. However, this process was time consuming and not reliable in the discovery of specific enzymes. Moreover, over 99% of all microbes are still unculturable today. Fortunately, breakthroughs in deoxyribonucleic acid (DNA) sequencing and computer processing power allowed for more methodical alternatives such as *metagenomics*.<sup>59</sup>

In metagenomics, the entire DNA of a given environmental sample is extracted and cloned into bacterial cloning vectors for later expression. The library of genes ultimately generated can then be sequenced and searched for homologous enzymes (**Figure 7 - A**). Although sometimes inaccurate, homology proposes that the similarity in structure presented by different enzymes can correspond to similar activities.

A more thorough approach requires the phenotypic screening of all expressed enzymes from the environmental DNA with a substrate of interest (**Figure 7 - B**), followed by sequencing of the most promising results. Several more recent metagenomic approaches can be explored in the reference presented.<sup>60</sup>

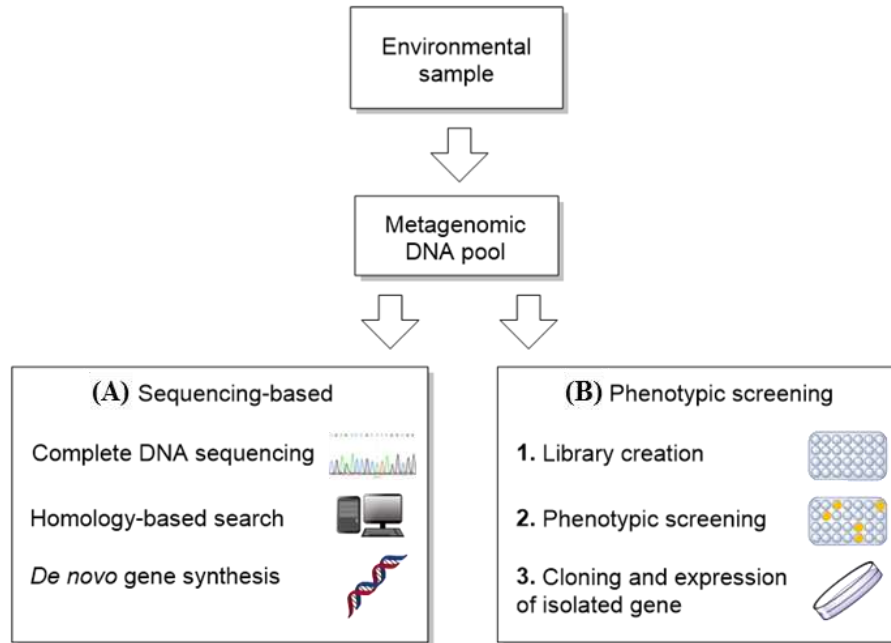


**Figure 7.** Metagenomics in gene discovery

### 1.2.2.2 Enzyme production: expression and purification

In the XX century, the development of enzymatic synthesis proceeded at a slow pace, hindered by long production and purification procedures. In fact, the isolation of enzymes from their native species - animals, plants, fungi or bacteria – for biocatalysis proved to be sometimes laborious and inefficient, encouraging scepticism in future industrial applications. The discovery of recombinant DNA in 1970 revolutionized this field, allowing scientists to express a given enzyme in a different host – heterologous expression. Nowadays, recombinant expression is widely used, with most enzymes overexpressed in bacterial or fungal hosts. Typical organisms include *Escherichia coli* and *Pichia pastoris* due to their high expression, easy culture and accessible genetic manipulation. Moreover, commercial strains of these organisms have been genetically modified to increase either plasmid replication or translation, to reduce the number of endonucleases and to increase growth rate. The engineered strain can then be used for either cloning or expression purposes.<sup>61</sup>

Several factors must be taken into account in the heterologous expression of protein. First, a pure sample of the gene of interest must be inserted into a suitable plasmid. A plasmid is a DNA molecule with self-replicating abilities, containing an appropriate origin of replication. This unit can also contain, among others, a transcription toolbox, markers for antibiotic



resistance and one or several genes. Circular plasmids are used in *E. coli* for extensive replication in the cytoplasm while linearized plasmids are used in *P. pastoris* for insertion in the host's genome.<sup>62,63</sup>

The plasmid must then be passively transported through the cell's membrane to the intracellular medium. For that, it requires an increased membrane permeability generated by the exposure to harsh physical conditions, in a procedure called transformation. In *E. coli* a sudden rise in temperature in the presence of divalent cations is enough to force plasmid DNA to enter the cell through the cell pores (heat shock), while in *P. pastoris* a more delicate procedure is required to avoid cell damage where an electrical current can generate transient holes in the cell's membrane (electroporation).<sup>62,63</sup> Finally, the recombinant cell can be grown in an appropriate culture and purified with one of the procedures extensively reported elsewhere.<sup>64</sup>

One additional topic must be addressed for the reader to fully understand the following work. Codon bias defines the preference of each organism for specific degenerate codons over others, establishing that adverse consequences can arrive from "silent mutations". According to the literature, codon bias can affect protein folding and influence protein expression for a factor up to 1000. Several causes have been identified for this phenomenon, including differences in tRNA (transfer ribonucleic acid) and codon frequency, in the spacial proximity between codons recognized by the same tRNA and in the unfavourable interactions between specific consecutive tRNA's.<sup>65</sup>

Two different strategies can provide a quick solution to these problems. First, it is suggested that expression in a more complex organism, with a larger genome, can reduce the impact of frequency bias. This method can be particularly effective if the new organism has a smaller genetic distance to the native one. In alternative, and more effectively, it is now possible to codon-optimize a gene for a target organism with carefully designed algorithms and create the modified gene by *de novo* synthesis. Nevertheless, the costs of DNA synthesis remain significant for most research groups and must be taken into account. Also, and as mentioned before, codon-optimization can be ineffective, as significant changes to the codon sequence can alter protein folding and lead to the expression of inactive enzyme.<sup>65,66</sup>

### 1.2.2.3 Enzyme engineering

The emergence of enzymes as sustainable catalysts in the transformation of natural chemicals has driven research for its application in non-natural compounds as well. Synthetic biology has addressed this issue with the development of enzyme engineering. Early experiments in mutagenesis were laborious and full mutation of all amino acids in a given enzyme, followed by its phenotypic screening, is still not physically possible. To explain, even the complete mutation of a 10 amino acid long protein requires the screening of over 10 trillion sequences. To further difficult enzyme optimization, the misconception of additivity - the activity of a double mutated enzyme can be predicted as an improved activity of the two single mutants - has been more recently replaced for epistasis, in which the effect of a mutation can be affected by the remaining protein sequence. This concept can be summarized by the “fitness landscape” presented in **Figure 8**, where the route towards the enzyme with optimum activity can go through several misleading local maximums and even mutations that, in that particular step, cause a decrease in activity.<sup>67</sup>

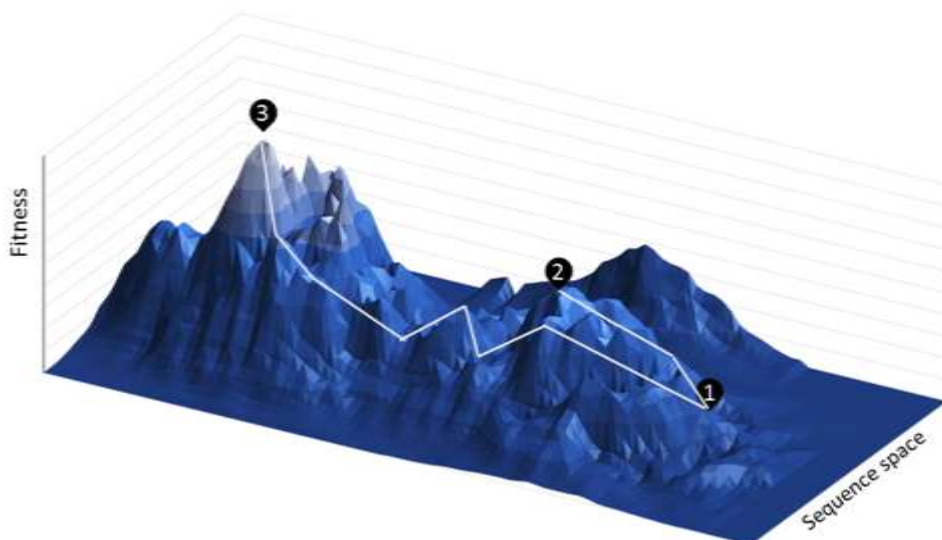


**Figure 8.** Simulated fitness landscape in directed evolution. The activity of a given enzyme **1** can be optimized to peak **2**, where a local maximum can be mistaken for the optimal activity, or peak **3**, where several misleading disadvantageous mutations are required to reach the global activity maximum. Adapted from Shaffe, T..<sup>68</sup>

Directed evolution tries to overcome this difficulty by mimicking natural evolution with a twist (**Figure 9**). For the purpose of this work, it can be defined as the protein engineering of enzymes, by iterative rounds of mutagenesis, for a pre-defined purpose. Procedures for the identification of the best desired mutants, selection or screening, are quite specific and will not be described in this chapter. Nevertheless, the reader is encouraged to explore solid-support selection methods and more recent high throughput screening assays.<sup>69</sup> Nowadays, the procedures involved in generating enzyme variation are the most debatable and three of the most generally applied techniques are here summarized.

Random mutagenesis by error-prone polymerase chain reaction (epPCR) is perhaps the first and most basic method in directed evolution (**Figure 9 - 2a**). It involves the use of altered PCR conditions to increase the error rate in DNA replication, generating randomly mutated DNA sequences. Although common, this method comprehends several limitations, including a high ratio of incomplete or insoluble proteins. In fact, it has been reported that up to 3 in every 64 mutations generate a new stop codon, leading only to partial protein expression. Furthermore, consecutive mutations and complete libraries cannot be obtained by this technique. Nevertheless, random mutation can still be important as a quick method to reveal unpredictable mutations that can alter a protein's secondary structure and significantly improve its activity.<sup>70</sup>

DNA shuffling was first reported by Stemmer *et al.* as a technique for the creation of highly chimeric gene libraries, formed by the fragmentation of several homologous genes, followed by recombination and PCR amplification (**Figure 9 - 2b**). Unfortunately, it is reported that a reduction in variability is usually found due to bias similar to the ones previously mentioned in epPCR. This technique has also been used to better assess multiple mutations by recombining single mutated gene fragments, obtained by either epPCR or site-directed mutagenesis.<sup>70,71</sup>

In focus in this particular work is site-directed mutagenesis (SDM), an *in vitro* method that uses PCR with mutagenic primers to introduce specific sequence changes (**Figure 9 - 2c**). This technique is widely used in the creation of gene libraries, designing primers so that a mixture of bases is found at a specific location, in a so called degenerate codon. A list with the most used degenerate codons, encoding for different sets of amino acids, is referred

elsewhere. A large number of samples is usually required to attain all 20 amino acids in a given position, limiting the number of mutations viable in a research laboratory.<sup>70</sup>

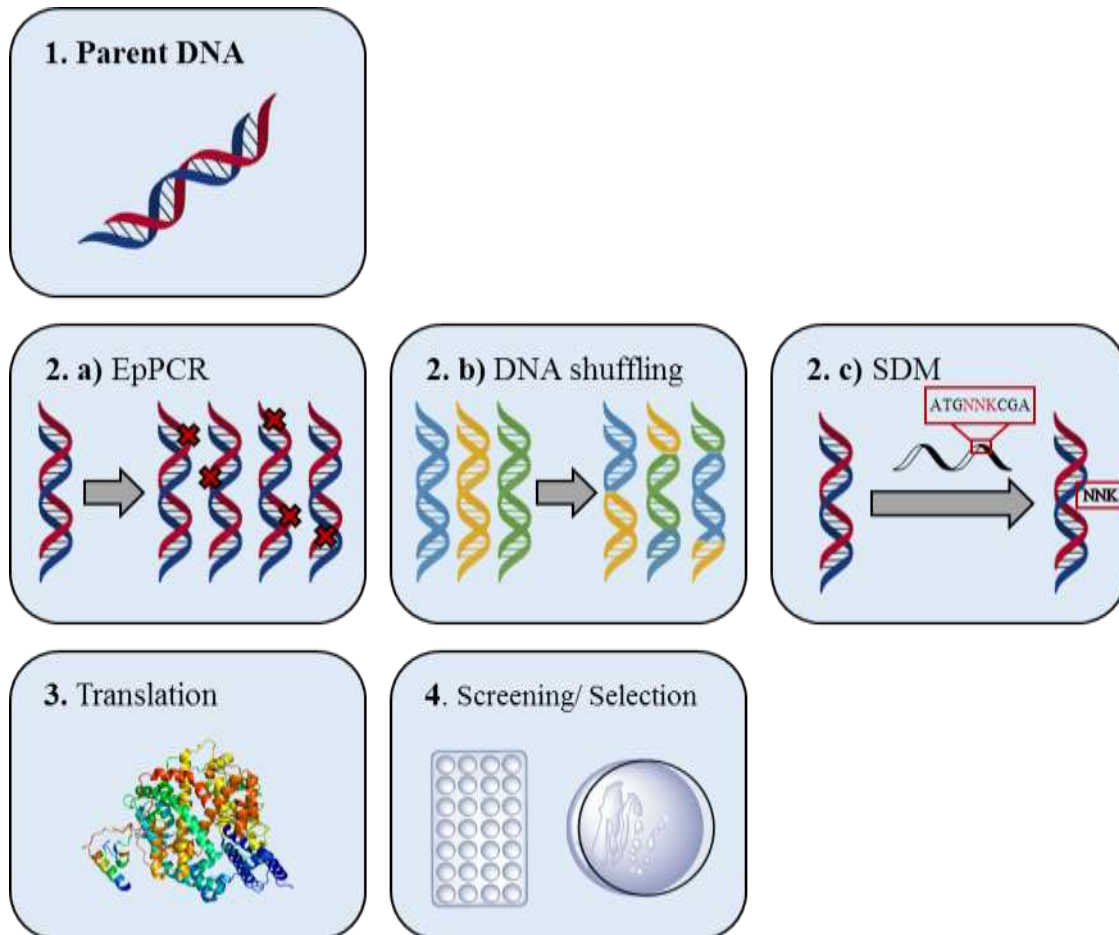


**Figure 9.** Example of an enzyme engineering experiment. It is highlighted that iterative cycles of this experiment are usually performed to achieve optimal activity.

### 1.2.3 Enzymes employed in chiral amine synthesis

Several classes of enzymes have been used in the synthesis of chiral amines, through the kinetic resolution of racemic substrates or the asymmetric synthesis from ketones, imines or  $\alpha$ -unsaturated acids. These classes are summed up in **Figure 10**.

Asymmetric synthesis			Kinetic Resolution		
NH <sub>2</sub> R	NH <sub>3</sub>	NH <sub>3</sub>		CH <sub>3</sub> COOiPr	NH <sub>3</sub> BH <sub>3</sub>
<b>Transaminase</b>	<b>Amine Dehydrogenase</b>	<b>Ammonia Lyase</b>	<b>Imine Reductase</b>	<b>Lipase</b>	<b>Amine Oxidase</b>

**Figure 10.** Enzymes used in the synthesis of chiral amines: examples

Ammonia lyases (AL) (E.C. 4.3.1) are a sub-class of enzymes with narrow substrate scopes that catalyse the reversible break of a C-N bond, often forming a double bond in the process and releasing ammonia. Remarkably, a methylaspartate ammonia lyase variant has been reported that can catalyse the addition to 2-methylfumaric acid of a variety of primary amines containing alkyl, benzyl and electron-rich substituents.<sup>72</sup>

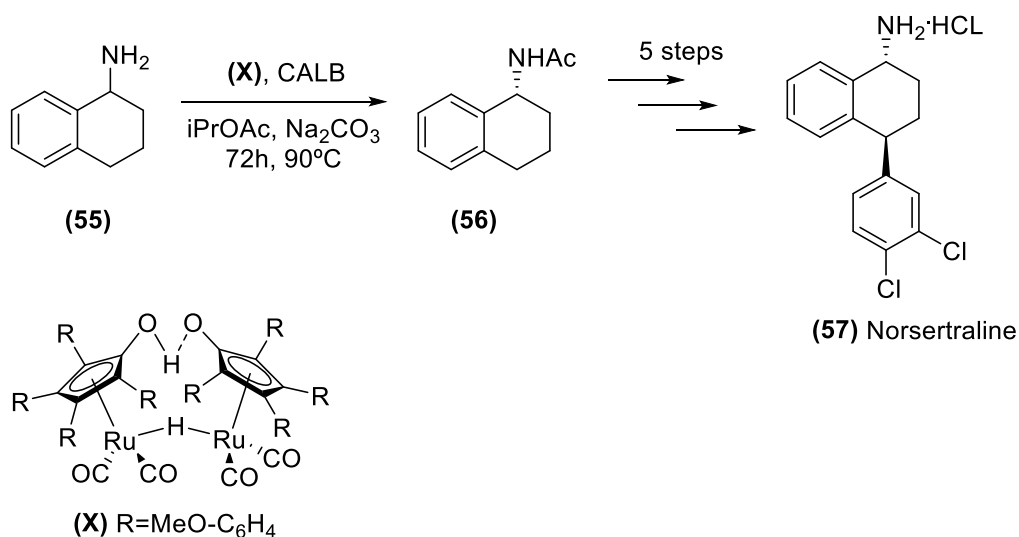
Nevertheless, the reader is guided towards phenylalanine ammonia lyase (PAL) as a promising enzyme for future applications. This enzyme is specific for the deamination or synthesis of L-Phe and, to a lesser extent, L-Tyr,<sup>73</sup> but directed evolution experiments have recently been reported that allow halogen substituents in the aromatic ring.<sup>74</sup> Two important uses of this lyase, the synthesis of L-Phe (**42 a**), an aspartame precursor, and 2-halogenated phenylalanine<sup>75</sup> (**43**), an indoline precursor (**44**), are presented in **Scheme 8**.





Two enzymes have been extensively reported for the deracemisation of chiral amines. Lipases can catalyse the enantioselective hydrolysis or synthesis of esters (Esterases - E.C. 3.1.1) and are currently one of the leading biocatalysts in lipid bio-industry. Moreover, they present high stability in organic solvents and an unusually high substrate scope, making them ideal for kinetic resolution experiments and future industrial application.<sup>85</sup>

*Candida antarctica* Lipase B (CAL-B) is the most common lipase for organic synthesis, already applied in industrial synthesis by Bayer and BASF. In fact, BASF has developed an immobilization procedure for CAL-B, thus reducing the need for high catalyst concentration.<sup>86,87</sup> Nevertheless, the more recent use of CAL-B in the DKR of primary amines is highlighted for its high yield, and metal complexes are commonly used in the ester hydrolysis. The synthesis of a norsertraline precursor (**56**) by the DKR of (**55**) with CAL-B and a ruthenium catalyst was reported with high yield (70%) and exceptional e.e. (99%), as seen in **Scheme 12**.<sup>88</sup>



**Scheme 12.** Chemoenzymatic synthesis of norsertraline (**57**).

Amine oxidases (AO) can also be used for the deracemisation of chiral amines. AO are oxidoreductases with important physiological functions in detoxification, cell growth, signalling and biosynthesis of alkaloids. They are found in numerous organisms and can be classified in two types: type I enzymes, copper-dependent, and type II enzymes, flavin-dependent. Type I AOs use copper and pyrroloquinoline quinone as co-factors and the formed imine remains covalently bound to the protein in the end of the reaction, limiting their applicability in biocatalysis. Type II AOs, on the contrary, are flavin-dependent and have been extensively used in enzymatic synthesis (E.C. 1.4.3.4).<sup>89</sup>



Several flavin adenine dinucleotide (FAD)-dependent AOs have been reported so far, including diamine oxidase<sup>90</sup>, several amino acid oxidases<sup>91</sup> and 6-hydroxy-D-nicotine oxidase (HDNO). HDNO (E.C. 1.5.3.6) is a 49kDa monomeric enzyme found in some soil bacteria, such as *Arthrobacter nicotinovorans*, where it is a key enzyme in the degradation of nicotine. It has been assigned to the *p*-cresol methylhydroxylase-vanillyl-alcohol oxidase family and, remarkable, stands as the first discovered enzyme with the FAD co-factor covalently bound.<sup>92</sup> Nowadays, it is estimated that approximately 10% of all flavoproteins have a covalently bond co-factor, significantly increasing the enzymes' redox potential, protein stability and preventing co-factor release.<sup>93</sup>

Crystal structure analysis has shown that HDNO possesses a large active centre, capable of accommodating additional substrates. In fact, a recent article by Heath, *et. al.* has studied the substrate scope of HDNO from *Arthrobacter nicotinovorans* and found it to be active with 8 different amines, including substituted derivatives of nicotine. Moreover, a double mutant was engineered and used in the deracemisation of additional tetrahydroisoquinoline (**58**, **60** and **61**) and tryptoline (**59**) derivatives (**Figure 11**).<sup>94</sup>

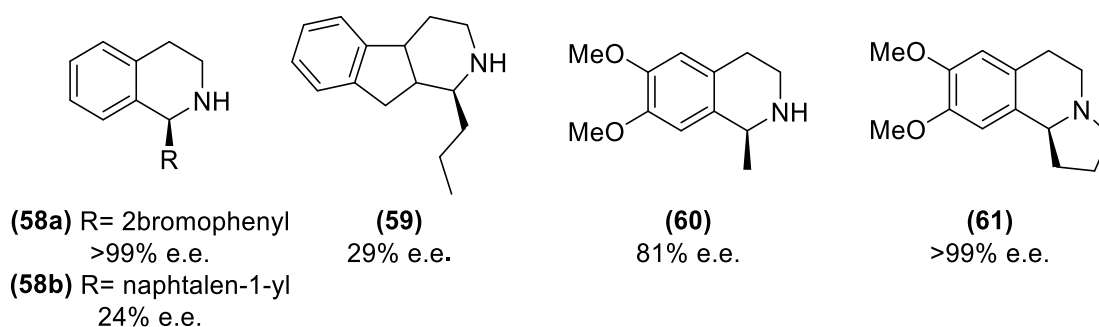


**Figure 11.** Deracemisation of tetrahydroisoquinoline and tryptoline derivatives with the E350L/E352D HDNO mutant.

Monoamine oxidase (MAO) remains one of the most important AO, referred as “the mother of all amine oxidases” in a book published by SpringerMedicine.<sup>95</sup> It catalyses the oxidative deamination of biogenic primary amines by producing H<sub>2</sub>O<sub>2</sub>. In humans, MAO exists mainly in the brain and peripheral tissues in the form of two isozymes: A and B. Although similar in sequence (70% sequence identity), these two isozymes differ in their accepted substrates and functions in the brain: MAO A shows higher affinity towards serotonin (**62**), norepinephrine (**64**) and dopamine (**20**) and has been related to aggressiveness while

MAO B has a higher affinity for phenylethylamine (**63**), benzylamine (**65**) and dopamine (**20**) and has been implicated in Parkinson's disease (**Figure 12**).<sup>96</sup>

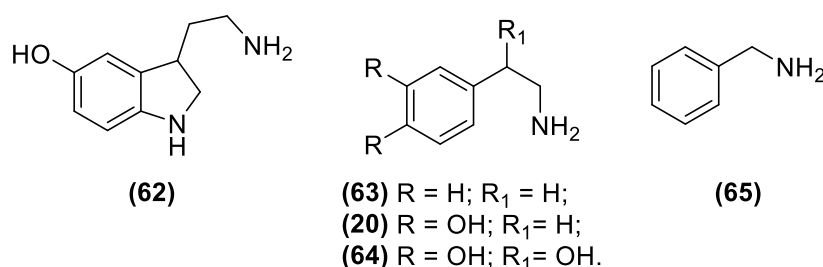


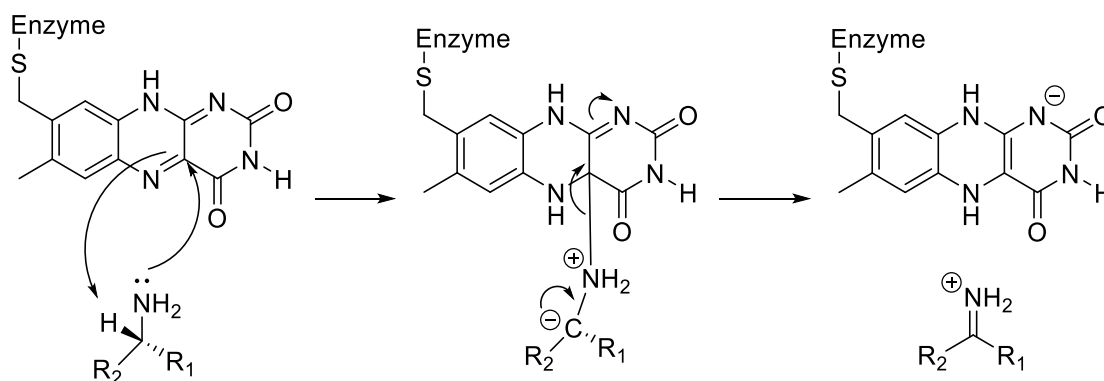
**Figure 12.** Common MAO A and MAO B natural substrates

Type I and II non-membrane bound MAO can be found in lower eukaryotes, oxidizing amines as nitrogen sources. From those, a flavin-dependent MAO from *Aspergillus niger* (MAO-N) has been extensively engineered for biocatalysis. Besides, its importance in the work here presented justifies the separate description that follows.<sup>97</sup>

#### 1.2.4 Monoamine oxidase from *Aspergillus niger*

MAO-N was first cloned in 1995 by Schilling *et al.* with a butylamine-induced culture. In fact, the article suggests this enzyme as an evolutionary prototype of mammalian MAO-A and MAO-B.<sup>97</sup> The same author readily cloned this enzyme in *E-coli*, reporting a length of 495 amino acid residues correspondent to 55.6 kDa.<sup>98</sup>

As previously stated, MAO-N is a FAD-dependent enzyme, but the mechanism through which the redox reaction occurs is still subject to controversy. According to our research, a computational study by Erdem *et al.* supports the polar nucleophilic mechanism proposed by Miller and Edmondson shown in **Scheme 13**. The authors found good correlations between the experimental reaction rate and activation energy of MAO-A with *p*-substituted benzylamines and quantum chemical calculations based on this mechanism.<sup>99</sup>



**Scheme 13.** Modified polar mechanism for amine oxidation

#### 1.2.4.1 Crystal structure and active site

As far as we can ascertain the crystal structure of MAO-N wild type (wt) has never been determined. Yet, Atkin *et al.* reported and analysed the structure of MAO-N D5, with five amino acid substitutions, back in 2008 (**Figure 13**). It is reported that its asymmetric unit is constituted by eight monomers each containing 17  $\alpha$ -helices and 21  $\beta$ -sheets. Moreover, this enzyme shows a similar structure to human MAO near the FAD molecule, both showing a  $\sim 30^\circ$  angle in the isoalloxazine ring. MAO-N D5 also lacks a protruding helix present in MAO A and B, thought responsible for membrane binding.<sup>100</sup>

The active site of MAO-N is formed by a single large hydrophobic cavity, on the *re* face of FAD's ring system, and an "aromatic cage", containing the co-factor and formed by the flavin and W430 and F466 amino acid residues. In fact, it is suggested these amino acids are essential to the enzyme's activity, playing significant steric and electronic functions. The hydrophobic pocket extends to the protein surface, and three hydrophobic residues, M242, M246 and Y238, are proposed as a "gate" for substrate entrance into the active site. It is suggested that the hydrophobic character of this entrance channel can be determinant in MAO-N's selectivity towards small cyclic non-polar substrates.

Furthermore, it is noted that the amino acid residues mutated in all directed evolution experiments directly interfere with the active site, and Atkin *et al.* note that two of the most significant mutations alter the aromatic cage and the substrate binding site, possibly improving the electronic distribution and releasing steric constraints, respectively.<sup>100</sup>

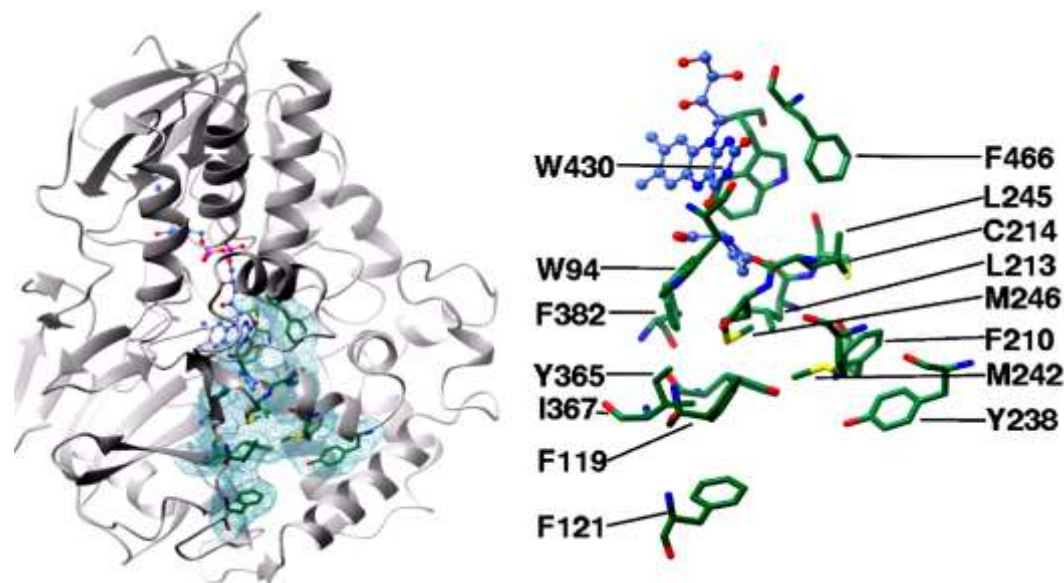
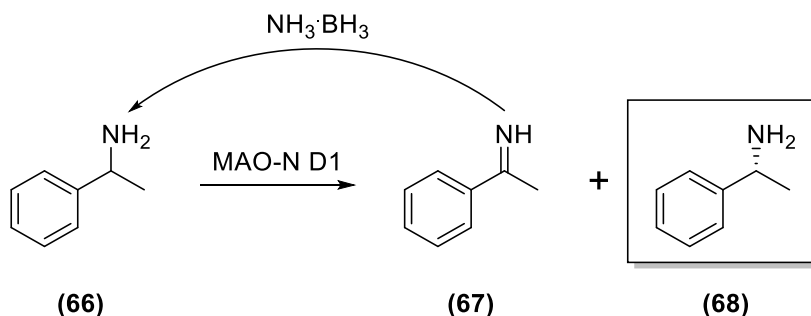


**Figure 13.** Proposed hydrophobic cavity in MAO-N D5. Right: residues forming the hydrophobic cavity in green and the FAD co-factor in blue. Adapted from Atkin *et al.*<sup>100</sup>

#### 1.2.4.2 State of art: increasing the substrate scope of MAO-N by directed evolution

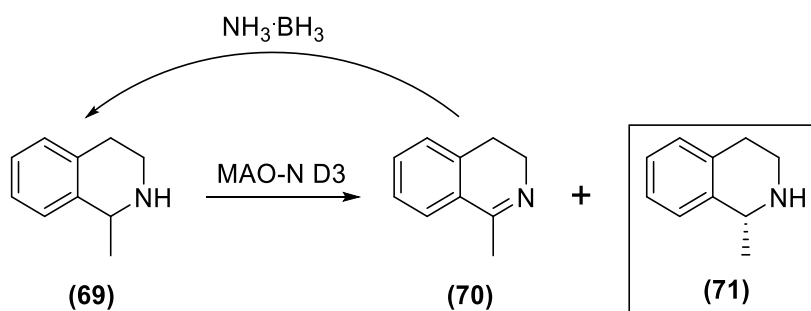
Research in the use of MAO-N for biocatalysis started with substrate scope studies by Sablin *et al.*<sup>101</sup>, who limited the activity of this enzyme to a few simple primary amines. Since then, a remarkable work by the Turner group at the Manchester Institute of Biotechnology (MIB) has increased its utility by consecutive rounds of directed evolution and established efficient oxidation and deracemisation procedures.

The first reported evolutionary studies on MAO-N date back to 2002, when Alexeeva *et al* used random mutagenesis and a solid phase colorimetric assay to discover a single MAO-N D1 mutant - N336S - with increased activity towards  $\alpha$ -methylbenzylamine (AMBA) (**66**). In the same article, a DKR experiment with a reducing agent, ammonia-borane complex, was first reported for the synthesis of (*R*)-AMBA (**68**) with 77% yield and 93% e.e. (**Scheme 14**).<sup>102</sup> Soon after, the substrate scope of this mutant was determined, showing high activity toward a broader range of primary amines, preferably flanked by a small alkyl group and a bulky aryl group. Significant activity of any MAO-N variant towards 1-methyltetrahydroisoquinoline (1-MTQ), a secondary amine, is first stated in this article.<sup>103</sup>



**Scheme 14.** Dynamic kinetic resolution of AMBA

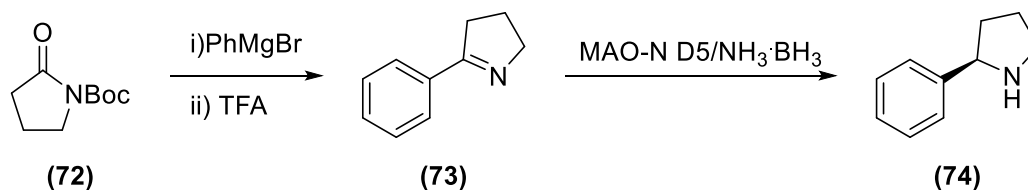
Additional random mutagenesis was performed on MAO-N D1 by Carr *et al.* in order to increase MAO-N's activity towards secondary amines. A double mutant - M248K/I246M - was found with high activity towards secondary amines and named MAO-N D3. This mutant presented a 5-fold increase in activity for 1-MTQ (**69**) relative to MAO-N D1. A small-scale deracemisation reaction was performed with this substrate to afford (*R*)-1-MTQ (**71**) with 71% yield and 99% e.e. over 48 hours (**Scheme 15**). Moreover, immobilization of the enzyme in Eupergit C resin increased the yield to 95% while maintaining the e.e., but required 98 hours for completion.<sup>104</sup>



**Scheme 15.** DKR in the deracemisation of 1-MTQ.

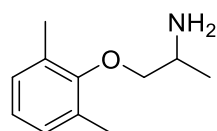
Dunsmore *et al.* continued the previous work by screening a recently found MAO-N D5 mutant – I246M/N336S/M348K/T384N/D385S – with a number of secondary and tertiary amines, reporting remarkable activity with N-methylated substrates. This new mutant was used in a chemoenzymatic reaction for the synthesis of chiral secondary amines (**74**) from prochiral aminoketone compounds (**72**) (**Scheme 16**).<sup>105</sup>

Also, an article by Foulkes *et al.* reports the use of MAO-N D5 with nanoscale bioreduced Pd(0) particles/H<sub>2</sub> for the deracemisation of 1-MTQ with 96% yield. However, it is stated that separate reactions are required for the oxidation and reduction steps, complicating the overall procedure.<sup>106</sup>



**Scheme 16.** Chemoenzymatic route for the synthesis of (*R*)-2-phenylpyrrolidine

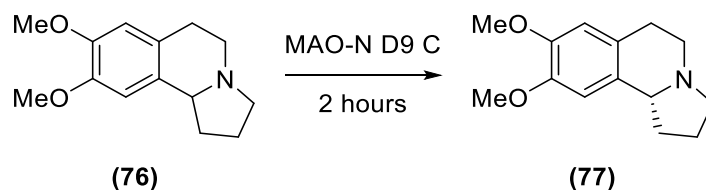
Surprisingly, an article outside Turner's group was found regarding the directed evolution of MAO-N D5 for the deracemisation of mexiletine (**75**) (**Figure 14**). By SDM based on the results from docking studies, and posterior screening assays, Chen *et al.* reported three new mutants based on MAO-N D5 – F210V/L213C, F210V/I367T and F210V/L213C/I367T – with enhanced activity towards this substrate. According to their studies, the F210V mutation can widen both the binding cavity and entrance channel, and L213C and F210V mutations combined can cause the formation of a new disulphide bond that enlarges the binding pocket by disulphide bond stretching.<sup>107</sup>



**(75)** (*rac*)-Mexiletine

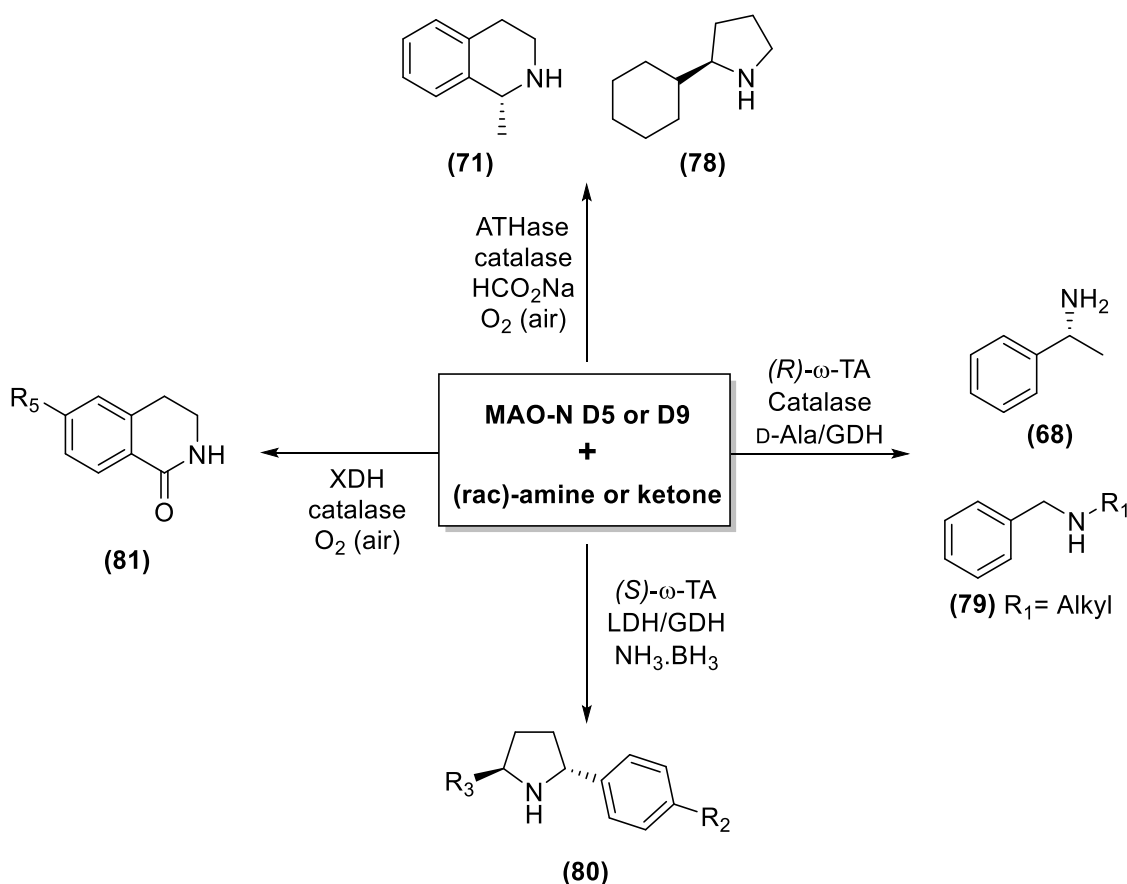
**Figure 14.** Structure of mexiletine

Meanwhile, Rowles *et al.* further improved MAO-N activity for the deracemisation of crispine A.<sup>108</sup> Four target residues from the entrance channel were identified by molecular modelling for their steric interaction with this substrate, and the parent enzyme subjected to two rounds of saturated double mutagenesis and solid-phase screening. A new mutant, MAO-N D9 C, was found with a 990-fold increase activity towards crispine A (**76**). The additional mutations – F210L/L213T/M242Q/M246T – widened the entrance channel by changing the orientation of the side-chains in these residues. Lastly, the deracemisation of crispine A with MAO-N D9 C is reported with >99% e.e. within 2 hours (**Scheme 17**).



**Scheme 17.** Deracemisation of crispine A with MAO-N D9 C

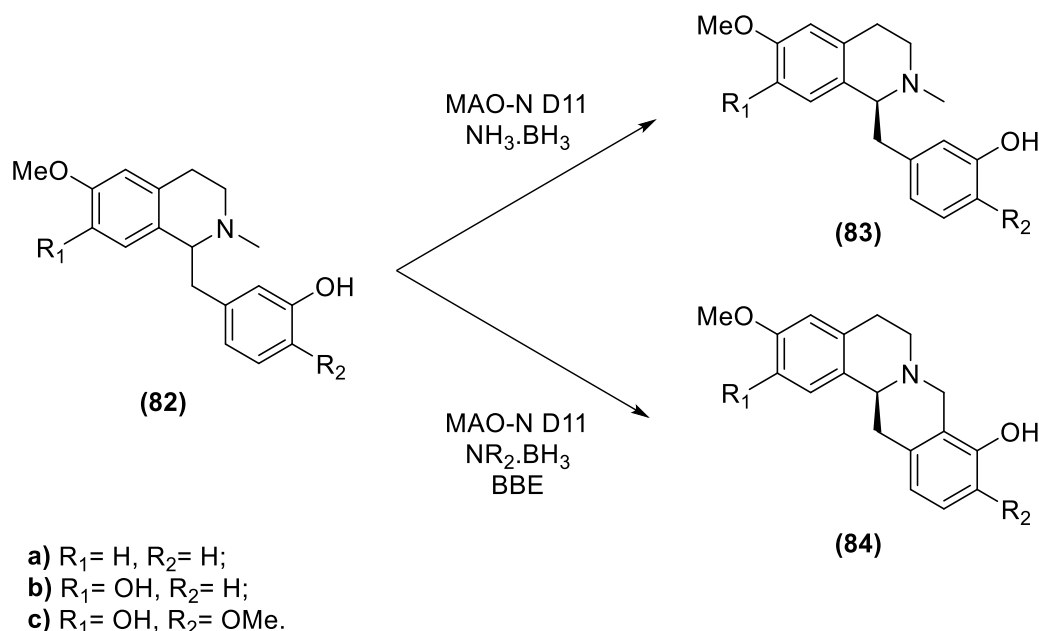
Four enzymatic cascade reactions have been reported for the synthesis of highly enantiopure primary and secondary amines with great yield, by the use of additional enzymes ( $\omega$ -TA, xanthine dehydrogenase (XDH) or IRED) or an artificial transfer-hydrogenase (ATHase). A brief summary of these reactions can be seen in **Scheme 18**.<sup>80,109–111</sup>



**Scheme 18.** Enzymatic synthesis of enantiopure chiral amines with MAO-N D5 or D9 variants

The last reported MAO-N mutant within the literature is MAO-N D11, surprisingly obtained by a simple change in an already mutated residue in MAO-N D9 – W430H to W430G.<sup>112</sup> It proved effective for the deracemisation of bulky amines such as 1-phenyltetrahydroisoquinoline. This new mutant has been recently explored for the

deracemisation of 1-benzyl-*N*-methyltetrahydroisoquinoline derivatives (**83**), with excellent e.e. and good yields, and the synthesis of protoberberines (**84**) by a MAO-N D11/Berberine bridge enzyme (BBE)/NH<sub>3</sub>·BH<sub>3</sub> redox cascade, with excellent e.e. and yields (**Scheme 19**).<sup>113,114</sup>



**Scheme 19.** MAO-N D11 catalysed synthesis of enantiopure 1-benzyltetrahydroisoquinoline derivatives.

A recent unpublished work by Jane Kwok *et al.* at the Manchester Institute of Biotechnology reports a rational non-randomized method for the directed evolution of MAO-N starting from MAO-N D5.<sup>115</sup> With it, they expect to achieve a more efficient search of the enzyme's functional space in the future. This work in progress involves the creation of double mutant libraries in every segment of MAO-N's secondary structure and use a solid-phase screening assay to determine the mutants responsible for an increased activity with  $\alpha$ -AMBA. The researcher also states that the gene can be divided into three main regions: high variations, amino acid residues where mutations do not affect the enzyme's activity; high conservations, where any mutation reduces or completely eliminates enzyme activity; and strong selections, where a tendency is found towards specific mutations when sequencing the mutants with increased activity. These last areas have enormous potential in engineering and, so far, nine residues have been identified that show strong selection – C50T, S81T, S81C, Y86T, F128L, S205T/S206N, A266V, A289V and I356V. Although most of these residues are thought to



alter the entrance channel or the position of the FAD tricyclic ring, some are distal to the active site and therefore may present an oligomer formation or solubilisation role. An image of the MAO-N D5 gene divided by these regions can be seen in **Figure 15**.

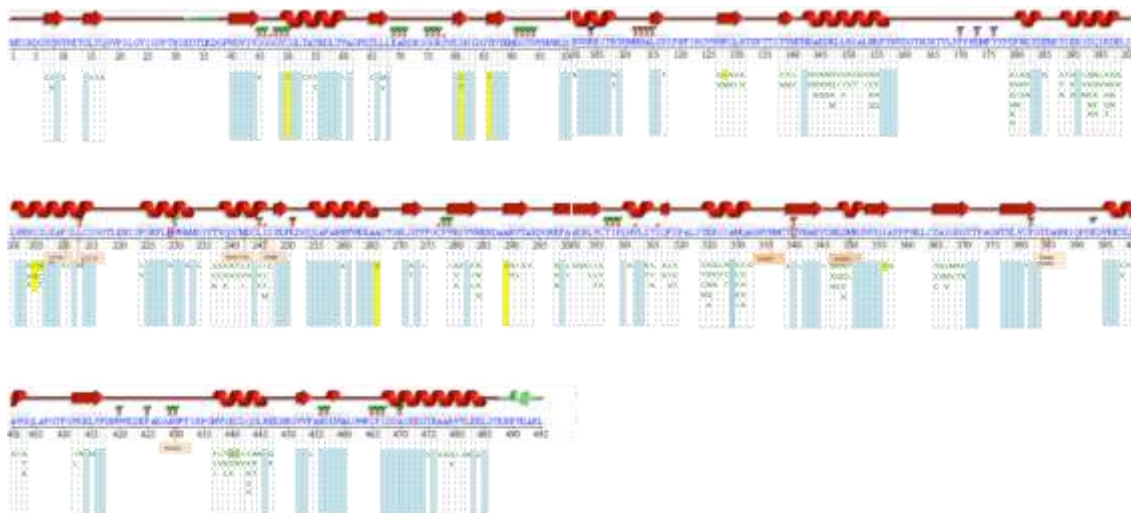


**Figure 15.** Summary of the solid phase screening of MAO-N mutants, with the MAO-N gene marked with the previously mentioned areas: high variations, in blue, high conservations, in white with green letters marking the majority residue, and strong selections, in yellow.<sup>115</sup>



### 1.3 SCOPE OF THIS WORK

Biocatalysis represents one of the most promising routes towards a sustainable future in the industrial production of fine chemicals. Particularly, monoamine oxidase from *Aspergillus niger* has been consistently engineered for the oxidation and deracemisation of chiral amines. Nevertheless, a limited substrate scope is still reported, and further evolution of this enzyme is still undergoing. As so, and given the opportunity presented by working with the Turner group, highly experienced in MAO-N expression and evolution, in this work we aimed to further develop this high potential oxidase, and explore its potential use in cascade reactions.

To accomplish these goals, we:

- i) Established a target scaffold, THIQ, and devised a library of compounds capable of fully assessing MAO-N's substrate scope. The library used contained THIQs with a methyl substituent in all the positions of the bicyclic ring as well as 6,7-dimethoxytetrahydroisoquinoline (DMTHIQ) and 6,7-dimethoxy-1-methyltetrahydroisoquinoline (1-M-DMTHIQ), as seen in **Figure 16**;

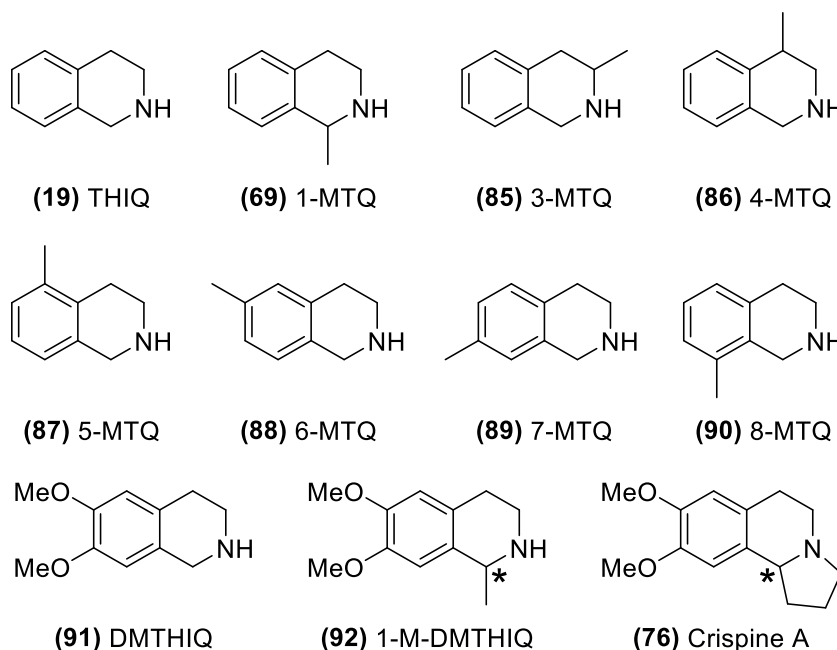


**Figure 16.** Tetrahydroisoquinoline substrates used within the scope of this work.

- ii) Expressed MAO-N D5, D9 and D11 in *E. coli* and purified sufficient enzyme for the specific activity assays. Expression of MAO-N D9 in *P. pastoris* was also attempted;

- iii) Perfected a colorimetric screening assay and used it to assess the activities of 11 MAO-N variants (**Table 1**) – MAO-N D5, D9, D11 and eight promising variants from the previously mentioned Jane Kwok *et al.* work<sup>115</sup>, from now on defined as MAO-N D12 (A-H) variants – with all the substrates previously mentioned;

**Table 1.** MAO-N variants used in the specific activity assays. The mutations I246M/N336S/M348K/T384N/D385S are present in all the variants below.

MAO-N variant	C50	S81	F128	S205/S206	F210	L213	M242	I246	A266	A289	I356	W430
<b>D5</b>	-	-	-	-	-	-	-	-	-	-	-	-
<b>D9</b>	-	-	-	-	L	T	Q	T	-	-	-	H
<b>D11</b>	-	-	-	-	L	T	Q	T	-	-	-	G
<b>D12 (A)</b>	-	-	-	-	-	-	-	-	V	-	-	-
<b>D12 (B)</b>	T	-	-	-	-	-	-	-	-	-	-	-
<b>D12 (C)</b>	-	-	L	-	-	-	-	-	-	-	-	-
<b>D12 (D)</b>	-	-	-	-	-	-	-	-	-	-	V	-
<b>D12 (E)</b>	-	C	-	-	-	-	-	-	-	-	-	-
<b>D12 (F)</b>	-	T	-	-	-	-	-	-	-	-	-	-
<b>D12 (G)</b>	-	-	-	T/N	-	-	-	-	-	-	-	-
<b>D12 (H)</b>	-	-	-	-	-	-	-	-	-	V	-	-

- iv) Used the data obtained from the previous experiments to develop a new MAO-N D13 mutant, based on MAO-N D9, and tested its ability to oxidize and deracemize 1-M-DMTHIQ;
- v) Used MAO-N D5, D9, D11 and HDNO E350L/E352D - developed by Heath *et al.*<sup>94</sup> and from now on simply designated as “HDNO” - in the deracemisation of the chiral substrates aforementioned;
- vi) Presented the proof of concept for a novel one-pot three step synthesis of unnatural tetrahydroisoquinoline amino acids by the oxidation, cyanation and selective hydrolysis of their C1 unsubstituted counterparts

# CHAPTER 2. EXPERIMENTAL SECTION



## GENERAL INFORMATION

MAO-N D5, D9 and D11 genes in pET16b plasmids were obtained from the plasmid library of the *Manchester Institute of Biotechnology*. Empty pPicZ $\alpha$  C vectors from Invitrogen™ were used for protein expression in *P. pastoris*. Competent *E. coli* cells - BL21(DE3), NEB® 5-alpha and Rosetta™ - were purchased from New England Biolabs® Inc.. Moreover, competent *P. pastoris* GS115 and X-33 cells from Invitrogen™ had been previously grown in the MIB and stored at -80°C for use in this project.

Substrates used in the specific activity assays and biotransformations were either commercially available by Sigma Aldrich and Flurochem or supplied by Orion Pharma, UK. The solvents used were high-performance liquid chromatography (HPLC) grade or analytical grade.

<sup>1</sup>H and <sup>13</sup>C NMR spectra were recorder on a Bruker Avance 400 (400.1 MHz for <sup>1</sup>H and 100.6MHz for <sup>13</sup>C) without additional internal standard. Chemical shifts are reported in  $\delta$  (ppm) and multiplicities defined as follows: s – singlet; d – doublet; t – triplet; m – multiplet. HPLC measurements were performed on Agilent machines equipped with diode arrays and 1100 or 1200 series modules. Columns and conditions used in this work are indicated separately for each run.

## 2.1 PLASMID SELECTION

### 2.1.1 pET16b (*E. coli*)

A 5711 base pair (bp) long pET16b vector was used in the expression of MAO-N variants (**Figure 17**). Apart from the origin of replication (ori), this plasmid first presents a gene encoding resistance to the antibiotic ampicillin (**F**), allowing for the selection of successful transformants in a medium with this particular antibiotic. Then, a *lacI* gene and a *lac operon* (**C**) are present and lead to a regulation of protein expression by lactose. *LacI* encodes for the expression of the lac repressor protein, which binds to the lac operon and stops the transcription of the gene of interest. The presence of either lactose or isopropyl  $\beta$ -D-1-thiogalactopyranoside (IPTG) induces protein expression by interacting with the *lac* repressor and preventing its binding to the operon.

Both the lac operon and the gene of interest are inserted between the T7 promoter (**B**) and T7 terminator (**E**), responsible for its the transcription by the T7 RNA polymerase present in the *E. coli* strains used. Although not naturally present in *E. coli*, this polymerase has been engineered into the bacteria as it synthesizes RNA at a much faster rate than the native polymerase. Finally, a chain of 10 histidine codons (**D**) is included and transcribed with MAO-N. In this manner, the histidines are translated in the end of the wanted protein and its strong coordination with  $\text{Ni}^{+2}$  can be used for a quick purification procedure.<sup>116</sup>

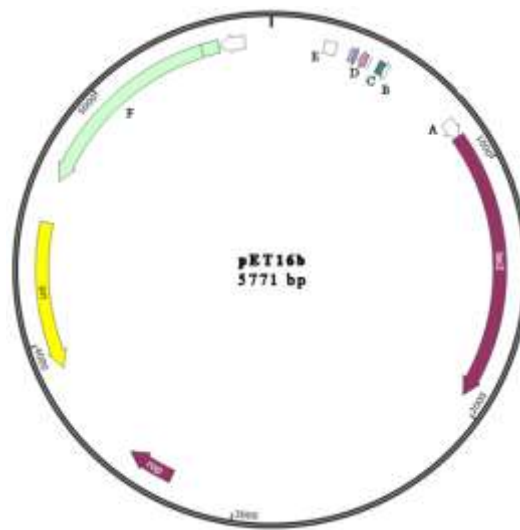


**Figure 17.** Scheme of an empty pET16b plasmid. (**A**) Lac promoter; (**B**) T7 promoter; (**C**) Lac operon; (**D**) 10x Histidine Tag; (**E**) T7 terminator; (**F**) Ampicillin resistance marker.

### 2.1.2 pPicZ $\alpha$ C (*P. pastoris*)

In this work a 3.6 kilobases (kb) pPicZ- $\alpha$  C vector was used for the insertion of MAO-N D9 gene into the genome of *P. pastoris* (**Figure 18**). An increased transformation and expression complexity is found in this organism as the procedure involves the incorporation of the target gene into the organism's genome. As so, some additional features are required in the plasmid.<sup>62</sup>

First, an alcohol oxidase 1 (AOX1) promoter and terminator are used, allowing for a methanol induced protein expression. Then, the presence of a  $\alpha$ -factor, expressed with the desired gene, causes the segregation of MAO-N D9 to the extracellular medium. Moreover, a 6x Histidine Tag is used to facilitate protein purification. Finally, an antibiotic (Zeocin<sup>TM</sup>) resistance marker is introduced to allow the selection of successful transformants.<sup>62</sup>



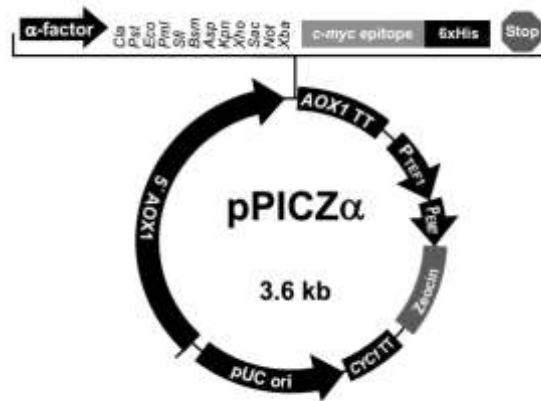


**Figure 18.** Scheme of an empty pPicZα C plasmid. Adapted from Lezdey et al..<sup>117</sup>

## 2.2 TRANSFORMATION PROTOCOLS

### 2.2.1 *E. coli* BL21 (DE3)

Available plasmid DNA of D5, D9 and D11 mutants of MAO-N in a pET16b vector were transformed into chemically competent *E. coli* BL21(DE3) cells by heat shock. Approximately 50 ng of circular plasmid DNA were added to 50  $\mu$ L of cells, followed by thawing on ice for 30 minutes. The cells were heat shocked for 40 seconds at 42°C and left on ice for 2 minutes to reduce cell damage. Next, 300  $\mu$ L of super optimal broth with catabolite repression (SOC) media was added and the mixture was left incubating for one hour at 37°C. The resulting culture was spread on lysogeny broth (LB) plates with ampicillin (100 mg/L) and left to grow overnight at 37°C.

### 2.2.2 *E. coli* NEB<sup>®</sup> 5-alpha

A similar procedure was used to transform MAO-N D9 plasmid DNA into a Bio-Rad NEB<sup>®</sup> 5-alpha cloning strain. Low salt LB plates with Zeocin<sup>™</sup> were required for a correct antibiotic selection when transforming MAO-N in a pPicZα C vector.

### 2.2.3 *E. coli* Rosetta<sup>™</sup> (DE3)

The transformation was carried out using the procedure previously described in point 2.2.1.

#### 2.2.4 *P. pastoris* GS115

Transformation of the MAO-N D9 gene into *Pichia pastoris* GS115 cells was achieved by electroporation of the pPicZα C plasmid containing the gene of interest. First, circular plasmid DNA was linearized with a restriction enzyme digestion. 2 μL of a suitable restriction enzyme – PmeI, New England Biolabs® Inc. - was added to approximately 20 μg of plasmid DNA in 30 μL of water. After overnight incubation at 37°C, linearized plasmid DNA was purified using a QIAquick PCR Purification Kit.

*P. pastoris* GS115 cells were grown on a LB plate for 96 hours at 30°C. A single colony was used to incubate 5 mL of YPD (yeast extract peptone dextrose) media in a 50 mL falcon tube and grown overnight at 30°C. Then, 500 mL of fresh medium in a 2 litre Erlenmeyer were inoculated with 0.1 mL or 0.2 mL of the overnight culture and left growing at 30°C until an OD600 between 1.3 and 1.5 is reached (approximately 16 hours). The incubation of two separate media with different amounts of cells allowed us to choose the one closer to the desired optical density (OD) for transformation. This value is extremely important as a higher cell density, passing the log phase, can lead to a reduction in cell viability after electroporation.

Cells were then centrifuged at 1500 g and 4°C for 10 min. The cell pellet was collected and resuspended in 500 mL of ice-cold, sterile water and centrifuged again under the same conditions. This step was repeated one more time with 250 mL of water.

Next, cells were resuspended in 20 mL of ice-cold, sterile 1 M sorbitol, transferred to a 50 mL falcon tube and centrifuged again. Finally, the cells were resuspended in 1 mL of 1 M sorbitol to a final volume close to 1.5 mL and kept on ice to be used within the hour.

For the electroporation step, 80 μL of cells were mixed with 5-10 μg of linearized DNA in an ice-cold 0.2 cm electroporation cuvette. After 5 min incubation on ice, the cells were pulsed at 2,500V for 5 ms using a Gene Pulser MXcell™ Electroporation System, Bio-Rad Laboratories. Ice-cold 1 M sorbitol (1 mL) was immediately added and cells left to regenerate for one hour at 30°C without shaking. The mixture was then centrifuged and cells resuspended in 300 μL of sorbitol. 100 μL were spread on YPD plates containing 100, 500 and 1000 mg/L of Zeocin™. Higher antibiotic concentration allowed for a better selection of multi-copy recombinants. The plates were incubated, protected from light, at 30°C for 5

days. Successful insertion was verified by Touchdown PCR using insert primers from the ligation independent cloning followed by agarose gel electrophoresis.

### 2.2.5 *P. pastoris* X-33

A similar procedure to the one used on 2.2.4 was applied to this transformation.

## 2.3 GROWTH OF MAO-N IN *E. coli*

A single colony was used to inoculate a 5 mL pre-culture of LB media with ampicillin (100 mg/L), which was grown at 37°C overnight. 2 L Erlenmeyer flasks containing 500 mL of Terrific Broth (TB) medium with ampicillin (100 mg/L) were inoculated with 2 mL of pre-culture and incubated for 48 hours at 25°C. Additional experiments with different incubation parameters were performed for MAO-N D9 and can be found in **Table 2**.

One additional experiment was attempted using IPTG induction. To a 2 L Erlenmeyer flask containing 500 mL of TB medium with ampicillin (100 mg/L) was added 2 mL of pre-culture and incubated until an OD of 0.6-0.8 was reached. 1 M IPTG was added to a final concentration of 0.2 mM and the culture incubated at 20°C overnight.

After incubation, the cells were collected by centrifugation at 4000 rpm and 4°C for 30 minutes, followed by resuspension in 15 mL of phosphate buffer (pH 8.0, 100 mM) and further centrifugation. The cell pellet was collected and collected and stored at -20°C. In standard conditions, approximately 10 g of cell paste were obtained per incubation.

**Table 2.** Experiment parameters for MAO-N D9 expression in *E. coli*

Experiment	<i>E. coli</i> strain	Medium	Time (h)	Temperature (°C)
1	BL21(DE3)	TB	48	37
2	BL21(DE3)	TB	24	37
3	BL21(DE3)	TB	72	25
4	BL21(DE3)	TB	24	30
5	BL21(DE3)	TB	48	30
6	BL21(DE3)	LB	48	30
7	NEB <sup>®</sup> 5-alpha	TB	48	30
8	Rosetta <sup>™</sup>	TB	48	30

## **2.4 PURIFICATION OF MAO-N**

One gram of cell paste was resuspended in 10 mL of buffer A (100 mM KPi, pH 7.7, 5 mM imidazole) and cooled to 4°C. Cell lysis was achieved through ultrasonication (20 s on, 20 s off, 20 cycles). After centrifugation (20000 rpm, 4°C, 30 min) the supernatant was loaded on a column with approximately 1 mL of Ni-NTA Agarose from QIAGEN. The column was closed and mixed for 1 hour. After eluting and collecting the flow-through, 10 mL of buffer B (100 mM KPi, pH 7.7, 30 mM imidazole) was added to remove unbound protein and collected as the wash-through. Finally, the protein was eluted with 10 mL of buffer C (100 mM KPi, pH 7.7, 250 mM imidazole) and collected in 1 mL fractions.

All fractions were analysed by SDS-PAGE to ensure a correct purification. MAO-N containing fractions were pooled and concentrated using a Sartorius Vivaspin 20 spin column (30 kDa cut-off) with centrifugation at 4000 rpm for 20 minute cycles until a final volume near 2.5 mL was reached. The solution was then desalted using a PD-10 Sephadex column (GE Healthcare) to a final volume of 3.5 mL in phosphate buffer.

## **2.5 SDS-PAGE**

Polyacrylamide gel electrophoresis (PAGE) is a technique used to separate macromolecules, for identification and quantification purposes, by its mobility in a polyacrylamide gel when subjected to an electric current. With proteins, sodium dodecyl sulphate (SDS) is commonly used to cause complete denaturation and simultaneously induce a negative charge to the protein, allowing a separation based mainly on size.

In this work 20 µL of 2x Laemli Buffer (MicroMol) were added to 20 µL of protein sample. Proteins were denatured in a heat block at 104°C for 10 min and 20 µL of the resulting solution was applied to each well of the gel. A 10 to 180 kDa PageRuler™ Prestained Protein Ladder was added to the first well to confirm the expected weight of the protein and the gel run for 30 min at 230 V.

## **2.6 PROTEIN QUANTIFICATION: BRADFORD PROTEIN ASSAY**

Purified protein was quantified using a Bradford protein assay. This assay is based in the binding of a dye (Coomassie Brilliant Blue G-250) to the protein, generating a shift in the absorption spectrum to a maximum of 595 nm. As so, it is possible to estimate the protein

concentration on a given sample by comparison of the absorption at 595 nm with one of a standard protein with a known concentration – in this case bovine serum albumin (BSA). The calibration curve used is presented in **Equation 1** and the corresponding graph can be seen in **Figure A1.1**.

$$y = 0.6543x + 0.3441 \quad (R^2 = 0.994)$$

**Equation 1.** Calibration curve for protein concentration in the Bradford protein assay

In this assay, 200  $\mu\text{L}$  of 1X Bradford reagent (Bio Rad) was added to 10  $\mu\text{L}$  of either BSA or sample in a 96 well plate. After incubating at room temperature for at least 10 minutes, the absorbance at 595 nm was measured with a Tecan Infinite<sup>®</sup> M200 microplate reader.

## 2.7 SPECIFIC ACTIVITY ASSAYS

In a 96 well plate, 50  $\mu\text{L}$  of horseradish peroxidase (HRP) (0.20 mg/mL in phosphate buffer), 50  $\mu\text{L}$  of a 10 mM solution of substrate in phosphate buffer (pH=8.0) and 50  $\mu\text{L}$  of solution A were added to each well. 50  $\mu\text{L}$  of a 0.10 or 0.05 mg/mL enzyme solution was quickly added and the absorbance at 510 nm was monitored at 30°C for the next 20 min using a Tecan Infinite<sup>®</sup> M200 microplate reader. Two replicas of each assay were made and the average value and standard deviation used in further calculations.

Solution A: Previously mixed solution of 37.5  $\mu\text{L}$  of 4-aminoantipirine (4-AAP) (50 mg/mL of water) and 150  $\mu\text{L}$  of 2,4,6-tribromo-3-hydroxybenzoic acid (TBHBA) (75 mg/mL of DMSO), diluted to 1,500 mL with phosphate buffer.

## 2.8 DNA PROTOCOLS

### 2.8.1 Preparation of plasmid DNA from *E. coli*

A single colony was used to inoculate a 5 mL LB culture with the appropriate antibiotic. The culture was incubated overnight at 37°C and plasmid DNA was isolated using the QIAprep Spin Miniprep Kit, QIAGEN. In order to increase final plasmid concentration, 35  $\mu\text{L}$  of nuclease-free warm water were used to elute the DNA.

### **2.8.2 Determination of DNA concentration**

DNA concentration was calculated using a NanoDrop ND-1000 spectrophotometer. The purity of the sample was assessed by the difference between in the absorbance spectrum of DNA – maximum at 260 nm - and proteins – maximum at 280 nm. A ratio of A<sub>260</sub>/A<sub>280</sub> between 1.8 and 2.1 was usually obtained and falls into standard values for pure DNA samples.

### **2.8.3 Agarose gel electrophoresis**

An agarose gel consists in a matrix of polymeric oligosaccharides with pores that allow the passage of biomolecules. An electric current is applied that induces a migration of DNA towards the anode through the pores of the gel, generating a separation by molecular weight.

In this experiment, a 1% agarose gel (0.5 g of agarose dissolved in 50 mL of TAE (tris-acetate-EDTA) buffer) was prepared and allowed to solidify in the cast. Next, 5 µL of reaction mixture – typically the direct result of a PCR experiment – were mixed with 1 µL of 6x DNA Loading Dye and transferred to the agarose wells along with a 1 kb Prestained DNA Ladder. The gel was then run in TAE buffer at 100 V for 30 min and the results visualized under ultraviolet light.

### **2.8.4 Ligation independent cloning: insertion of MAO-N D9 gene into pPicZα C empty vector**

Ligation independent cloning is a technique developed as an alternative to restriction enzyme/ligation cloning. It discards the need for a time consuming ligation step by amplifying both the insert and the empty plasmid with overhangs, that is, sequences of DNA non-complementary to the DNA being amplified. These overhangs are, however, complementary to each other, as described in **Figure 19**, and ligate once the results of both amplifications are combined. When all four overhangs are joined together, the desired circular plasmid with the gene of interest is obtained.

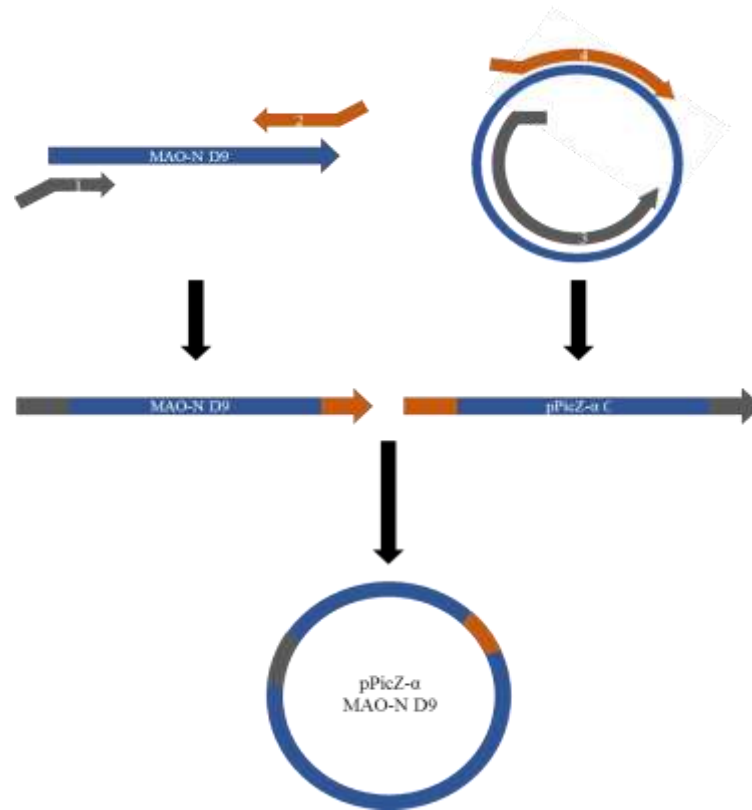


**Figure 19.** Ligation independent cloning for the insertion of MAO-N D9 gene into a pPicZ $\alpha$  C empty vector

Primers for both the insert and the empty vector are presented in **Table 3**. Amplification of both DNA sequences was done by Phusion<sup>®</sup> PCR, according to **Tables 4** and **5**, and purified with a QIAGEN PCR purification kit. Successful amplification was verified by agarose gel electrophoresis and the linearized DNA was stored at -20°C for further use.

**Table 3.** List of the primers used in the ligation independent cloning.

Primer name	Sequence
Forward Insert	TCTCGAGAAAAGAGAGGCTGAAGCTATGACCTCCCGTGACGGTTACCACT
Reverse Insert	AATGATGATGATGATGATGGTCGACCAAACGAGCCTTCACCTCCCTCTTC
Forward Vector	GAAGAGGGAGGTGAAGGCTCGTTTGGTCGACCATCATCATCATCATCATT
Reverse Vector	ACTGGTAACCGTCACGGGAGGTCATAGCTTCAGCCTCTCTTTTCTCGAGA

**Table 4.** Phusion<sup>®</sup> PCR mix

Component	HF buffer PCR
H <sub>2</sub> O	36.5 µL
5 x Phusion HF buffer	10 µL
10 mM dNTPs	1 µL
Primer mixture 10 mM	1 µL
MAO-N D9 / pPicZα C plasmids	1 µL
Phusion DNA polymerase	0.5 µL

**Table 5.** Phusion<sup>®</sup> PCR cycle program. A) MAO-N D9; B) pPicZα C.

Cycle step	Temperature	Time	Cycles
<b>Initial denaturation</b>	98°C	30 s	1
<b>Denaturation</b>	98°C	30 s	30 cycles
<b>Annealing</b>	58°C	30 s	
<b>Extension</b>	72°C	30s (A)/ 2 minutes (B)	
<b>Final extension</b>	72°C	5 minutes	1

Both insert and vector DNA with overhangs were later mixed and incubated at room temperature until only circular plasmid was found on the agarose gel electrophoresis. The resulting plasmid was directly transformed in *E. coli* NEB<sup>®</sup> 5-alpha and an overnight culture (250 rpm, 37 °C) was spread on a low salt LB/Zeocin<sup>™</sup> plate and incubated at 37 °C.

Several colonies were chosen and used in an overnight culture at 37 °C and 250 rpm. Plasmid DNA was purified and stored for future use in linearization/electroporation.

### 2.8.5 Site-directed mutagenesis

A site-directed mutagenesis experiment was performed for the mutation of the S205 and S206 amino acids of MAO-N D9. A set of primers was designed in such a way so the mutated region rested in the middle of the forward primer. This primer possessed two non-complementary bases in its sequence that, despite not pairing with the DNA, are transcribed and alter the enzyme's protein sequence.

The following 25 base-long mutagenic primers (**Table 6**) were ordered through Eurofins Scientific<sup>®</sup> and dissolved to a concentration of 100 µmol/mL in nuclease-free water.



**Table 6.** List of mutagenic primers used in the double mutation (mutagenic base pairs in bold).

Primer name	Sequence
Forward primer	CTTAATGAACGGACTA <b>AT</b> CTGGAAGCGTTGATATTGACC
Reverse primer	GCTCAACTCATCCCGGATTTGATCAATCCG

Mutant strand synthesis (PCR) was prepared in 0.2 mL PCR tubes with the reagents presented in **Table 7**. Both High-Fidelity and GC buffers were used to ensure a good amplification. The cycle program used follows in **Table 8**.

**Table 7.** Site-directed mutagenesis PCR reaction mix

Component	HF buffer PCR	GC buffer PCR
H <sub>2</sub> O	36.5 µL	35 µL
5 x Phusion HF buffer	10 µL	-
5 x Phusion GC buffer	-	10 µL
10 mM dNTPs	1 µL	1 µL
Primer mixture 10 mM	1 µL	1 µL
Dimethyl sulfoxide	-	1.5 µL
MAO-N D9 plasmid DNA	1 µL	1 µL
Phusion DNA polymerase	0.5 µL	0.5 µL

**Table 8.** Site-directed mutagenesis PCR cycle program

Cycle step	Temperature	Time	Cycles
<b>Initial denaturation</b>	98 °C	30 s	1
<b>Denaturation</b>	98 °C	30 s	30 cycles
<b>Annealing</b>	58 °C	30 s	
<b>Extension</b>	72 °C	2 minutes	
<b>Final extension</b>	72 °C	5 minutes	1

Success in the amplification was verified by agarose gel electrophoresis. Resulting DNA was purified with a Qiagen PCR purification kit and transformed in *E. coli* cloning strain (NEB<sup>®</sup> 5-alpha) according to the protocol above.

After selective cell growth in LB plates with ampicillin, four random colonies were selected and used to incubate a 5 mL LB/Ampicillin medium which was grown overnight at 250 rpm and 37 °C. Plasmid DNA was purified, concentrated and sent to sequencing to confirm a successful mutation. Finally, the mutated plasmid DNA was transformed in *E. coli* BL21(DE3) and cells grown according to the protocol above.

## 2.9 BIOTRANSFORMATIONS

### 2.9.1 Amine deracemisations with MAO-N D5/D9/D11 or HDNO

To a 15 mL falcon tube with 5 mL of a 10 mM solution of substrate in phosphate buffer (pH 8.0), 0.5 grams of cell pellet were added. When required, the substrate was previously dissolved in 50  $\mu$ L of DMSO. Five equivalents of ammonia-borane complex ( $\text{BH}_3\text{NH}_3$ ) were also introduced and pH adjusted to 8 by addition of 1M HCl.

The reaction mixture was incubated at 250 rpm and 37 °C and the e.e. monitored by HPLC, working up small samples at appropriate time intervals. To a 250  $\mu$ L aliquot of reaction mixture 40  $\mu$ L of 5M NaOH and 250  $\mu$ L of TBME were added. The solution was vigorously mixed and centrifuged at 13000 rpm for 1 min. The organic phase was separated, dried with anhydrous sodium sulphate and run on a normal-phase HPLC. Conversion was verified by normal-phase HPLC, by comparison with standards. When not commercially available, imine compounds were synthesized by large scale biotransformations and conversion determined by  $^1\text{H}$  NMR. These were directly used as standards for HPLC.

### 2.9.2 MAO-N D9/D11 or HDNO imine formation reactions

A similar procedure to the above mentioned was used for these biotransformations. 0.1 grams of cell pellet were added to 1 mL of a 10 mM solution of substrate in phosphate buffer. The reactions were incubated at 250 rpm and 37 °C and monitored by HPLC as previously described. When not commercially available, imine compounds were synthesized by large scale biotransformations and conversion determined by  $^1\text{H}$  NMR. These were directly used as standards for HPLC.

Large scale biotransformations were done in a 5 mL scale and extracted after 48 hours with 3 x 5 mL of ethyl ether. The organic phase was dried and concentrated, and the product was analysed by  $^1\text{H}$  and  $^{13}\text{C}$  NMR.

### 2.9.3 HPLC analysis: determination of the relative response factor

The relative response factor (RRF) allows an accurate comparison of the concentration of two compounds in an HPLC run by its peak area. It can be calculated according to **Equation 2**, whose values can be obtained from the HPLC runs of standards of each compound.

$RRF_{(A/B)} = \frac{P_a/C_a}{P_b/C_b}$ , where P is the peak area, C the concentration of the sample injected and A and B different compounds.

#### Equation 2. Relative response factor

The determination of the RRF between 6,7-dimethoxy-1-methyl-3,4-dihydroisoquinoline (**A**) and 6,7-dimethoxy-1-methyltetrahydroisoquinoline (**B**) is presented as an example. In **Figure 20**, equimolar standards of both compounds were run at the HPLC and peak area determined. In such conditions as  $C_A = C_B$ ,

$$RRF_{(A/B)} = \frac{P_A}{P_B} \Rightarrow RRF_{(A/B)} = \frac{54521.5}{19347.8} = 2.82$$

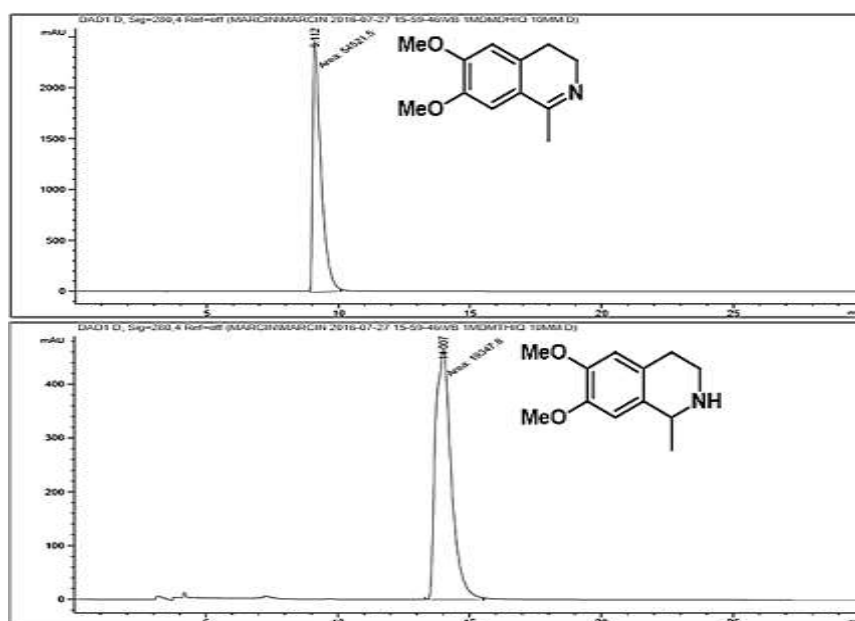


**Figure 20.** Normal phase HPLC trace (CHIRACEL<sup>®</sup> OD-H 250 mm x 4.6 mm, 5  $\mu$ m, eluent: hexane/isopropanol/diethylamine = 90/10/0.1, 1 mL/min, 280 nm) of a 10 mM standard solution of either 6,7-dimethoxy-1-methyl-3,4-dihydroisoquinoline (top) or 6,7-dimethoxy-1-methyltetrahydroisoquinoline (bottom).

### 2.9.4 Nitrilase catalysed hydrolysis

Commercially available lyophilized cell-free extract of six nitrilases was used in the following biotransformations. To 1 mL of a 20 mM solution of cyano substrate in phosphate buffer (pH 8.0) was added 3 mg of the corresponding enzyme. The mixture was incubated at 150 rpm and 30 °C for 72 hours, after which a sample was taken and analysed by reverse-phase HPLC. Additional 3 mg of enzyme were added and the reaction was incubated for more 48 hours, followed by new HPLC analysis. HPLC samples were prepared by centrifugation of a 200 µL aliquot at 13200 rpm followed by a 1:2 dilution of the supernatant in methanol and posterior 1:2 dilutions in methanol/water 50/50. Product concentration was calculated according to **Equation 3**, whose graphic can be consulted in **Figure A1.2**.

$$y = 3807x \quad (R^2 = 0.987)$$

**Equation 3.** Calibration curve of tetrahydroisoquinoline-1-carboxylic acid concentration.

## 2.10 CHEMICAL REACTIONS

### 2.10.1 Cyanation of 3,4-dihydroisoquinolines

A 1 M solution of potassium cyanide (1.5 eq.) was added to a 1.5 M solution of 3,4-dihydroisoquinoline in water previously acidified with diluted sulphuric acid, according to a procedure by Beumont *et al.*<sup>118</sup> The reaction was left stirring at room temperature for 1 hour. After extraction with ethyl ether, the yield was determined by <sup>1</sup>H and <sup>13</sup>C NMR. Decomposition of the cyano compounds occurred quickly at room temperature and, as so, the product was kept at -4 °C.

# CHAPTER 3. RESULTS AND DISCUSSION



### 3.1 PROTEIN EXPRESSION

#### 3.1.1 Protein expression in *E. coli*

After transforming MAO-N D5, D9 and D11 plasmids into competent BL21(DE3) cells and expressing and purifying the protein using the protocol described in **Chapter 2**, the adequate MAO-N variant's presence was verified by SDS-PAGE (**Figure 21**). Success was confirmed by the presence of a single band in the polyacrylamide gel between 60 and 70 kDa, eluted between fractions 2 and 7. With 495 amino acid residues, MAO-N has a molecular weight of approximately 60 kDa.

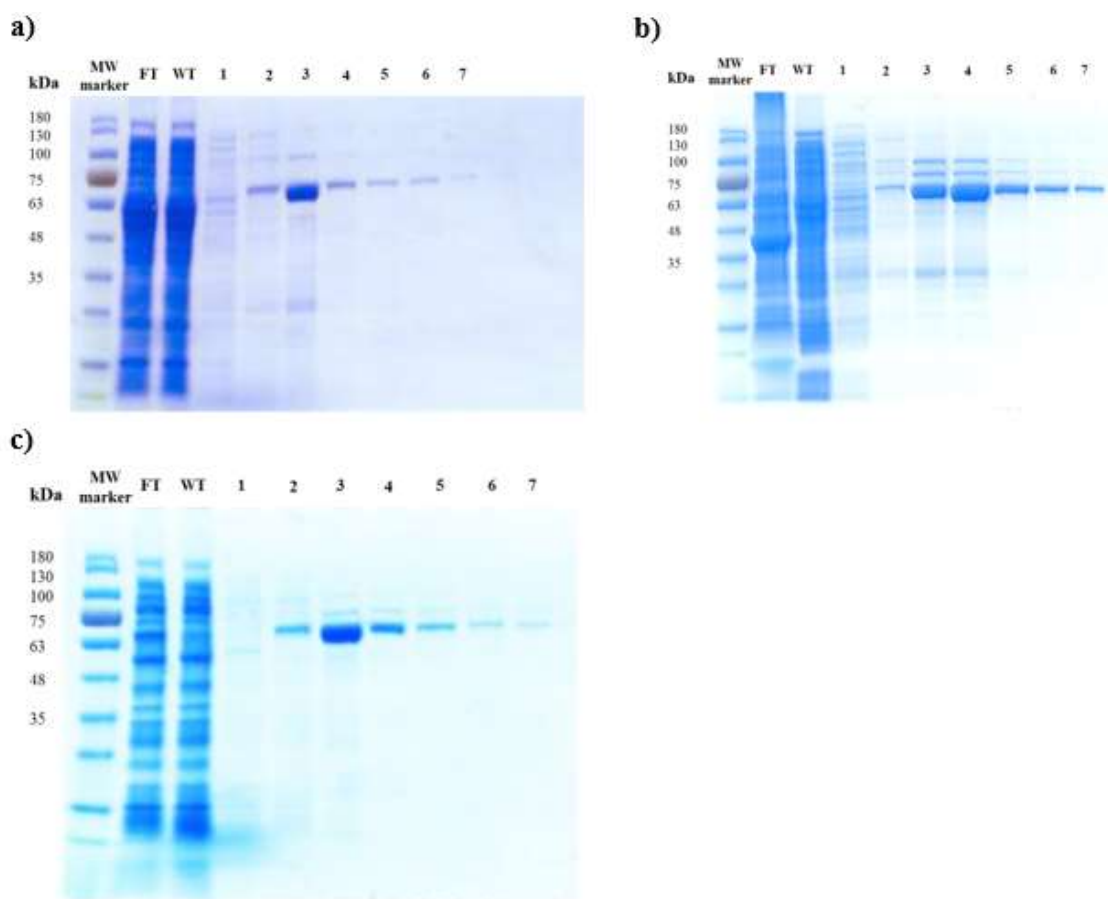


**Figure 21.** SDS-PAGE gel of MAO-N variant's purification. The protein ladder, marked at 75 kDa, was run in the first well, followed by the flow-through (FT), the wash-through (WT) and the elution fractions by order. a) MAO-N D5; b) MAO-N D9; c) MAO-N D11.

The obtained solutions were subjected to the Bradford protein assay and protein concentrations calculated by comparison with a BSA calibration curve (**Figure A1.1**). Results show that 3.5 mL of MAO-N D5, D9 or D11 solutions had a concentration ranging from 0.63 to 1.59 mg/mL (**Figure 22**). Moreover, the increased number of mutations in MAO-N D9 and MAO-N D11 seem to difficult enzyme expression. These results were taken into account in the specific activity assays that follow.

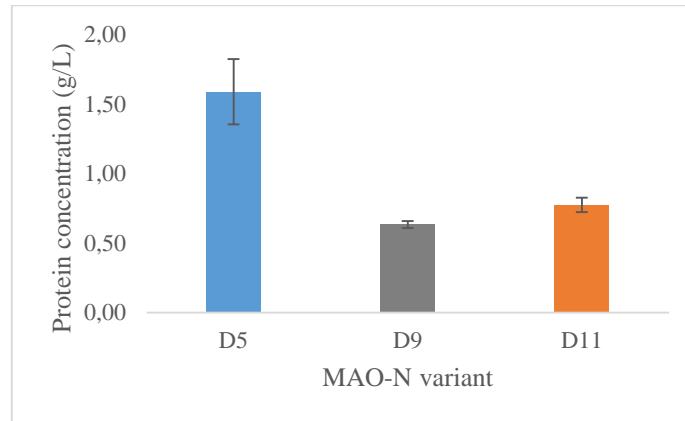


**Figure 22.** Protein concentration of MAO-N variants calculated by the Bradford Assay

Additional expression of MAO-N D9 was attempted with different incubation conditions and *E. coli* strains but, unfortunately, SDS-PAGE analysis showed no significant amount of protein after purification. Troubleshooting of this results lead to the analysis of the DNA sequence of MAO-N wt, D5 and D9. Large differences were found in the codon frequencies of MAO-N wt and MAO-N D5, indicating that the D5 variant had been previously codon optimized for expression in *E. coli* – see **1.2.2.2** for further reference. On the other hand, MAO-N D9 sequencing showed this enzyme had not been codon optimized, which could justify its low expression in this organism.

### 3.1.2 Protein expression in *P. pastoris*

*P. pastoris* is a methylotrophic organism widely used for heterologous protein expression. It presents several advantages in its ability to secrete proteins and reach high cell densities. Moreover, it is a suitable host to test our hypothesis that MAO-N D9 did not express due to a lack of codon optimization, as yeast stands more similar to the native host, *Aspergillus niger*.<sup>62</sup>



In this work, MAO-N D9 gene was inserted in a pPicZ $\alpha$  C empty vector by ligation independent cloning. Cloning success was confirmed by DNA sequencing. Also, the presence of the MAO-N gene was verified by subjecting the circular plasmid to two restriction enzymes, XhoI and BamHI, that selectively cut the gene in two segments of 1872 bp and 3100 bp. Successful cleavage was verified by agarose gel electrophoresis (**Figure 23**).

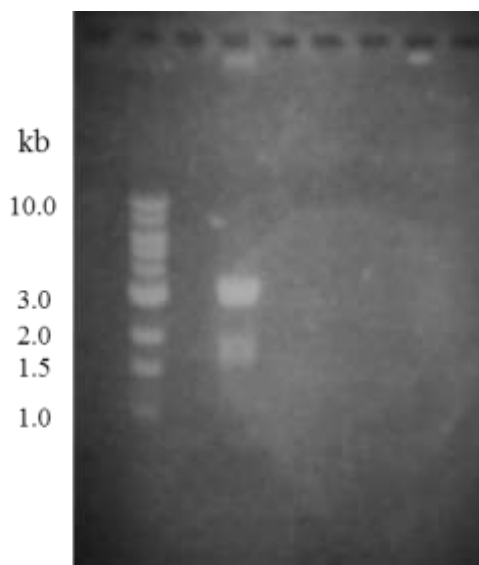


**Figure 23.** Agarose gel electrophoresis of MAO-N D9 in pPicZ $\alpha$  C after action of the restriction enzymes XhoI and BamHI.

The complete circular plasmid was linearized with a PmeI restriction enzyme for transformation into *P. pastoris* cells. Insertion of plasmid DNA in *P. pastoris* was achieved by electroporation. Unfortunately, transformation efficiencies for this organism are considerable lower than with *E. coli* as the plasmid needs not only to enter the cell but also be incorporated in the host's genome. In order to achieve successful insertion, care must be taken with cell viability and concentration of DNA and cell in the electroporation cuvette. Moreover, cell growth with several concentrations of antibiotic is required for the selection of the best multi-copy recombinants, that is, multiple insertion of the gene in the host's genome.

Transformation of MAO-N into *P. pastoris* was attempted for five times before successful transformants were found. Even then, only two colonies grew on an YPD plate with 1000  $\mu$ g/ml Zeocin<sup>TM</sup>. PCR of both colonies, with the previous primers from the ligation independent cloning, followed by agarose gel electrophoresis revealed the presence of a band

around 1.5 kb, corresponding to amplification of the MAO-N D9 gene (**Figure 24**). This confirmed a successful insertion of the target gene. Besides, the high intensity of the band suggests the insertion of multiple copies into the *P. pastoris* genome, therefore increasing the likelihood of high MAO-N D9 expression in future cell growth experiments.

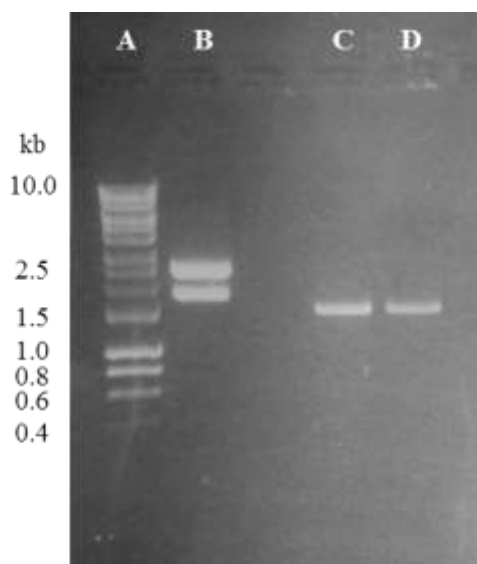
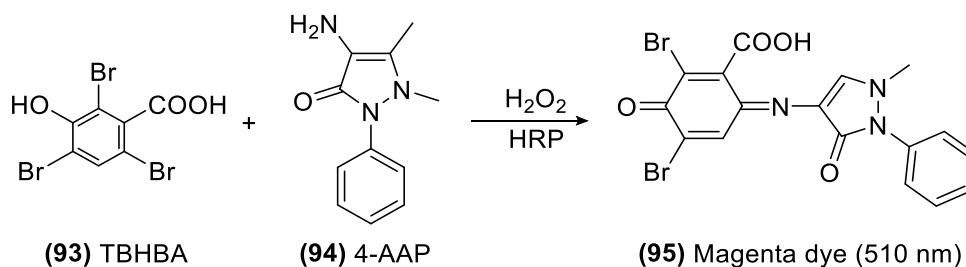


**Figure 24.** Agarose gel electrophoresis of the results from the Touchdown PCRs for the amplification of MAO-N D9 gene in *P. pastoris*' genome. A) 1 kb DNA ladder; B) Unrelated run; C) Touchdown PCR with colony 1; D) Touchdown PCR with colony 2.

## 3.2 SUBSTRATE SCOPE OF MAO-N IN THE OXIDATION OF TETRAHYDROISOQUINOLINES

### 3.2.1 Overview

A colorimetric specific activity assay was optimized to quickly determine the activity of MAO-N variants with THIQ substrates. MAO-N can catalyse the oxidation of primary and secondary amines to imines, producing hydrogen peroxide as a sub product. In the presence of HRP,  $H_2O_2$  can catalyse the oxidative coupling of TBHBA with 4-AAP, producing a highly stable magenta dye (**Scheme 20**). Its concentration can be monitored measuring the absorbance at 510 nm. Moreover, when plotting absorbance vs time, a direct proportionality can be found between the slope of the graphic obtained and the specific activity of the enzyme.



**Scheme 20.** Oxidative coupling of TBHBA and 4-AAP

Eleven different substrates were used in this analysis, as mentioned in **Figure 16**, and tested with the MAO-N variants found in **Table 1**. Besides the already reported MAO-N D5, D9 and D11 mutants, eight mutants, selected from a library of single and double mutations on MAO-N D5 under development by Jane Kwok *et al.*<sup>115</sup>, were studied for the first time with THIQ substrates. The absorbance of all reactions was monitored over time, the specific activity calculated accordingly and the results presented in the following **Figures 25 to 29**.

### 3.2.2 Specific activity assays

The specific activity of MAO-N variants with  $\alpha$ -AMBA (**66**) (see structure in **Scheme 14**) and THIQ (**19**) (see structure in **Figure 16**) is presented in **Figure 25**.  $\alpha$ -AMBA was used as a positive control to confirm that the enzyme was expressed in its active conformation. As expected, all variants showed activity with this substrate. However, its similarity with the natural substrate of this enzyme seems to evidence that a greater change in the enzyme's active site, as seen in MAO-N D11, can lead to a significant decrease in activity with simple substrates.

Surprisingly, all MAO-N D12 variants had higher specific activities with THIQ than with  $\alpha$ -AMBA, reaching a surprising 7-fold increase in activity for D12 (H). In fact, the new engineered mutants appeared to follow a different evolutionary route than the previously reported with MAO-N D9 and D11, maintaining and even improving MAO-N D5's preference for unsubstituted THIQ over  $\alpha$ -AMBA.

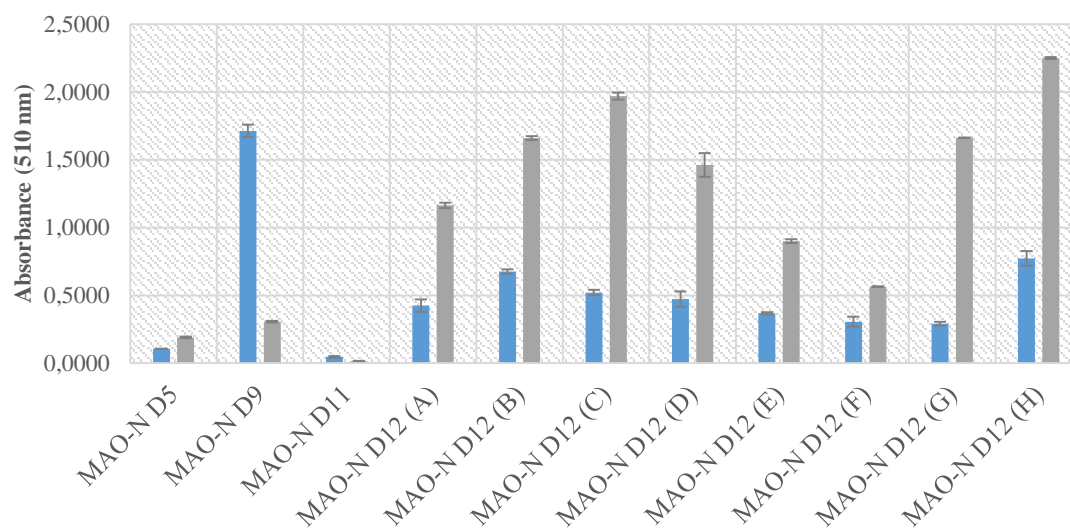


**Figure 25.** Specific activity of MAO-N variants with racemic  $\alpha$ -AMBA – in blue – and THIQ – in grey.

The procedure was repeated with MTQs. In **Figure 26** and **27** it is possible to assess the influence of an increased steric hindrance near the amine group to the activity of all MAO-N variants. First, and as expected, MAO-N D9 showed significantly higher activity with this substrate than other mutants.

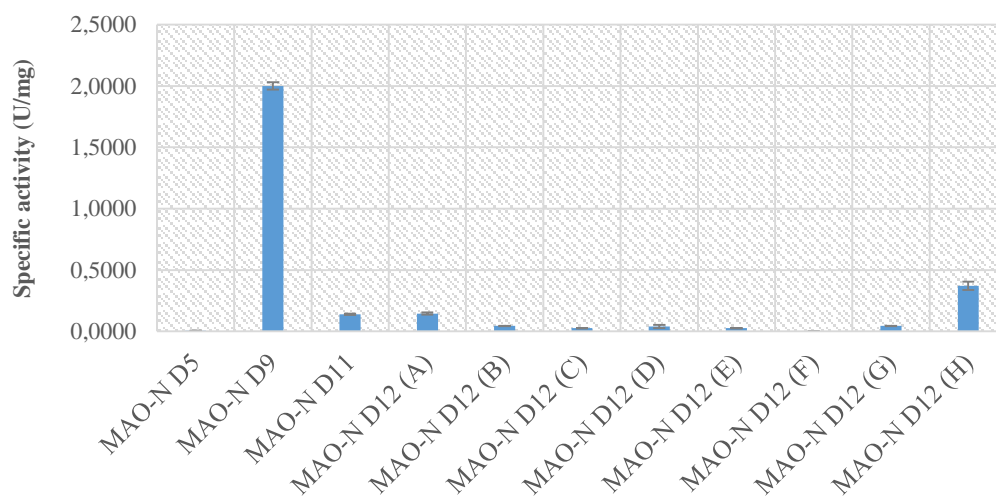


**Figure 26.** Specific activity of MAO-N variants with 1-MTQ

Still, different results were found when comparing substitutions in the remaining positions of the pyrimidine ring, as these substrates were not easily accepted by any enzyme variant. First, and in contrast with MAO-N D9 and D11, the activity of MAO-N D12 variants with 4-MTQ (**86**) (see structure in **Figure 16**) appeared to be much higher than with 3-MTQ (**85**) (see structure in **Figure 16**). Most importantly, MAO-N D12 mutants showed the highest activity so far reported for 4-MTQ, with an up to 17-fold improvement from MAO-N D5.

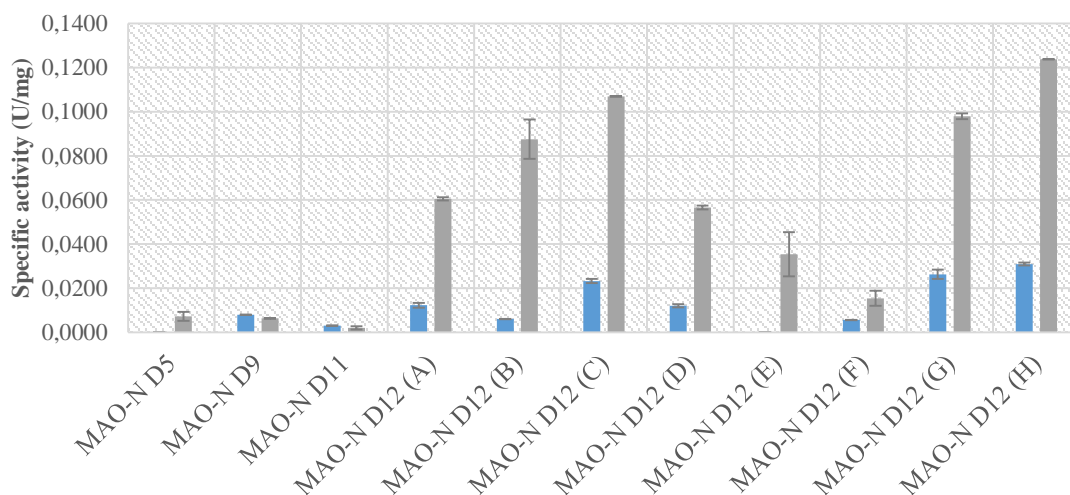


**Figure 27.** Specific activity of MAO-N variants with 3-MTQ – in blue – and 4-MTQ – in grey.

Next, the activity of MAO-N variants with THIQ with substituents in the aromatic ring was determined. **Figure 28** shows that MAO-N D9 presented exceptional activity with 5,6 and 8-MTQ - (**87**), (**88**) and (**90**), respectively (see structures in **Figure 16**). Nevertheless, the new MAO-N D12 mutants showed a significant increase in activity from MAO-N D5, up to 16-fold. Consistent with the results is the higher acceptance by these new mutants of 5-MTQ, presenting a similar activity profile to MAO-N D5. Remarkably, some MAO-N D12 variants are now the most promising enzymes for the oxidation of these methylated THIQs.

Finally, very low activities were found testing all MAO-N variants with 7-MTQ (**89**) (see structure in **Figure 16**), and only MAO-N D12 (C) and (G) showed any significant activity at 0.0051 and 0.027 U/mg, respectively.

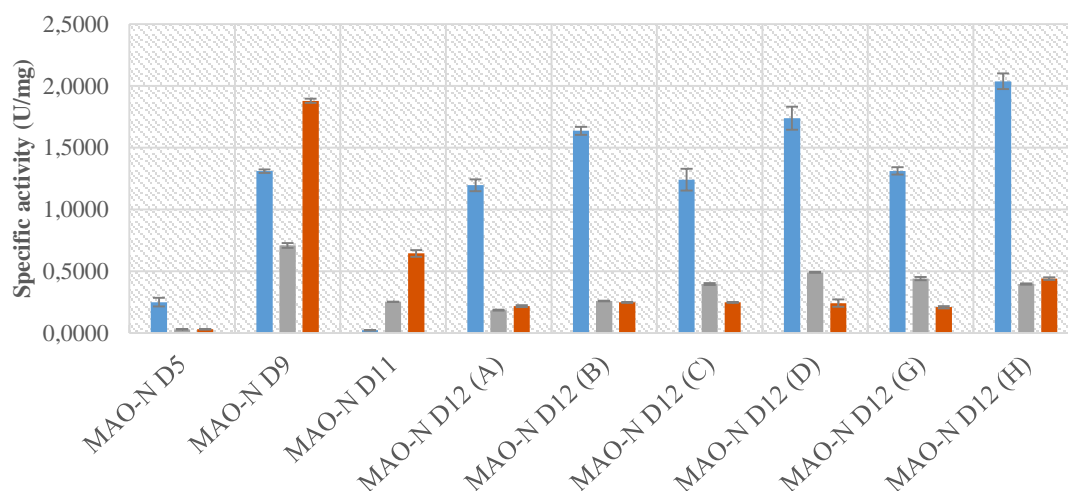


**Figure 28.** Specific activity of MAO-N variants with 5-MTQ, in blue, 6-MTQ, in grey, and 8-MTQ, in orange.

It is known that MAO-N does not accept 6,7-dimethoxy substituents in its aromatic ring but no study as so far determined if mere steric hindrance is involved or a change in the electronic distribution of the molecule. Given the exceptional activity obtained from MAO-N D12 mutants with THIQs, in general, and particularly with 7-MTQ, the specific activity of all MAO-N variants with DMTHIQ (**91**) (see structure in **Figure 16**) and 1-M-DMTHIQ (**92**) (see structure in **Figure 16**) was also determined and is presented in **Figure 29**.

All the enzymes tested showed very low activities with dimethoxylated substrates. Nevertheless, MAO-N D9, MAO-N D12 (C) and MAO-N D12 (G) had the highest activity of all variants with DMTHIQ. Remarkably, MAO-N D9 maintained its activity when tested with 1-M-DMTHIQ and MAO-N D12 (C) suffered only a slight decrease in activity. In contrast, MAO-N D12 (G) proved to be completely unable to oxidize this substrate.

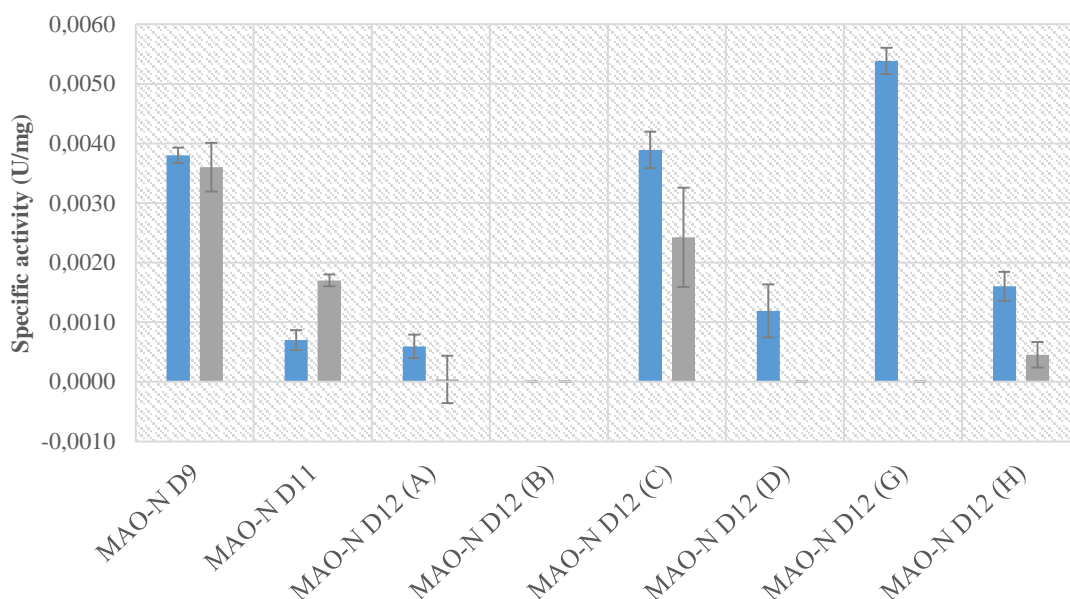


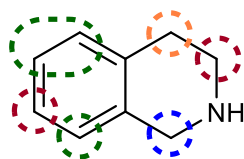
**Figure 29.** Specific activity of some MAO-N variants with DMTHIQ, in blue, and 1-M-DMTHIQ, in grey.

### 3.2.3 Final discussion

In this section a specific activity assay was used to study the substrate scope of several engineered MAO-N variants with THIQ derivatives, with interesting results. A summary of the results aforementioned is presented in **Figure 31**. First, it seems clear that the substrate's substitution pattern can have a huge influence in the enzyme's activity (**Figure 30**). Although simple non-polar substitutions in the 5, 6 or 8 positions can maintain or even improve the activity of some MAO-N variants, substitutions in the 7 position do not seem to be accepted at all. Moreover, the four mutations present in MAO-N D9 and not in MAO-N D5, shown in **Table 1**, appear essential in the acceptance of small substituents in C1 by the enzyme. In fact, the low activity seen in MAO-N D11 with 1-MTQ, by comparison with MAO-N D9, indicates that the only different amino acid between these mutants, W430, may be responsible for this selective behaviour.

Second, C3 and C4 substitutions can significantly hinder the enzyme's activity, by either changing the electronic properties of the molecule, and subsequently altering the amine's pKa, or making it difficult to accommodate the target molecule inside the active pocket. It is our belief that the increase in activity seen in some MAO-N D12 mutants supports the second hypothesis, as the change in the enzyme's secondary structure, far from the aromatic

cage, is more likely to alter the shape or size of the active pocket and, therefore, its ability to accommodate larger substrates.



(19) THIQ

**Figure 30.** Summary of the activity of MAO-N variants with methyl substituted THIQs, with the circles representing the carbons in which the methyl group was added. Green -high activity with most tested variants; orange – average activity with most tested variants; red – very low activity with all tested variants; blue – high activity only with MAO-N D9.

Finally, the results showed remarkable activities for MAO-N D12 (C) and D12 (G) with dimethoxylated substrates, similar or even higher than the activity here reported with MAO-N D9. Nevertheless, while MAO-N D12 (C) maintained its activity with 1-M-DMTHIQ, the (G) variant was completely inactive with this substrate. What's more, this behaviour was comparable to the one seen in 1-MTQ, where this last variant showed complete loss in activity by the addition of a 1-methyl substitution. This suggests an inability by the enzyme to accept C1 substitutions, therefore limiting its substrate scope. As so and as previously stated, the increase in the size of the active pocket caused by the mutations present in MAO-N D9, especially in the W430 residue, can be essential for the accommodation of C1 substituted THIQ's in the active site.



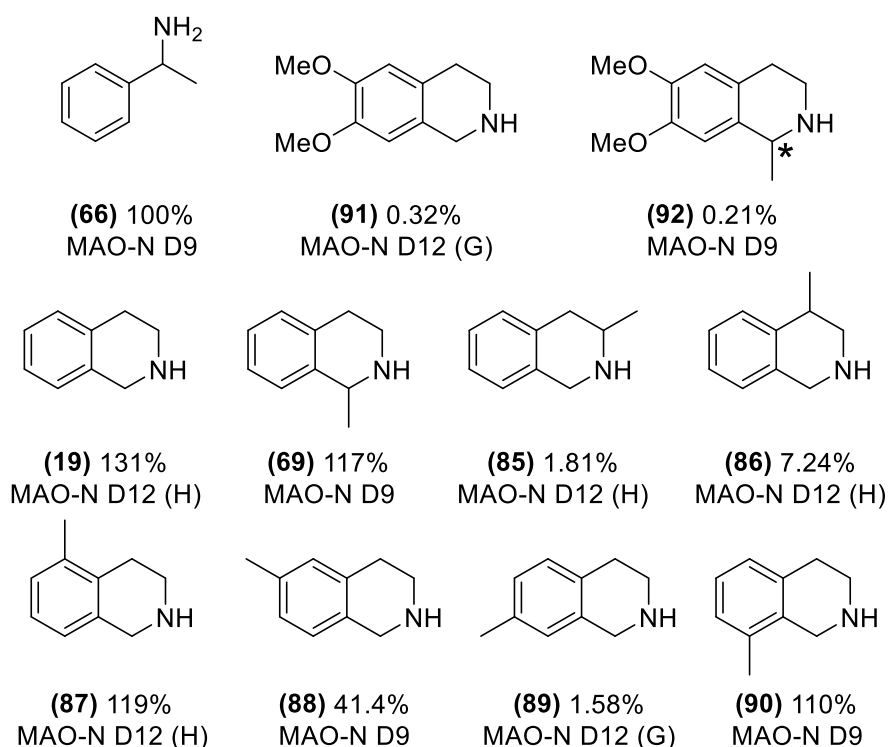


**Figure 31.** Summary of the mutants with best activity towards each one of the substrates tested. The values presented are relative to the best activity determined for  $\alpha$ -AMBA (MAO-N D9)

### 3.3 DIRECTED EVOLUTION OF MAO-N D9 BY SITE-DIRECTED MUTAGENESIS

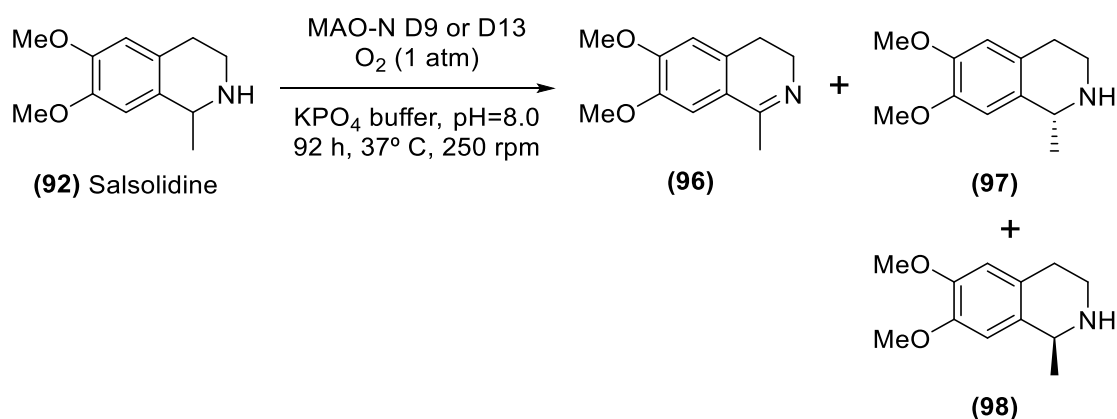
#### 3.3.1 Overview

The MAO-N D12 (G) mutant presented remarkable activity towards DMTHIQ, the highest activity ever reported by a MAO-N variant. Unfortunately, this mutant seems to lose all activity by the presence of a substitution in C1. On the other hand, MAO-N D9 presented similar activities with both substrates, easily accommodating the additional methyl group. Following the principle of additivity, explained in Chapter 1, we set out to see if the addition of the two additional mutations in MAO-N D12 (G) – S205T S206N – to MAO-N D9 could generate a new enzyme with increased activity towards 1-M-DMTHIQ.

### 3.3.2 Oxidation and deracemization of salsolidine

The double point mutation was performed by both GC and HF PCR with designed mutagenic primers and success confirmed by sequencing of overnight cultures in NEB<sup>®</sup> 5-alpha. For the purposes of this work the new mutant was named MAO-N D13.

MAO-N D13 was expressed in *E. coli* BL21(DE3) but purification did not yield any significant amount of protein. As so, specific activity assays couldn't be performed with the new mutant. Nevertheless, biotransformations were set to verify the enzyme's ability to oxidise (*rac*)-1M-DMTHIQ (**92**) to 6,7-dimethoxy-1-methyl-3,4-dihydroisoquinoline (**96**) and the results analysed by HPLC (**Scheme 21**). The relative response factor was 2.82, calculated as described in the experimental section.



**Scheme 21.** Oxidation of 1-M-DMTHIQ with MAO-N variants

MAO-N D9 was used as a negative control. A whole-cell biotransformation was set using MAO-N D9 in *E. coli* BL21(DE3) and its results presented in **Figure 32**. Only 0.92% yield was found after 4 days, confirming previous results that this mutant could not catalyse the aforementioned reaction. On the other hand, the new MAO-N D13 mutant achieved a remarkable yield of 29.8% in the same time period, showing an over 30-fold increase in activity. Amazingly, it appears to be the first ever recorded successful biotransformation of dimethoxylated tetrahydroisoquinolines with a MAO-N variant.

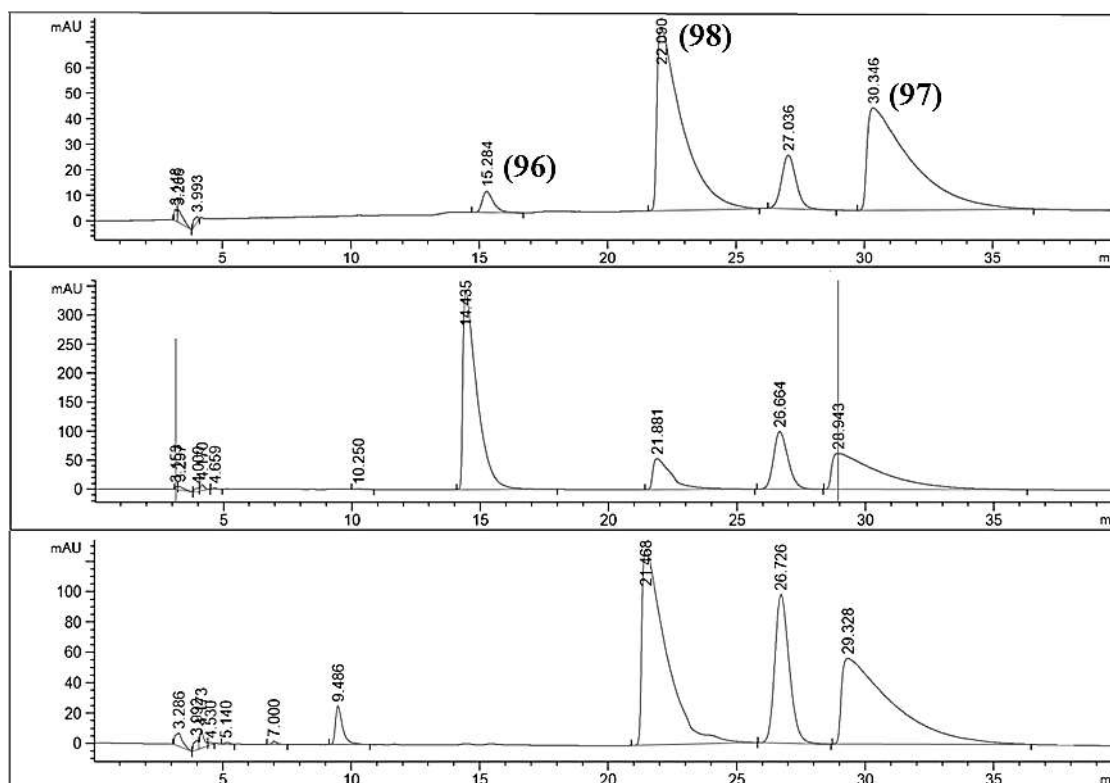


**Figure 32.** Normal phase HPLC trace (CHIRACEL<sup>®</sup> OD-H 250 mm x 4.6 mm, 5  $\mu$ m, eluent: hexane/isopropanol/diethylamine = 95/5/0.1, 1 mL/min, 280 nm) of three biotransformations: oxidation of **(92)** with MAO-N D9 (top), oxidation of **(92)** with MAO-N D13 (middle) and deracemisation of **(92)** with MAO-N D13 (bottom).  $RT_{[(S)\text{-amine}]}$  = 21.79 min\*;  $RT_{[(R)\text{-amine}]}$  = 28.89 min\* ;  $RT_{[\text{imine}]}$  = 14.65 min. \*Enantiomer peaks identified according to the literature.<sup>94</sup>

Moreover, analysis of the remaining amine peaks showed a 49.5% enantiomeric excess of the (*R*) enantiomer **(97)**, with no significant decrease in its peak area (by comparison with a 10mM racemic standard), indicating MAO-N D13 to be very selective towards (*S*)-1-M-DMTHIQ **(98)**. As so, the reaction yield could be calculated by the conversion of **(98)** to **(96)**, estimated at approximately 60%. These results showed that MAO-N D13 could, in theory, be used for the kinetic resolution of racemic 1-M-DMTHIQ due to its high activity and selectivity towards one enantiomer.

In light of these results, the dynamic kinetic resolution of 1-M-DMTHIQ with MAO-N D13 and  $\text{NH}_3\cdot\text{BH}_3$  was attempted. Unfortunately, no significant change in enantiomer concentration was found over a 4-day reaction period. The reaction rate appears too small to ensure enough cycles of oxidation-reduction in a reasonable time period. No further

reactions were attempted, but an increase in enzyme loading could, in theory, lead to better results. Nevertheless, the identification of a new MAO-N mutant with increased activity is still remarkable and can stand as a starting point for further directed evolution experiments targeting dimethoxylated substrates.

## 3.4 DYNAMIC KINETIC RESOLUTION OF CHIRAL TETRAHYDROISOQUINOLINES

### 3.4.1 Overview

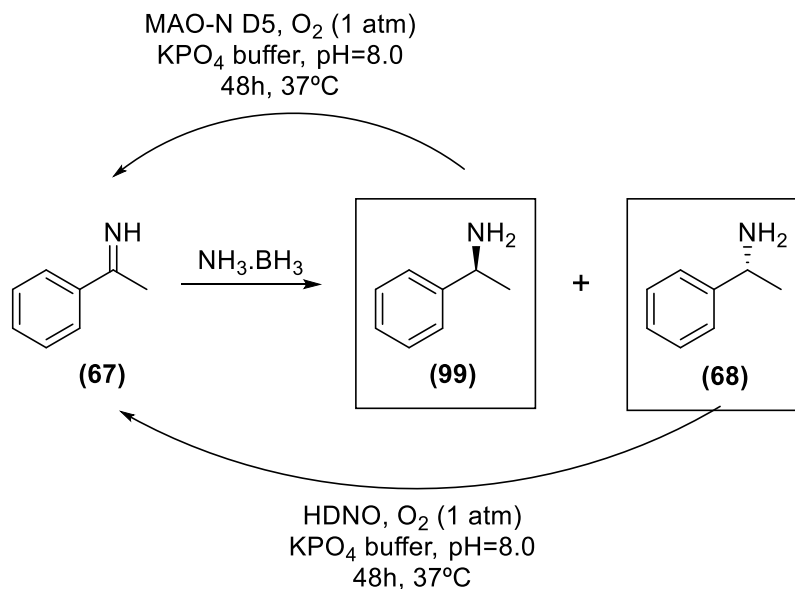
Pure chiral amines are increasingly common in the pharmaceutical industry, driving a constant search for new and sustainable methods towards their synthesis or resolution. In this section, four enzymes - MAO-N D5, D9, D11 and HDNO - were investigated for their ability to oxidase several chiral amines.

DKR of chiral amines with MAO-N variants has been previously described in **Chapter 1**. It has remarkable advantages to common resolution methods, as it can reach 100% yield and have a low environmental impact. In this work, HDNO and an appropriate MAO-N variant, according to the literature, were used for the deracemisation of  $\alpha$ -AMBA and several tetrahydroisoquinolines, as follows.

### 3.4.2 Resolution of chiral amines

#### 3.4.2.1 $\alpha$ -Methylbenzylamine

The deracemisation of  $\alpha$ -AMBA with MAO-N D5 has been previously reported with great success, as stated in Chapter 1. In this work, both MAO-N D5 and HDNO were used in this reaction (**Scheme 22**) and, surprisingly, appear to have reverse selectivity. With MAO-N D5, an e.e. of 74% of the (*R*) enantiomer (**68**) was reached within 2 hours, and complete deracemization should shortly follow (**Figure 33**). Contrarily, an e.e. of only 16% of (*S*)- $\alpha$ -AMBA (**99**) was obtained with HDNO after two days, proving that, although selective towards this isomer, this enzyme is not very active.



**Scheme 22.** Deracemisation of  $\alpha$ -AMBA with MAO-N D5 and HDNO

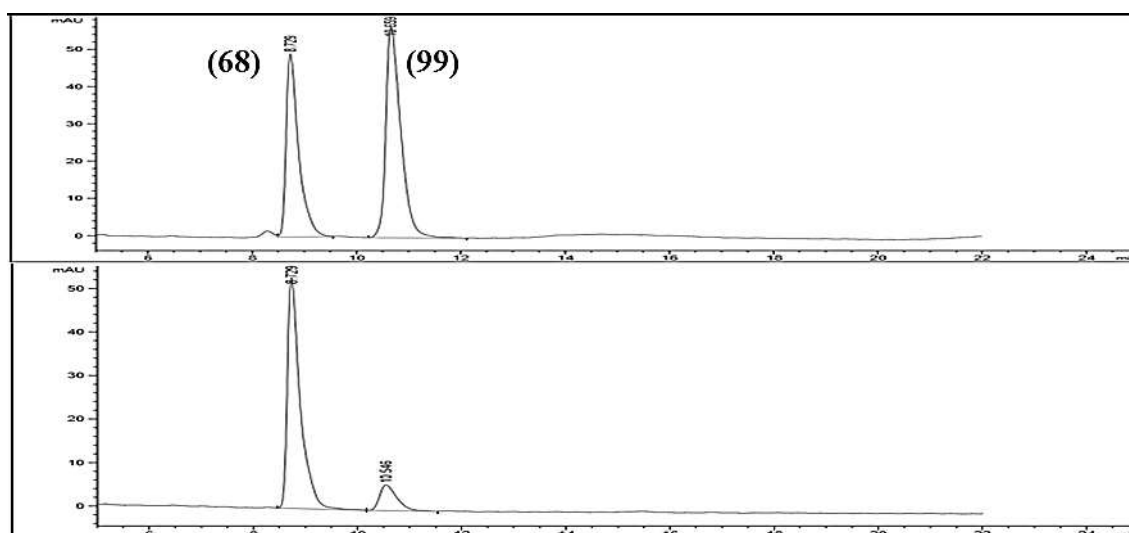
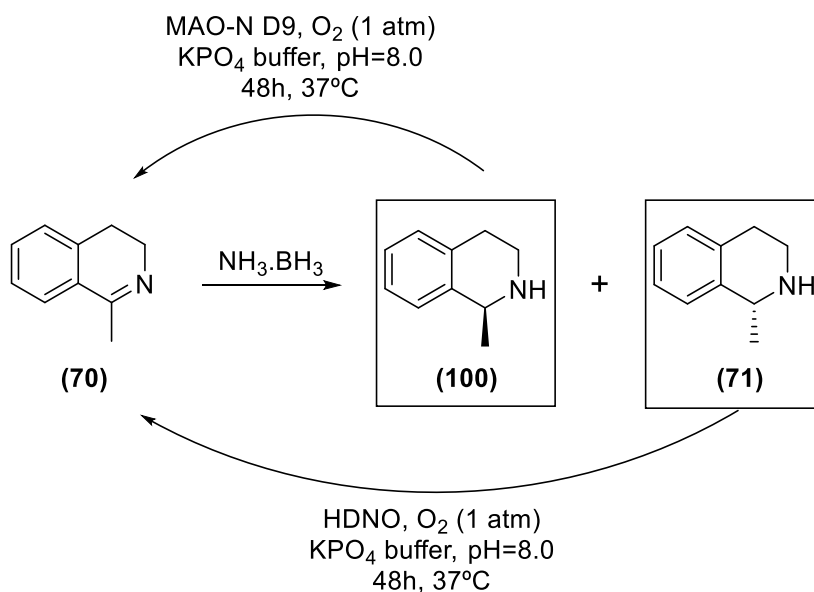


**Figure 33.** Normal phase HPLC trace (CHIRACEL<sup>®</sup> OD-H 250 mm x 4.6 mm, 5  $\mu$ m, eluent: hexane/isopropanol/diethylamine = 95/5/0.1, 1 mL/min, 254 nm) of the deracemisation of  $\alpha$ -AMBA with HDNO (top) or MAO-N D5 (bottom). **RT**<sub>[(R)-amine]</sub> = **8.77 min**; **RT**<sub>[(S)-amine]</sub> = **10.67 min**.

### 3.4.2.2 1-Methyltetrahydroisoquinoline

A similar procedure was used for 1-MTQ (**Scheme 23**) and the HPLC results shown in **Figure 34**. MAO-N D9 was the monoamine oxidase variant used in this experiment due to its high activity with this substrate, previously reported in **Chapter 3**. Full conversion to (R)-MTQ (**71**) was found with MAO-N D9 after two hours, while with HDNO only 29.9%

e.e. of (*S*)-MTQ (**100**) was attained after 2 days. Even so, this result presents an increase in activity for HDNO, by comparison with  $\alpha$ -AMBA.



**Scheme 23.** Deracemisation of 1-MTQ with MAO-N D9 and HDNO

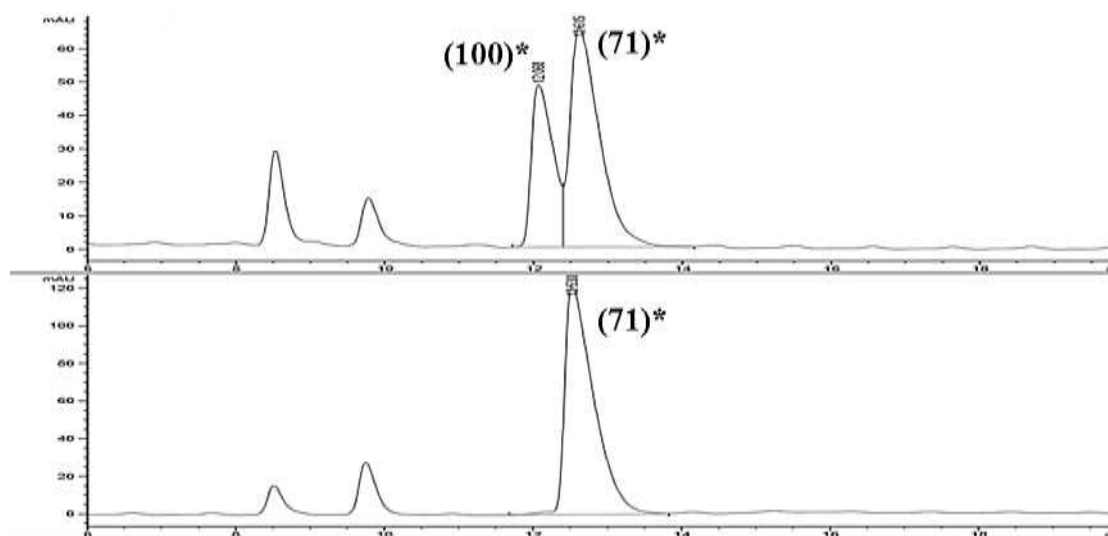
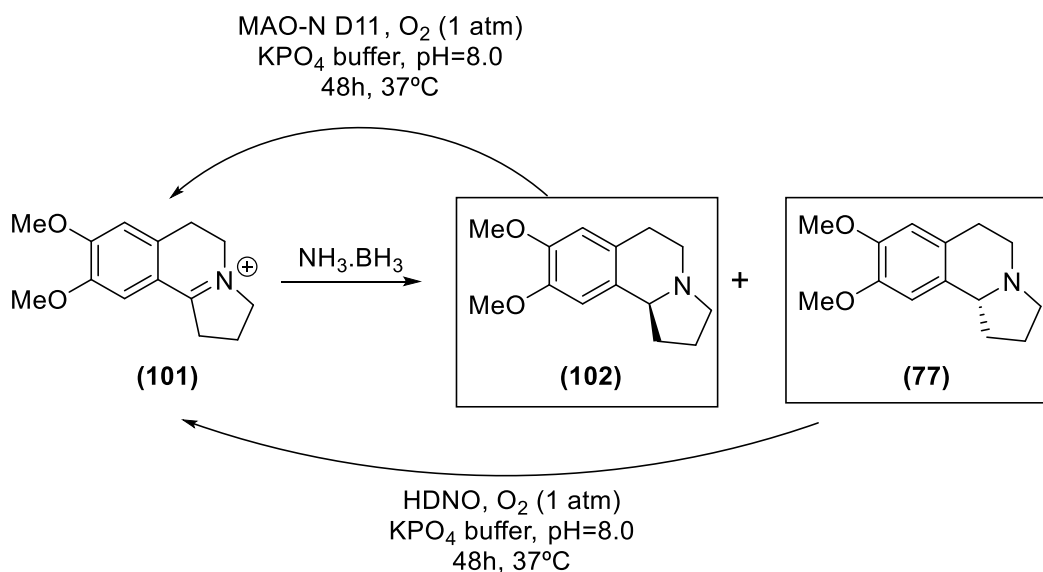


**Figure 34.** Normal phase HPLC trace (CHIRACEL<sup>®</sup> OD-H 250 mm x 4.6 mm, 5  $\mu$ m, eluent: hexane/isopropanol/diethylamine = 98/2/0.1, 1 mL/min, 254 nm) of the deracemisation of 1-MTQ with HDNO (top) or MAO-N D9 (bottom). **RT**<sub>[(*S*)-amine]</sub> = **12.13 min**; **RT**<sub>[(*R*)-amine]</sub> = **12.68 min**.

\*Enantiomer peaks identified by comparison with known literature.<sup>103</sup>

## 3.4.2.3 Crispine A

Finally, the deracemization of Crispine A, a known antitumor drug, was attempted with HDNO and MAO-N D11 (**Scheme 24**). Unfortunately, only 15.8% e.e. of (*R*)-Crispine (**77**) was found after 2 days (**Figure 35**). Also, HDNO proved to be either inactive or non-selective towards this substrate. Nevertheless, the low activity of MAO-N D11 with Crispine A could be justified by the increased difficulty in the oxidation of tertiary amines, as no mention of catalytic loading was made in previous articles.



**Scheme 24.** Deracemisation of Crispine A with MAO-N D11 and HDNO

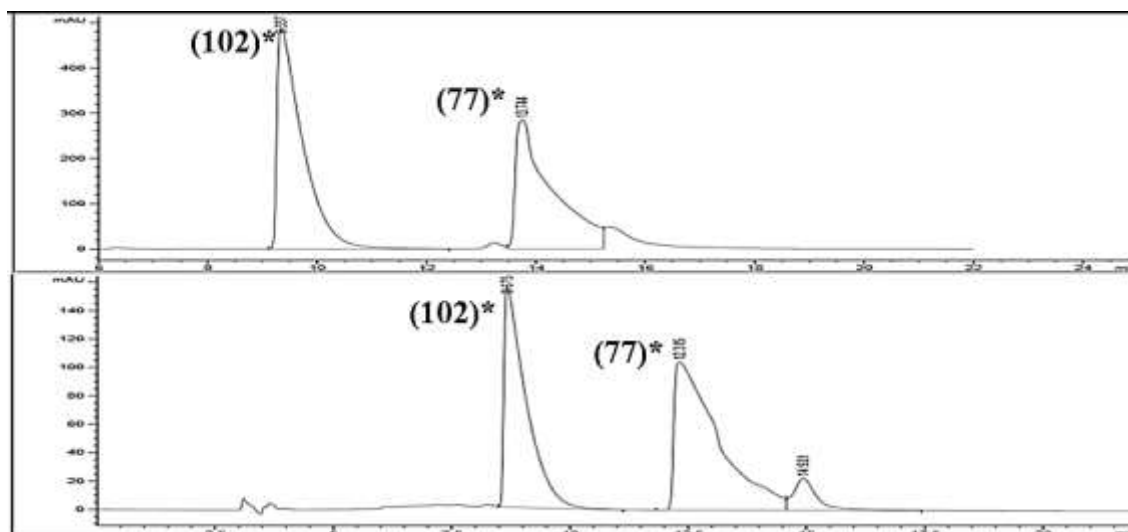


**Figure 35.** Normal phase HPLC trace (CHIRACEL<sup>®</sup> OD-H 250 mm x 4.6 mm, 5  $\mu$ m, eluent: hexane/isopropanol/diethylamine = 90/10/0.1 (top) or 95/5/0.1 (bottom), 1 mL/min, 254 nm) of the deracemisation of Crispine A with HDNO (top) or MAO-N D11 (bottom). **RT<sub>[(S)-amine]</sub> = 12.13 min; RT<sub>[(R)-amine]</sub> = 12.68 min.**

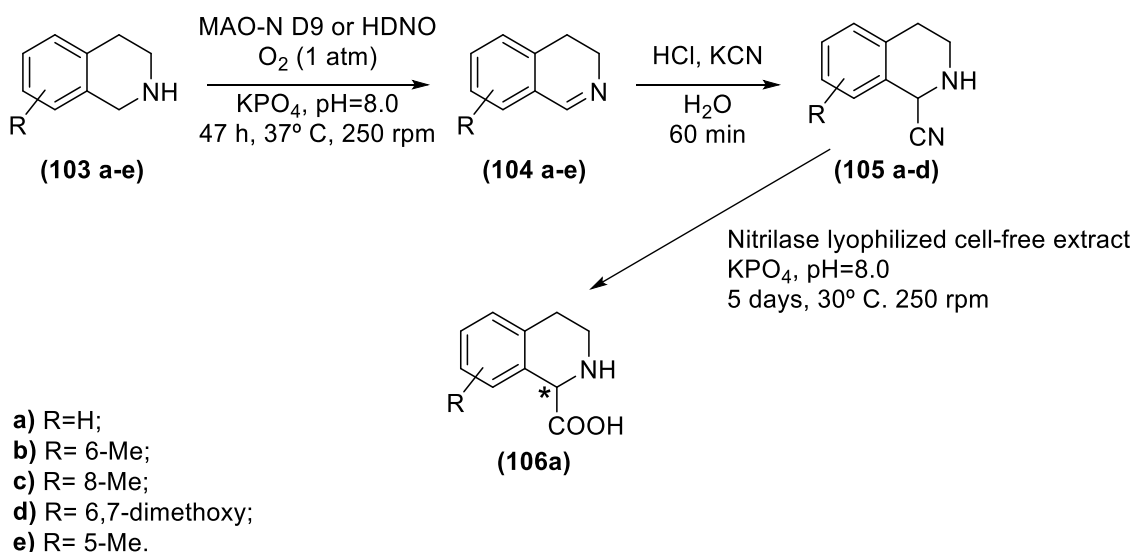
\*Enantiomer peaks identified by comparison with known literature.<sup>94</sup>



### 3.5 ONE POT THREE STEP CASCADE FOR THE C1 FUNCTIONALIZATION OF TETRAHYDROISOQUINOLINES

#### 3.5.1 Overview

Functionalized THIQs can act as precursors to important alkaloids with known pharmacological applications. In this work, a one-pot three step cascade reaction was devised to synthesize tetrahydroisoquinoline-1-carboxylic acids (**106**) (Scheme 25). First, MAO-N D9, D12 (G) or HDNO were used in the conversion of several THIQs (**103 a-e**) to the corresponding 3,4-dihydroisoquinoline analogues (**104 a-e**), as described in Chapter 2. These were treated with potassium cyanide in an acid environment to yield 1-cyanotetrahydroisoquinolines (**105 a-d**). The cyano compounds were then selectively hydrolysed by commercial nitrilases, and both the conversion and enantiomeric excess determined by reverse-phase HPLC.



**Scheme 25.** Cascade reaction for the stereoselective synthesis of tetrahydroisoquinoline-1-carboxylic acids. Compound (**19**) was renumbered to (**103a**) to allow a better comprehension of the following results by the reader.

## 3.5.2 Synthesis of 3,4-dihydroisoquinolines

### 3.5.2.1 Overview

MAO-N D9, D12 (G) or HDNO were used in the oxidation of several THIQs. First, small biotransformations were set and analysed by HPLC. When near full conversion was reached within 48 hours, the biotransformations were replicated in a larger scale and analysed by  $^1\text{H}$  NMR, as presented. The obtained 3,4-dihydroisoquinolines (**104 a-e**), confirmed by  $^1\text{H}$  NMR, were used in the determination of response factors, and the final yield was calculated from the previous small scale HPLC runs. An exception is made for 3,4-dihydroisoquinoline (**104a**) as the commercial imine standard was available.

The  $^1\text{H}$  NMR spectrum of 5-methyl-3,4-dihydroisoquinoline as a direct result of the oxidation of 5-MTQ by MAO-N D9 is shown in **Figure 36** as an example. First, the H-1 peak can be seen at 8.25 ppm in the form of a triplet, coupling at long distance with the H-3 protons. It suffers the inductive deshielding effect of the highly electronegative nitrogen atom, as well as the anisotropic deshielding effect caused by the C1=N double bond conjugated with the aromatic ring.

Next, the signals correspondent to the three aromatic protons can be seen between 7.05 and 7.20 ppm, all suffering the anisotropic effect of the aromatic ring. The signal from the H-8 proton appears as a doublet, coupling with H-7, at a higher chemical shift due to the increased anisotropic effect from the C1=N bond and the inductive effect of the nitrogen atom. At 7.14 ppm appears the H-7 signal as a triplet, by coupling of this proton with H-6 and H-8. Finally, the signal of H-6 appears at 7.07 ppm as a doublet, coupling with H-7.

The signals from the aliphatic protons appear last in the  $^1\text{H}$  NMR spectrum, with H-3 and H-4 signals presenting an downfield shift due to their proximity to the heteroatom and the aromatic ring. In fact, the direct bond to the nitrogen atom causes a downfield shift of the H-3 signal (3.72 ppm) that appears as a double triplet by coupling with H-1 and the H-3 protons. Next, the signal from H-4 appears as a triplet at 2.62 ppm, coupling only with H-3. Finally, the H-9 protons' signal from the methyl group appears as a singlet at 2.22 ppm, suffering only slightly the anisotropic effect of the aromatic ring.

6-MTQ and 8-MTQ present similar  $^1\text{H}$  NMR spectra, with some slight differences in the chemical shift of the signals correspondent to the aromatic protons. Nevertheless, these signals were easily assigned by their multiplicity. On the other hand, the spectrum of

6,7-dimethoxy-3,4-dihydroisoquinoline shows significant differences due to the addition of electronegative atoms. First, the signals of the methyl protons adjacent to an oxygen atom appear as singlets at 3.83 and 3.85 ppm, suffering its deprotective inductive effect. Then, the aromatic protons' (H-5 and H-8) signal present a downfield shift due to its *ortho* position to the methoxy groups, suffering an important resonance deprotecting effect.

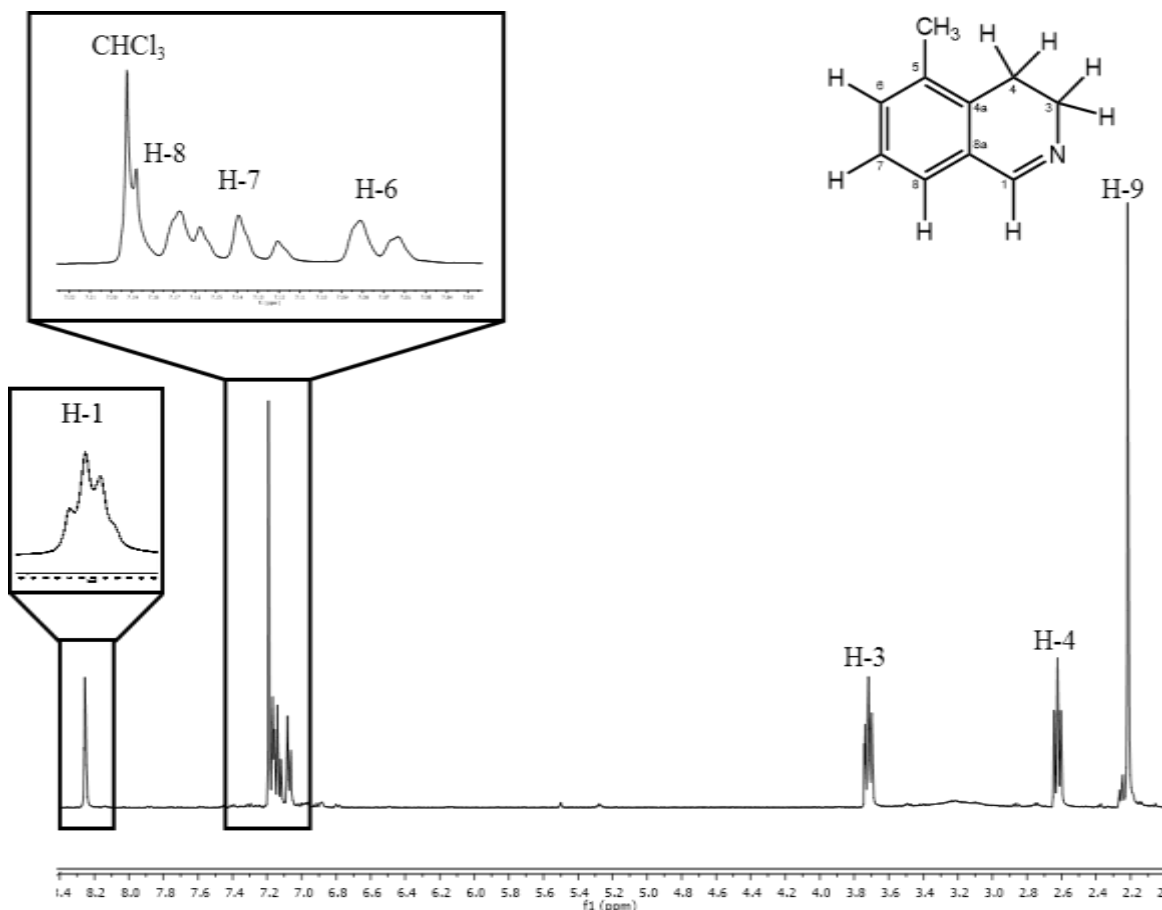


**Figure 36.**  $^1\text{H}$  NMR spectrum of 5-methyl-3,4-dihydroisoquinoline as a direct result of an oxidation by MAO-N D9

### 3.5.2.2 3,4-Dihydroisoquinoline

The oxidation of THIQ (**103a**) with MAO-N D9 or HDNO was monitored over a 48-hour period. A yield over 99% was reached with MAO-N D9, as shown in **Figure 37**. On the other hand, a reduced yield of 50.1% was determined for HDNO in this time period.

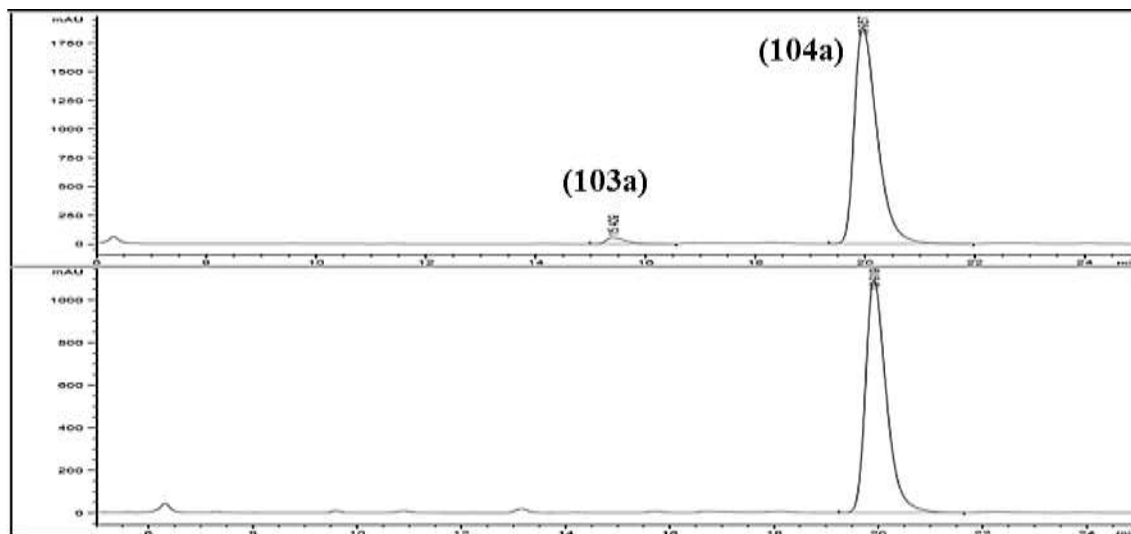
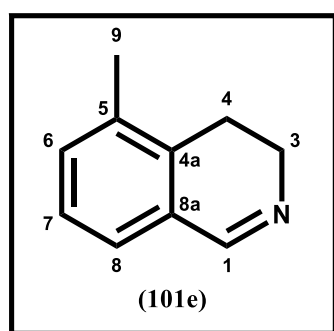


**Figure 37.** Normal phase HPLC trace (CHIRAPACK<sup>®</sup> IC<sup>™</sup> 250 mm x 4.6 mm, 5  $\mu$ m, eluent: hexane/isopropanol/diethylamine = 95/5/0.1, 1 mL/min, 254 nm) of the oxidation of (103a) with HDNO (top) and MAO-N D9 (bottom).  $RT_{[amine]} = 15.03$  min;  $RT_{[imine]} = 20.14$  min.

### 3.5.2.3 5-Methyl-3,4-dihydroisoquinoline

MAO-N D9 was used in the synthesis of 5-methyl-3,4-dihydroisoquinoline (104e) with >99% yield after 2 days, as reported in **Figure 38**. Oxidation with HDNO was also attempted but resulted only in a 23.3% yield.



<sup>1</sup>H NMR (400.13 MHz, CDCl<sub>3</sub>):  $\delta$  (ppm) = 2.22 (s, 3H, H-9); 2.62 (t, 2H, J 7.8 Hz, H-4); 3.72 (dt, 2H, J 7.8 and 2.0 Hz, H-3); 7.07 (d, 1H, J 7.3 Hz, H-6); 7.14 (t, 1H, J 7.3 Hz, H-7); 7.18 (d, 1H, J 8.2 Hz, H-8); 8.25 (t, 1H, J 2.0 Hz, H-1).

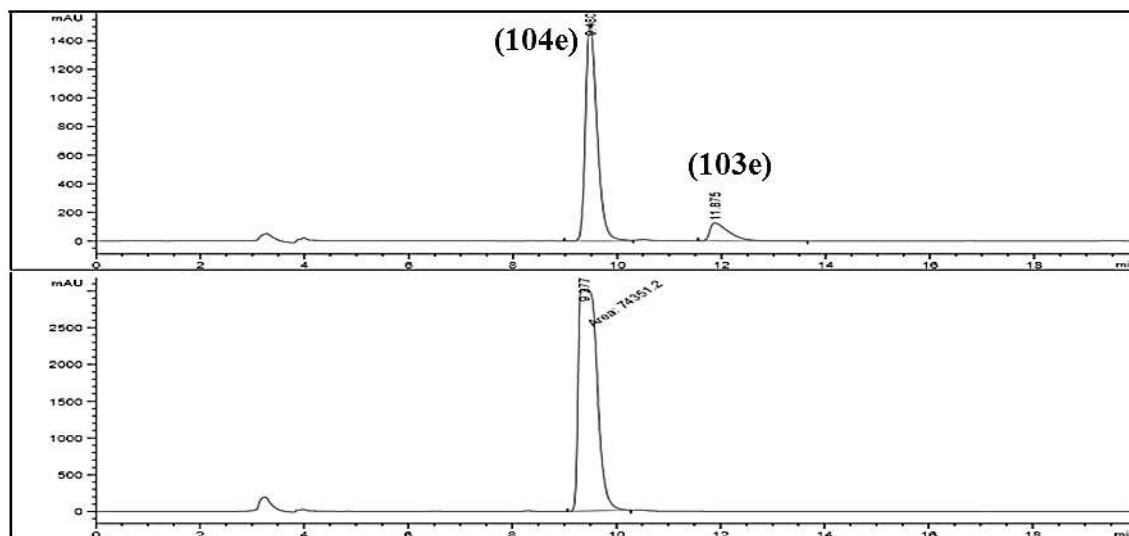
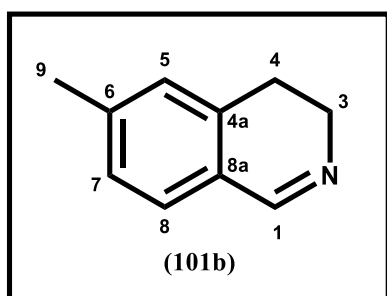


**Figure 38.** Normal phase HPLC trace (CHIRAPACK<sup>®</sup> OD-H 250 mm x 4.6 mm, 5  $\mu$ m, eluent: hexane/isopropanol/diethylamine = 95/5/0.1, 1 mL/min, 254 nm) of the oxidation of (103e) with HDNO (top) and MAO-N D9 (bottom).  $RT_{\text{[amine]}} = 12.01$  min;  $RT_{\text{[imine]}} = 9.51$  min.

### 3.5.2.4 6-Methyl-3,4-dihydroisoquinoline

MAO-N D9 successfully oxidised 6-MTQ (103b) with >90% yield in two days, as seen in **Figure 39**. This result is compatible with the high specific activity presented by this variant in the colorimetric assay. Moreover, HDNO also showed full conversion in this time interval. Still, an unknown compound in high concentration was detected by a peak at 10.4 min in the final HPLC, along with a decrease in the expected imine signal (7.49 min). The presence of an additional enzyme, expressed by the cell and capable of reacting with either the substrate or the product and thus generate a new compound, can explain this phenomenon. Also, but less likely, the unprompted oxidation of the imine (104b) to 6-methyl-3,4-dihydroisoquinolin-1(2*H*)-one may have occurred.



$^1\text{H NMR}$  (400.13 MHz,  $\text{CDCl}_3$ ):  $\delta$  (ppm) = 2.30 (s, 3H, H-9); 2.65 (t, 2H, J 7.8 Hz, H-4); 3.66-3.70 (m, 2H, H-3); 6.91 (s, 1H, H-5); 7.03 (d, 1H, J 7.6 Hz, H-7); 7.11 (d, 1H, J 7.6 Hz, H-8); 8.24 (t, 1H, J 2.0 Hz, H-1).

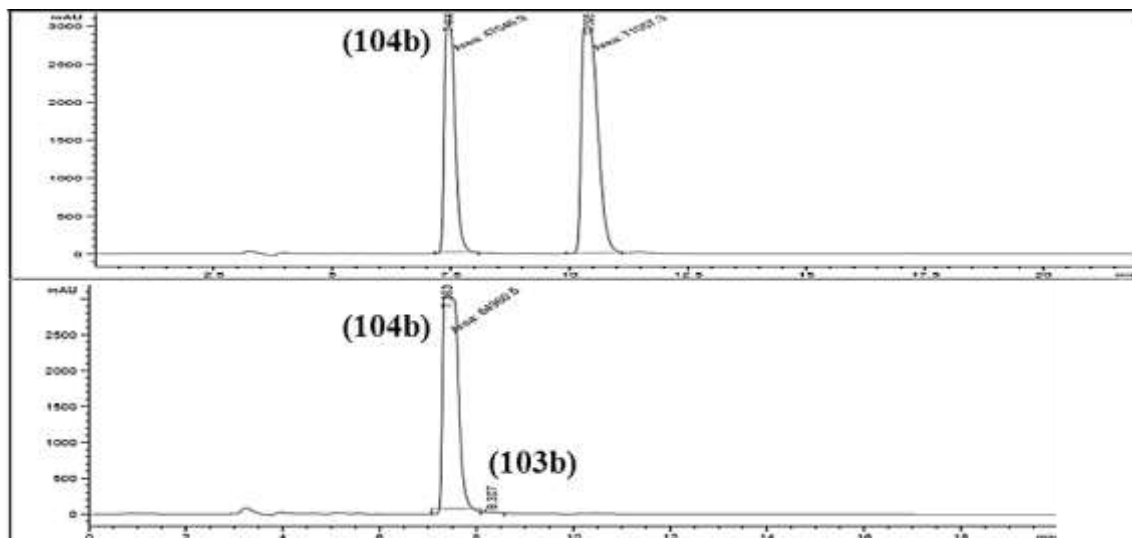
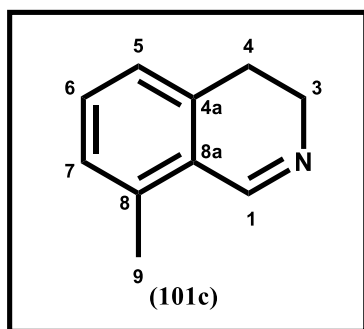


**Figure 39.** Normal phase HPLC trace (CHIRAPACK<sup>®</sup> OD-H 250 mm x 4.6 mm, 5  $\mu$ m, eluent: hexane/isopropanol/diethylamine = 95/5/0.1, 1 mL/min, 254 nm) of the oxidation of (103b) with HDNO (top) and MAO-N D9 (bottom).  $RT_{[amine]} = 8.34$  min;  $RT_{[imine]} = 7.49$  min.

### 3.5.2.5 8-Methyl-3,4-dihydroisoquinoline

Unsurprisingly, > 99 % yield was obtained in the oxidation of 8-MTQ (103c) with MAO-N D9. HDNO was also suitable for this reaction as a yield of 87% was achieved after only two days. The HPLC traces of both reactions can be seen in **Figure 40**.



$^1\text{H NMR}$  (400.13 MHz,  $\text{CDCl}_3$ ):  $\delta$  (ppm) = 2.41 (s, 3H, H-9); 2.64 (t, 2H, J 7.7 Hz, H-4); 3.62-3.67 (m, 2H, H-3); 6.92 (s, 1H, J 7.4 Hz, H-5); 7.01 (d, 1H, J 7.4 Hz, H-7); 7.17 (t, 1H, J 7.4 Hz, H-6); 8.57 (t, 1H, J 2.0 Hz, H-1).

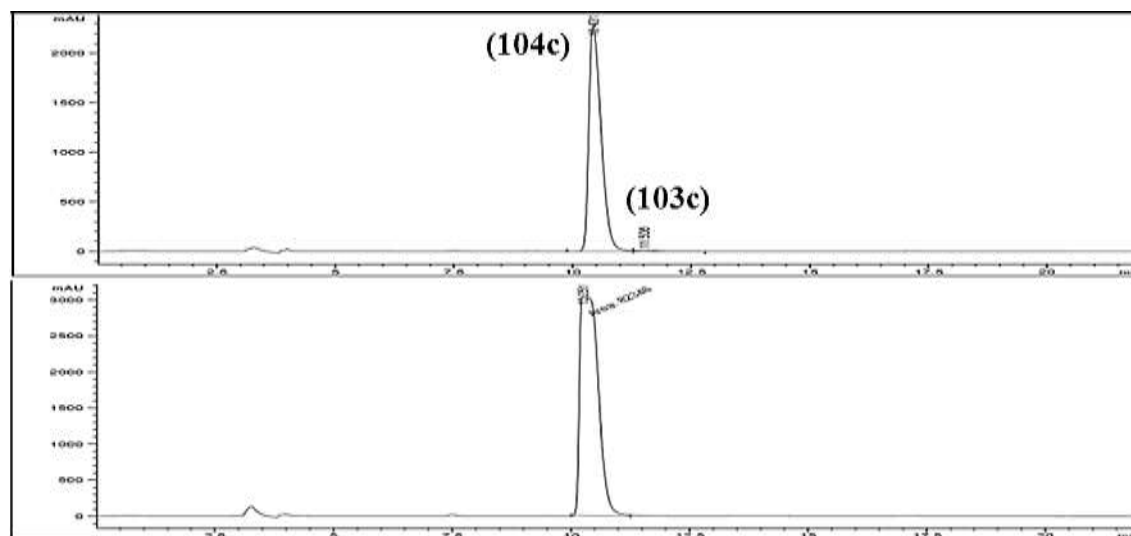
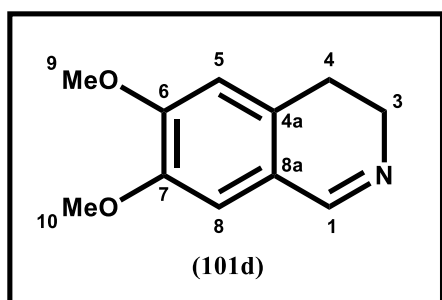


**Figure 40.** Normal phase HPLC trace (CHIRAPACK<sup>®</sup> OD-H 250 mm x 4.6 mm, 5  $\mu$ m, eluent: hexane/isopropanol/diethylamine = 95/5/0.1, 1 mL/min, 254 nm) of the oxidation of (103c) with HDNO (top) and MAO-N D9 (bottom).  $RT_{[amine]} = 11.36$  min;  $RT_{[imine]} = 10.48$  min.

### 3.5.2.6 6,7-Dimethoxy-3,4-dihydroisoquinoline

The oxidation of DMTHIQ (103d) with MAO-N D12 (G) and HDNO was attempted with limited success. Oddly, a shift was found in the substrate HPLC peak's location between the standard (~20 min) and the biotransformation runs (~27 min), preventing a correct calculation of the relative response factor. Nevertheless, the area of the imine (104d) peak in Figure 41 – (top), related to the HDNO biotransformation, is consistent to the product peak areas in previous experiments (~80000). Moreover, previous articles report full conversion of this substrate with HDNO. As so, this value was associated to full conversion to the imine, and yield in the MAO-N D12 (G) biotransformation calculated accordingly – 31.0 %. We highlight these values may not be accurate and must be used as reference with caution.



<sup>1</sup>H NMR (400.13 MHz, CDCl<sub>3</sub>):  $\delta$  (ppm) = 2.61 (t, 2H, J 7.5 Hz, H-4); 3.64-3.69 (m, 2H, H-3); 3.83 (s, 1H, OCH<sub>3</sub>); 3.85 (s, 1H, OCH<sub>3</sub>); 6.60 (s, 1H, H-5); 6.74 (s, 1H, H-8); 8.16 (t, 1H, J 2.0 Hz, H-1).

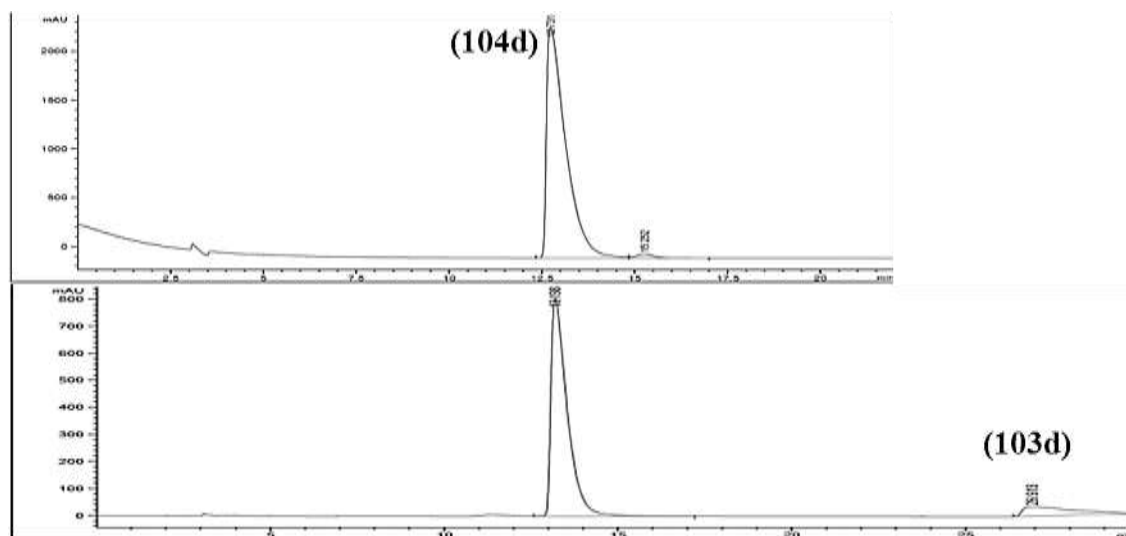
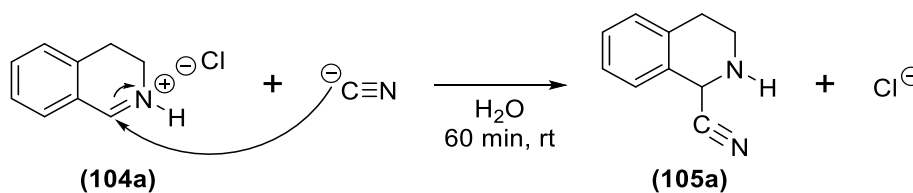


**Figure 41.** Normal phase HPLC trace (CHIRAPACK<sup>®</sup> OD-H 250 mm x 4.6 mm, 5  $\mu$ m, eluent: hexane/isopropanol/diethylamine = 90/10/0.1, 1 mL/min, 254 nm) of the oxidation of (**103d**) with HDNO (top) and MAO-N D12 (G) (bottom).  $RT_{[amine]}= 27.23$  min;  $RT_{[imine]}= 12.73$  min.

### 3.5.3 Synthesis of 1-cyanotetrahydroisoquinolines

1-Cyanotetrahydroisoquinolines (**105 a-d**) were synthesized from the corresponding imines (**104 a-d**) by the addition of cyanide in acid medium, according to the mechanism presented in **Scheme 26**. The previously reported imines from large scale biotransformations were extracted and used directly. <sup>1</sup>H NMR analysis was used to determine the yield of the synthesis of (**104**) and (**105**) compounds, as shown in the following example.



**Scheme 26.** Mechanism for the cyanation of 3,4-dihydroisoquinoline with cyanide

**Figure 42** shows the <sup>1</sup>H NMR spectrum of the reaction product from the cyanation of 3,4-dihydroisoquinoline. It is possible to see two very distinct signals whose ratio allowed an easy and accurate determination of the yield. The signal (**A**), corresponding to the H-1 proton from 3,4-dihydroisoquinoline, is present as a triplet at 8.26 ppm, as previously reported, while the signal corresponding to the same proton in



1-cyanotetrahydroisoquinoline appears as a singlet 4.96 ppm. Though suffering the deshielding inductive effect of the CN triple bond and nitrogen atom and the anisotropic effect of the aromatic ring, this proton did not suffer the previous anisotropic effect of the conjugated double bond, thus suffering a downfield shift. The presence of the equivalent THIQ (**103**), present due to an incomplete oxidation in the first step, can also be detected in some of the spectra by the presence of a singlet peak around 3.8 ppm, corresponding to the H-1 protons.

Additional characteristic 1-cyanotetrahydroisoquinoline signals could be found in the spectrum. First, the presence of a multiplet signal corresponding to the four aromatic protons, indistinguishable due to the lack of additional effects besides the anisotropic effect of the aromatic ring. Then, the presence of a very characteristic ABXY system constituted by the H-3 (AB) and H-4 (XY) protons, leading to three distinct NMR signals: an AB system at 3.2 ppm, in the form of a multiplet, and formed by the signals of the H-3 protons; a doublet of doublets signal (ddd) formed by the coupling of the H<sub>A</sub>-4 proton with H<sub>B</sub>-4 and both H-3 protons with different coupling constants; and a doublet of triplets (dt) formed by the coupling of the remaining H<sub>B</sub>-4 proton with H<sub>A</sub>-4 and with the two H-3 protons, in this case with similar coupling constants. An interesting phenomenon is therefore observed, as the orientation of the H-4 protons is not symmetrical and only one of them couples equally with both H-3 protons. Moreover, it could be verified that in most cases the central peaks of the ddd signal collapsed to form a larger central peak. Finally, the existence of a wide peak at 2.12 ppm, corresponding to the N-H proton, was also found in most spectra.

Important differences can be found in an additional <sup>1</sup>H NMR spectra of methylated 1-cyanotetrahydroisoquinolines. First, the methyl groups can be identified by a singlet signal around 2.25 ppm. Then, the signals corresponding to the aromatic protons can be assigned, with the H-5 and H-7 protons appearing more protected and the H-6 and H-8 protons more deshielded. Finally, in the spectra of 6,7-dimethoxy-1-cyanotetrahydroisoquinoline, the signals corresponding to the methyl groups appears at 3.79 and 3.80 ppm, due to inductive effect of the oxygen atom, and the signals from the aromatic protons suffer a significant upfield effect, due to the resonance effect of their *ortho* position to the methoxy groups.

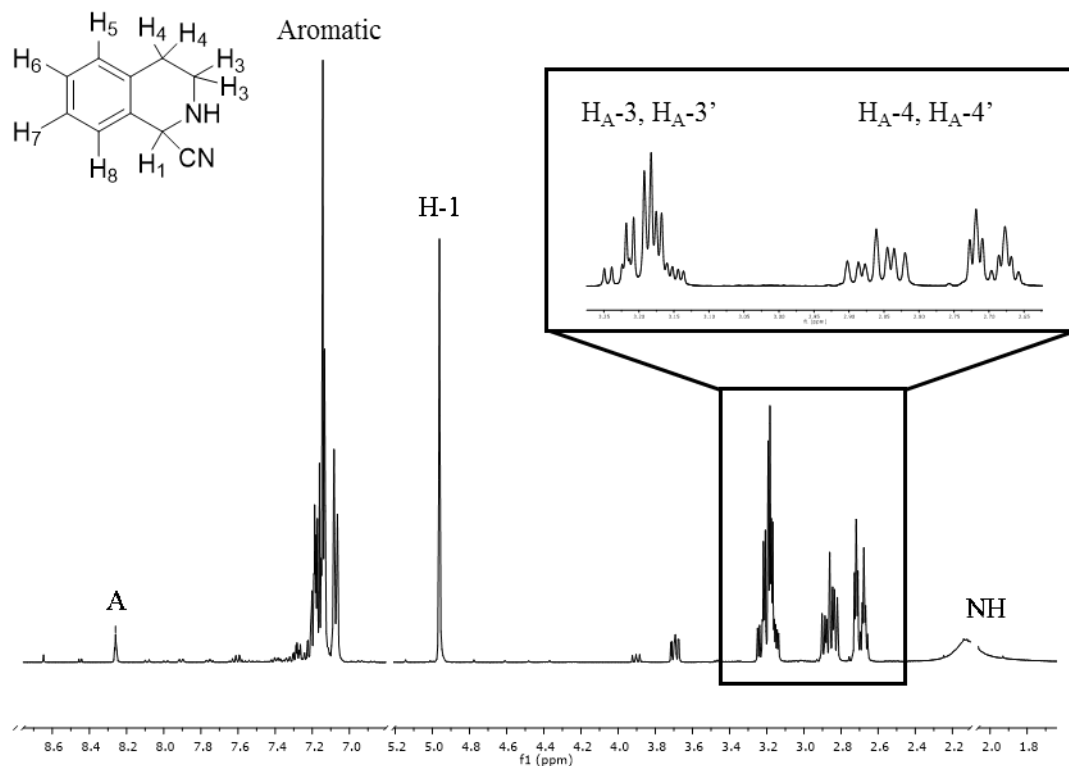


**Figure 42.**  $^1\text{H}$  NMR of the product from the cyanation of 3,4-dihydroisoquinoline

**Figure 43** further shows the  $^{13}\text{C}$  NMR spectrum of the same reaction and can serve as an example for the signal identification of 1-cyanotetrahydroisoquinolines. First, signals in the aliphatic area could be found at 28.23, 40.76 and 48.35 ppm, correspondent to the C-4, C-3 and C-1, respectively. An downfield shift was found in the last two carbons due to the inductive deshielding effect of the proximity to an electronegative atom (NH) and the inductive effect in C-1 of the proximity to a CN group. Next, the signal corresponding to the CN carbon can be seen at 120.2 ppm, suffering an downfield shift by its different hybridization ( $sp$ ) and the inductive effect of the nitrogen atom. Finally, the six signals corresponding to the aromatic carbon can be found between 125 and 135 ppm. First, the four CH signals could not be identified, appearing between 126 and 130 ppm. Then, the two quaternary carbon signals, C-4a and C-8a, were identified at a higher chemical shift (129.42 and 134.71 ppm) due to the inductive effect of an additional C-C bond. The C-8a signal appears at a higher chemical shift due to the additional inductive effect of the proximity to the nitrogen atom.

Some differences can also be found in the  $^{13}\text{C}$  NMR spectrum of the nitriles synthesized. First, the signal corresponding to the methyl carbon appears with the lowest chemical shift, suffering only slightly the inductive effect of the ring. Then, the additional quaternary carbon formed by the presence of a methyl group suffers a downfield effect due to the additional C-C bond, in the range of 10 ppm. Major changes to this spectrum are seen with **(105d)** (**Scheme 21**). First, the signals corresponding to the CH carbons appear at a lower chemical shift, with C-8 suffering the additional inductive effect of the proximity to the cyano group and nitrogen atom. Then, a similar shift is found with the quaternary carbons C-4a and C-8a, whose signal appears at 120.99 and 126.95 ppm. Last, the signals corresponding to the C-6 and C-7 quaternary carbons suffer the highest downfield effect due to the additional inductive effect of the oxygen atom, appearing at 147.87 and 149.17 ppm.

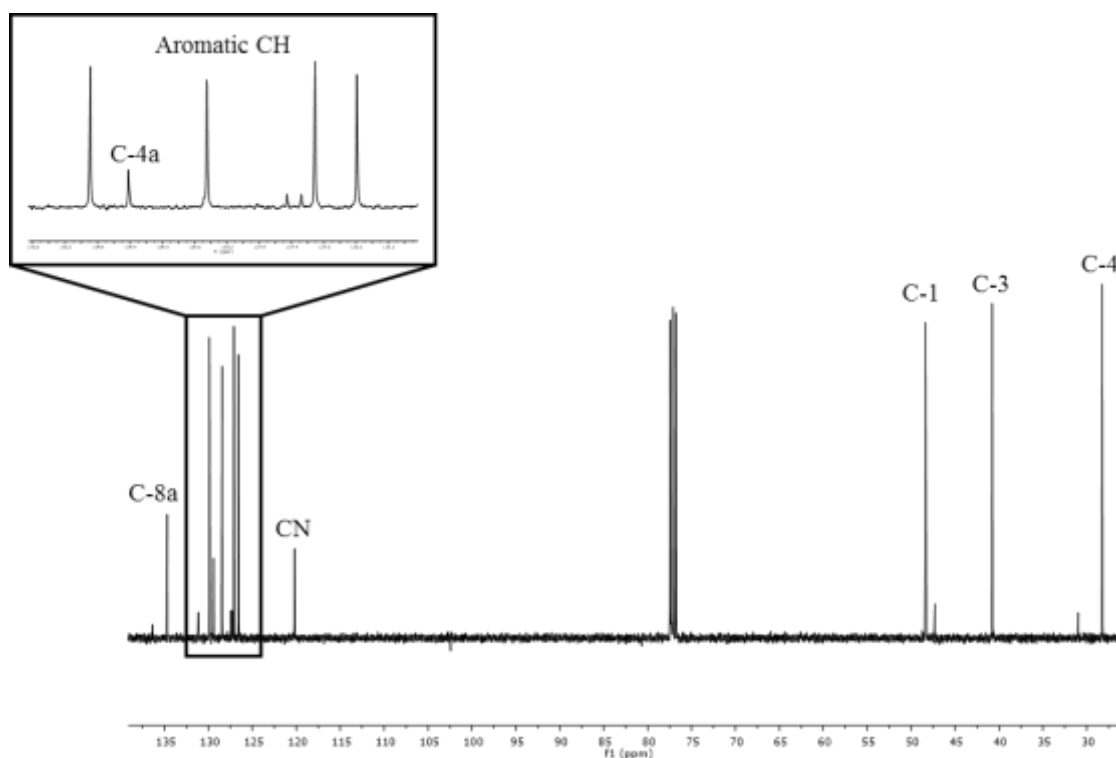
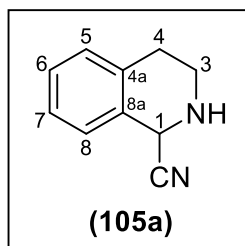


**Figure 43.**  $^{13}\text{C}$  NMR of the product from the cyanation of 3,4-dihydroisoquinoline

## 3.5.3.1 1-Cyanotetrahydroisoquinoline

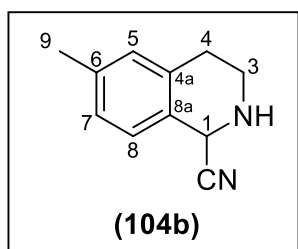


1-Cyanotetrahydroisoquinoline (**105a**) was synthesized from commercial 3,4-dihydroisoquinoline (**104a**) with 91.7 % yield.

**<sup>1</sup>H NMR (400.13 MHz, CDCl<sub>3</sub>):**  $\delta$  (ppm) = 2.10 (s, 1H, NH); 2.70 (dt, 1H, J 16.6 and 3.6 Hz, H-4); 2.86 (ddd, 1H, J 16.5, 10.1 and 6.3 Hz, H-4); 3.13 - 3.23 (m, 2H, H-3); 4.96 (s, 1H, H-1); 7.05 – 7.20 (m, 4H, H-5/H-6/H-7/H-8).

**<sup>13</sup>C NMR (100.6, CDCl<sub>3</sub>):**  $\delta$  (ppm) = 28.23 (C-4); 40.76 (C-3); 48.35 (C-1); 120.20 (CN); 126.59, 127.10, 128.45 and 129.90 (C-5, C-6, C-7 and C-8); 129.42 (C-4a); 134.71 (C-8a).

## 3.5.3.2 1-Cyano-6-methyltetrahydroisoquinoline

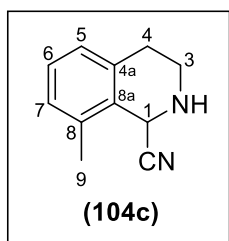


1-Cyano-6-methyltetrahydroisoquinoline (**105b**) was synthesized from 6-methyl-3,4-dihydroisoquinoline (**104b**) with 82.6 % yield. Yield of the two-step synthesis of the cyano compound from 6-MTQ was 70.7 %.

**<sup>1</sup>H NMR (400.13 MHz, CDCl<sub>3</sub>):**  $\delta$  (ppm) = 2.25 (s, 3H, H-9); 2.66-2.72 (m, 1H, H-4); 2.83 (ddd, 1H, J 16.4, 10.1 and 6.3 Hz, H-4); 3.14 - 3.25 (m, 2H, H-3); 4.94 (s, 1H, H-1); 6.90 (s, 1H, H-5); 6.96 (d, 1H, J 7.9 Hz, H-7); 7.04 (d, 1H, J 7.9 Hz, H-8).

**<sup>13</sup>C NMR (100.6 MHz, CDCl<sub>3</sub>):**  $\delta$  (ppm) = 21.13 (C-9); 28.22 (C-4); 40.81 (C-3); 48.15 (C-1); 120.29 (CN); 126.94, 127.46, 130.34 (C-5, C-7 and C-8); 129.82 (C-4a); 134.42 (C-8a); 138.27 (C-6).

## 3.5.3.3 1-Cyano-8-methyltetrahydroisoquinoline

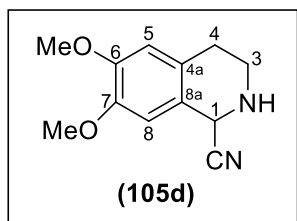


1-Cyano-8-methyltetrahydroisoquinoline (**105c**) was synthesized from 8-methyl-3,4-dihydroisoquinoline (**104c**) with 99.2 % yield. Yield of (**102c**) from 8-MTQ was 56.3 %.

**<sup>1</sup>H NMR (400.13 MHz, CDCl<sub>3</sub>):**  $\delta$  (ppm) = 2.28 (s, 3H, H-9); 2.68 (dt, 1H, J 16.6 and 2.7 Hz, H-4); 2.93 (m, 1H, H-4); 3.19 – 3.24 (m, 2H, H-3); 4.92 (s, 1H, H-1); 6.86 – 7.00 (m, 2H, H-5, H-7); 7.10 (t, 1H, J 7.6 Hz, H-6).

**<sup>13</sup>C NMR (100.6 MHz, CDCl<sub>3</sub>):**  $\delta$  (ppm) = 18.54 (C-9); 28.52 (C-4); 40.31 (C-3); 46.43 (C-1); 119.39 (CN); 127.70, 128.27 and 128.37 (C-5, C-6 and C-7); 127.93 (C-4a); 134.67 and 135.14 (C-8 and C-8a).

## 3.5.3.4 1-Cyano-6,7-dimethoxytetrahydroisoquinoline



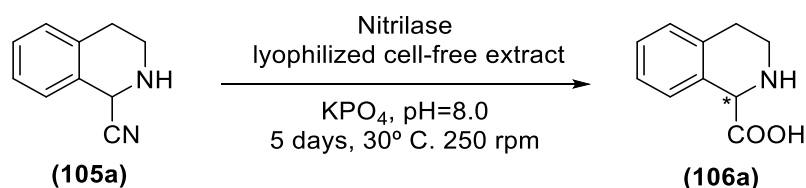
1-Cyano-6,7-dimethoxytetrahydroisoquinoline (**105d**) was synthesized from 6,7-dimethoxy-3,4-dihydroisoquinoline (**104d**) with 71.9 % yield. Accumulated yield for the synthesis of (**105d**) from DMTHIQ was 62.3 %.

**<sup>1</sup>H NMR (400 MHz, CDCl<sub>3</sub>):**  $\delta$  (ppm) = 2.61 (dt, 1H, J 16.4 and 3.6 Hz, H-4); 2.80 (ddd, 1H, J 16.4, 9.6 and 6.8 Hz, H-4); 3.16– 3.21 (m, 2H, H-3); 3.79 (s, 1H, OCH<sub>3</sub>); 3.80 (s, 1H, OCH<sub>3</sub>); 4.90 (s, 1H, H-1); 6.54 (s, 1H, H-5); 6.60 (s, 1H, H-8).

**<sup>13</sup>C NMR (100.6 MHz, CDCl<sub>3</sub>):**  $\delta$  (ppm) = 27.84 (C-4); 40.82 (C-3); 48.07 (C-1); 55.92 (OCH<sub>3</sub>); 56.06 (OCH<sub>3</sub>); 109.36 (C-5); 111.97 (C-8); 120.29 (CN); 120.99 (C-4a); 126.96 (C-8a); 147.87 and 149.17 (C-6 and C-7).

### 3.5.4 Nitrilase in the enantioselective hydrolysis of 1-cyanotetrahydroisoquinoline

To this moment, only 1-cyanotetrahydroisoquinoline was used in the nitrilase catalysed hydrolysis to tetrahydroisoquinoline-1-carboxylic acid (**Scheme 27**), according to the biotransformation described in **Chapter 2**. This substrate was used as is from previous experiments. The reaction was monitored by reverse-phase HPLC, showing loss of enzyme activity after 72 h. As so, more enzyme was added and the reaction monitored for an additional 48 h, leading to a total reaction time of 5 days.



**Scheme 27.** Stereoselective hydrolysis of (**105a**) with nitrilases for the synthesis of tetrahydroisoquinoline-1-carboxylic acid.

Yield in the synthesis of (**106a**) was determined by reverse-phase HPLC with a non-chiral column. A calibration curve was made with standard solutions of commercially available racemic product, as presented in **Annex 1**. Six different nitrilases from Prozomix® - N004, N006, N010, N014, N018, N020 – were tested for this reaction. Unfortunately, only N006 showed significant activity, with a yield of 12.6 % calculated by comparing the carboxylic acid's peak area in **Figure 44** with the calibration curve mentioned.

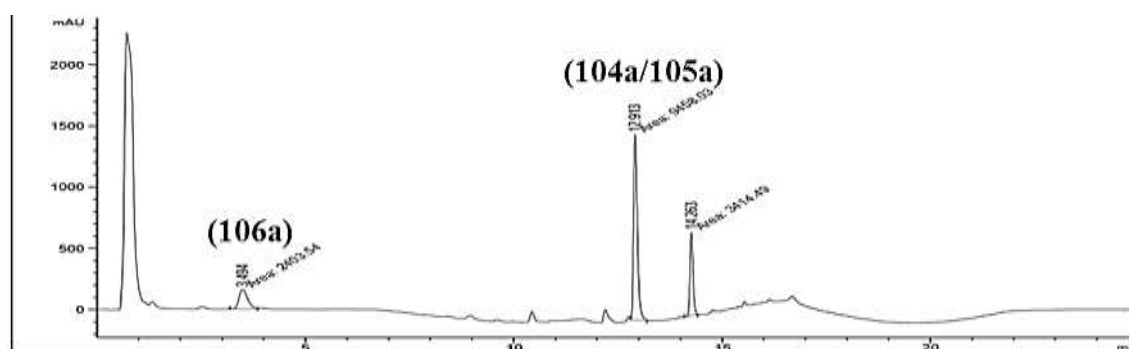


**Figure 44.** Reverse phase HPLC trace (ZORBAX Extend-C18 column 50 mm x 4.6 mm x 3.5  $\mu\text{m}$ , eluent:  $\text{NH}_4\text{OH}$  0.1 M pH=10/ methanol isocratic 90:10 (5 min), gradient from 90:10 to 10:90 (over 15 min), isocratic 10:90 (10 min), 1 mL/min, 40°C, 210 nm) of the biotransformation of unpurified (**105a**) with nitrilase N006.  $\text{RT}_{[\text{acid}]} = 3.35 \text{ min}$ ;  $\text{RT}_{[\text{imine}]} = 12.85 \text{ min}$ ;  $\text{RT}_{[\text{cyano}]} = 12.99 \text{ min}$ .

Next, the samples were run on a reverse-phase HPLC equipped with a chiral column, as shown in **Figure 45**. An enantiomeric excess of 88 % was found in the final run, evidencing the high selectivity of this nitrilase towards **105a**. However, only the racemic standard was available and, therefore, it is impossible to determine to which enantiomer is this enzyme selective.

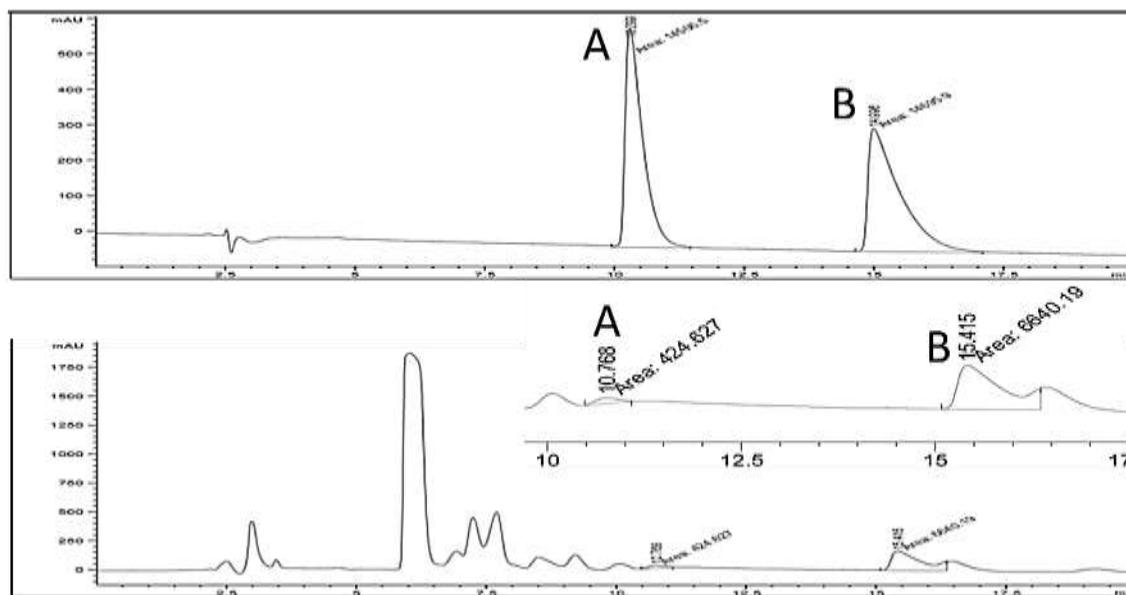


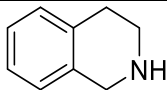
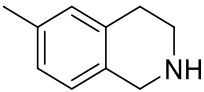
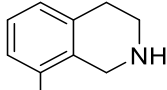
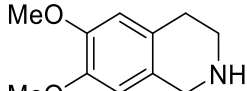
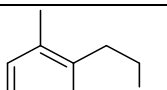
**Figure 45.** Reverse-phase chiral HPLC trace (Chirobiotic T column 250 mm x 46 mm x 5  $\mu$ m, eluent: water/ methanol = 60/40/, 0.8 mL/min, 40°C, 210 nm) of a tetrahydroisoquinoline-1-carboxylic acid 10mM standard (top) and the biotransformation of (**105a**) with nitrilase N006 (bottom). **A** and **B** identify the (**106a**) enantiomer peaks.

### 3.5.5 General discussion

A proof of concept was presented for the enantioselective green synthesis of tetrahydroisoquinoline-1-carboxylic acids from commercially available THIQs. For this synthesis, a one-pot three-step route was envisioned and applied to a range of substituted THIQ's. A summary the results can be found in **Table 9**.

**Table 9.** Summary table for the results described in section 3.5.

\*Accumulated yield from (**103**)

Substrate	Imine ( <b>104 a-e</b> ) *	Nitrile ( <b>105 a-d</b> ) *	Acid ( <b>106a</b> ) *
 <b>(103a)</b>	>99% MAO-N D9 50.1% HDNO	91.7%	12.6% <b>(88% e.e.)</b>
 <b>(103b)</b>	>90% MAO-N D9 >99% HDNO (conversion)	70.7%	-
 <b>(103c)</b>	>99% MAO-N D9 86.7% HDNO	56.3%	-
 <b>(103d)</b>	31.0% MAO-N D12 (G) >99% HDNO	62.3%	-
 <b>(103e)</b>	>99% MAO-N D9 23.3% HDNO	-	-



Results clearly show that MAO-N D9 promptly catalyses the oxidation of unsubstituted and 5, 6 or 8-methyl THIQs with excellent yields. However, 3, 4 and 7 substitutions are still not tolerated by this variant. These results appear consistent to the specific activity assays and further attest the limited substrate scope of MAO-N. Nevertheless, HDNO proved to be a great alternative in the oxidation of dimethoxylated THIQ, increasing the range of tetrahydroisoquinoline alkaloids covered by this method. Sadly, scale-up considerably lowered the conversion, limiting the future steps of this synthetic route.

All synthesized 3,4-dihydroisoquinolines were used in a cyanation reaction for the synthesis of 1-cyano compounds. Although good conversion was observed with all substrates, with a two-step overall yield over 57%, experiments showed that a slightly basic pH is required for the reaction to occur. Moreover, it is hypothesized that further studies in the scale-up of the enzymatic oxidation and further optimization of the cyanation procedure can potentially lead to overall yields over 90%.

Finally, 1-cyanotetrahydroisoquinoline was chosen to study its selective hydrolysis with six commercial nitrilases by Prozomix<sup>®</sup>. From those, only the N006 variant showed any significant activity with this substrate, reaching 12.6% yield with a remarkable e.e. of 88%. The great selectivity of this enzyme does limit the yield to a maximum of 50%, therefore raising the theoretical yield to around 25%. Moreover, we conjecture that a more regular addition of new enzyme to the reaction could increase the final yield, as results have shown that the enzyme lost all activity after 72 h. Nevertheless, the yield obtained must be thoroughly analysed, as a green synthetic route towards these high value compounds, using cheap and available reagents and performed in water at low temperatures had not been previously reported. In fact, a 100-fold price valorisation can be found between the commercial amine and the racemic acid synthesized.



# CHAPTER 4. CONCLUSIONS AND FUTURE PROSPECTS



In this work, the potential of biocatalysis in the synthesis of chiral amines with industrial and pharmacological applications was explored. In particular, monoamine oxidase variants from *Aspergillus niger* were used in the deracemisation and functionalization of tetrahydroisoquinolines. Also, the substrate scope of MAO-N variants with these substrates was studied and its results used in the design of a new mutant for the deracemisation of salsolidine.

It was determined that substitutions in the various positions of THIQ can seriously hinder or improve the activity of MAO-N variants. From these results a new mutant (MAO-N D13) was developed and proved effective in the oxidation of salsolidine. Unfortunately, DKR of this substrate could not be accomplished. Next, MAO-N variants and HDNO were used in the successful deracemisation of  $\alpha$ -AMBA and several THIQ derivatives.

Finally, a proof of concept is presented for the highly enantioselective one-pot three-step synthesis of tetrahydroisoquinoline-1-carboxylic acid from its C1 unsubstituted analogue. It is shown that this new cascade reaction can also potentially be applied to aromatic substituted THIQs. In fact, the production of a highly valuable chiral compound from a simple and easily obtainable derivative from petroleum can prove of great assistance in future industrial applications, placing a versatile functional group and therefore increasing its potential use as templates in the synthesis of tetrahydroisoquinoline alkaloids. More important, the synthesis of 1-carboxylic acid derivatives has only been briefly reported in the literature, and the pharmacological potential of this novel and complex  $\alpha$ -amino acids remains to be explored.

Nevertheless, the work performed during this master thesis stands only as a starting point in new potential routes for the development of MAO-N in biocatalysis. First, the expression of MAO-N D9 in the newly obtained *Pichia pastoris* cells must be finished to determine its ability to express large quantities of protein. If successful, this method can be used to express other variants and eventually substitute *E. coli* as the chosen organism for a relatively fast expression of great amounts of MAO-N.

Moreover, the search for MAO-N variants with diverse substrate scopes should continue, as shown in the remarkable results of the substrate screening. As an example, new variants with increased activity for 3-MTQ and 4-MTQ could prove effective in the oxidation of these substrates. Also, additional mutations to MAO-N D13, possibly from the mutations in the

MAO-N D12 mutants, could finally lead to a successful and fast deracemisation of salsolidine.

Considerable work is still required in the optimization of the enzymatic cascade shown above. Additional experiments could overcome the decrease in conversion verified in the scale-up of the amine oxidation, and optimization of the optimal pH conditions for the cyanation is still required. Moreover, the development of a protocol that does not require product extraction would prove advantageous in future applications, saving both time and solvents. Also, in a non-extracting protocol the use of a stoichiometric amount of cyanide would be preferential to avoid enzyme poisoning in the last step. Last, to increase the overall yield new nitrilases could be acquired and tested for its ability to selectively hydrolyse these cyano compounds.

In a wider perspective, investigation of the applicability of this new synthetic route to different substrates could lead to an increasingly used method to chiral amino acids. Also, the discovery of new mutants with unreported and exciting new characteristics can stimulate new applications for these enzymes. Most importantly, the development, in this work, of new segments for future exploration can hopefully encourage the scientific community to re-orient its investigation back to this overlooked high-potential monoamine oxidase.

## CHAPTER 5. REFERENCES





## Chapter 5. references

- (1) Flack, H. D. Louis Pasteur's Discovery of Molecular Chirality and Spontaneous Resolution in 1848, Together with a Complete Review of His Crystallographic and Chemical Work. *Acta Crystallogr.* **2009**, *A65*, 371–389.
- (2) Millership, J. S.; Fitzpatrick, A. Commonly Used Chiral Drugs: A Survey. *Chirality* **1993**, *5*, 573–576.
- (3) Vargesson, N. Thalidomide-Induced Teratogenesis: History and Mechanisms. *Birth Defects Res. C* **2015**, *105*, 140–156.
- (4) Gellad, W. F.; Choi, P.; Mizah, M.; Good, C. B.; Kesselheim, A. S. Assessing the Chiral Switch: Approval and Use of Single-Enantiomer Drugs, 2001 to 2011. *Am. J. Manag. Care* **2014**, *20*, e90–e97.
- (5) France, S.; Guerin, D. J.; Miller, S. J.; Lectka, T. Nucleophilic Chiral Amines as Catalysts in Asymmetric Synthesis. *Chem. Rev.* **2003**, *103*, 2985–3012.
- (6) Chiral resolving agents (accessed Oct 5, 2016).  
<http://www.sigmaaldrich.com/chemistry/chemistryproducts.html?TablePage=16265015>.
- (7) Axet, M. R.; Amoroso, F.; Bottari, G.; D'Amora, A.; Zangrando, E.; Faraone, F.; Drommi, D.; Saporita, M.; Carfagna, C.; Natanti, P.; Seraglia, R.; Milani, B. Application of Chiral Amine-Imine Ligands in Palladium-Catalyzed Polyketone Synthesis: Effect of Ligand Backbone on the Polymer Stereochemistry. *Organometallics* **2009**, *28*, 4464–4474.
- (8) Salvatore, R. N.; Yoon, C. H.; Jung, K. W. Synthesis of Secondary Amines. *Tetrahedron* **2001**, *57*, 7785–7811.
- (9) Lawrence, S. *Amines: Synthesis, Properties and Applications*, 1st Edition.; Cambridge University Press, **2004**.
- (10) Nugent, T. C.; El-Shazly, M. Chiral Amine Synthesis - Recent Developments and Trends for Enamide Reduction, Reductive Amination, and Imine Reduction. *Adv. Synth. Catal.* **2010**, *352*, 753–819.
- (11) Gawley, R. E.; Aubé, J. Introduction, General Principles, and Glossary of Stereochemical Terms. In *Principles of Asymmetric Synthesis*; Elsevier, **2012**; Vol. 1, pp 1–62.
- (12) Ghattas, G.; Chen, D.; Pan, F.; Klankermayer, J. Asymmetric Hydrogenation of Imines with a Recyclable Chiral Frustrated Lewis Pair Catalyst. *Dalton Trans.* **2012**, *41*, 9026–9028.
- (13) Salomó, E.; Orgué, S.; Riera, A.; Verdaguer, X. Highly Enantioselective Iridium-Catalyzed Hydrogenation of Cyclic Enamides. *Angew. Chem. Int. Ed.* **2016**, *55*, 7988–7992.
- (14) Lou, H.; Wang, Y.; Jin, E.; Lin, X. Organocatalytic Asymmetric Synthesis of Dihydrobenzoxazinones Bearing Trifluoromethylated Quaternary Stereocenters. *J. Org. Chem.* **2016**, *81*, 2019–2026.
- (15) Cai, X. H.; Xie, B. Recent Advances on Organocatalysed Asymmetric Mannich Reactions. *Arkivoc* **2013**, 264–293.
- (16) Hansen, K. B.; Hsiao, Y.; Xu, F.; Rivera, N.; Clausen, A.; Kubryk, M.; Krska, S.; Rosner, T.; Simmons, B.; Balsells, J.; Ikemoto, N.; Sun, Y.; Spindler, F.; Malan, C.; Grabowski, E. J. J.; Armstrong, J. D. Highly Efficient Asymmetric Synthesis of Sitagliptin. *J. Am. Chem. Soc.* **2009**, *131*, 8798–8804.
- (17) Mulzer, J. Introductory Remarks: Chiral Pool Syntheses and Diastereoselective Reactions. In *Comprehensive Chirality*; Elsevier, **2012**; Vol. 2, pp 1–8.
- (18) Dalpozzo, R. The Chiral Pool in the Pictet–Spengler Reaction for the Synthesis of  $\beta$ -Carbolines. *Molecules* **2016**, *21*, Article 699.
- (19) Pasteur, L. Recherches Sur Les Propriétés Spécifiques Des Deux Acides Qui Composent L'acide Racémique. *Ann. Chim. Phys.* **1850**, *28*, 56–117.
- (20) Pasteur, L. Transformation Des Acides Tartriques En Acide Racémique. Découverte de L'acide Tarrifique Inactif. Nouvelle Méthode de Séparation de L'acide Racémique En Acides Tarrifiques Droit et Gauche. *Comptes rendus Hebd. des séances l'Académie des Sci.* **1853**, *37*, 162–166.
- (21) Woelfle, M.; Seerden, J.-P.; de Gooijer, J.; Pouwer, K.; Olliaro, P.; Todd, M. H. Resolution of Praziquantel. *PLoS Negl. Trop. Dis.* **2011**, *5*, Article e1260.
- (22) Kagan, H. B.; Fiaud, J. C. Kinetic Resolution. In *Topics in Stereochemistry*; Eliel, E., Wilen, S., Eds.; John Wiley & Sons, Inc., 1988; Vol. 18, pp 249–330.

## Chapter 5. references

- (23) Rachwalski, M.; Vermue, N.; Rutjes, F. P. J. T. Recent Advances in Enzymatic and Chemical Deracemisation of Racemic Compounds. *Chem. Soc. Rev.* **2013**, *42*, 9268–9282.
- (24) Yasukawa, K.; Hasemi, R.; Asano, Y. Dynamic Kinetic Resolution of  $\alpha$ -Aminonitriles to Form Chiral  $\alpha$ -Amino Acids. *Adv. Synth. Catal.* **2011**, *353*, 2328–2332.
- (25) Hesse, M. Isoquinoline Alkaloids. In *Alkaloids: Nature's Curse or Blessing?*; Wallímann, P., Kisakürek, M., Eds.; VHCA, WILEY-VCH, **2003**; pp 36–54.
- (26) Ysern, M.; Ordoñez, L. Tetrahydroisoquinolines: A Review. *Prog. Neuro-psychopharmacol.* **1981**, *5*, 343–355.
- (27) Myers, R. D. Tetrahydroisoquinolines and Alcoholism: Where Are We Today? *Alcohol. Clin. Exp. Res.* **1996**, *20*, 498–500.
- (28) Naoi, M. Dopamine-Derived Salsolinol Derivatives as Endogenous Monoamine Oxidase Inhibitors: Occurrence, Metabolism and Function in Human Brains. *Neurotoxicology* **2004**, *25*, 193–204.
- (29) Yi, H.; Akao, Y.; Maruyama, W.; Chen, K.; Shih, J.; Naoi, M. Type A Monoamine Oxidase Is the Target of an Endogenous Dopaminergic Neurotoxin, N-Methyl-(R)Salsolinol, Leading to Apoptosis in SH-SY5Y Cells. *J. Neurochem.* **2006**, *96*, 541–549.
- (30) Roessner, V.; Walitza, S.; Riederer, F.; Hünnerkopf, R.; Rothenberger, A.; Gerlach, M.; Moser, A. Tetrahydroisoquinoline Derivatives: A New Perspective on Monoaminergic Dysfunction in Children with ADHD? *Behav. Brain Funct.* **2007**, *3*, Article 64.
- (31) Naito, R.; Yonetoku, Y.; Okamoto, Y.; Toyoshima, A.; Ikeda, K.; Takeuchi, M. Synthesis and Antimuscarinic Properties of Quinuclidin-3-yl 1,2,3,4-Tetrahydroisoquinoline-2-Carboxylate Derivatives as Novel Muscarinic Receptor Antagonists. *J. Med. Chem.* **2005**, *48*, 6597–6606.
- (32) Mang, G. M.; Dürst, T.; Bürki, H.; Imobersteg, S.; Abramowski, D.; Schuepbach, E.; Hoyer, D.; Fendt, M.; Gee, C. E. The Dual Orexin Receptor Antagonist Almorexant Induces Sleep and Decreases Orexin-Induced Locomotion by Blocking Orexin 2 Receptors. *Sleep* **2012**, *35*, 1625–1635.
- (33) Chander, S.; Ashok, P.; Singh, A.; Murugesan, S. De-Novo Design, Synthesis and Evaluation of Novel 6,7-Dimethoxy-1,2,3,4-Tetrahydroisoquinoline Derivatives as HIV-1 Reverse Transcriptase Inhibitors. *Chem. Cent. J.* **2015**, *9*, Article 33.
- (34) Gangapuram, M. Synthesis and Pharmacological Evolution of Tetrahydroisoquinolines as Anti Breast Cancer Agents. *J. Cancer Sci. Ther.* **2014**, *6*, 161–169.
- (35) Capparelli, E.; Zinzi, L.; Cantore, M.; Contino, M.; Perrone, M. G.; Luurtsema, G.; Berardi, F.; Perrone, R.; Colabufo, N. A. SAR Studies on Tetrahydroisoquinoline Derivatives: The Role of Flexibility and Bioisosterism To Raise Potency and Selectivity toward P-Glycoprotein. *J. Med. Chem.* **2014**, *57*, 9983–9994.
- (36) Kotha, S.; Deodhar, D.; Khedkar, P. Diversity-Oriented Synthesis of Medicinally Important 1,2,3,4-Tetrahydroisoquinoline-3-Carboxylic Acid (Tic) Derivatives and Higher Analogs. *Org. Biomol. Chem.* **2014**, *12*, 9054–9091.
- (37) Tsukiyama, M.; Ueki, T.; Yasuda, Y.; Kikuchi, H.; Akaishi, T.; Okumura, H.; Abe, K.  $\beta$  2 - Adrenoceptor-Mediated Tracheal Relaxation Induced by Higenamine from *Nandina Domestica* Thunberg. *Planta Med.* **2009**, *75*, 1393–1399.
- (38) Yin, J.; Xing, H.; Ye, J. Efficacy of Berberine in Patients with Type 2 Diabetes. *Metabolism* **2008**, *57*, 712–717.
- (39) Pang, B.; Zhao, L.-H.; Zhou, Q.; Zhao, T.; Wang, H.; Gu, C.; Tong, X. Application of Berberine on Treating Type 2 Diabetes Mellitus. *Int. J. Endocrinol.* **2015**, Article 905409.
- (40) Pictet, A.; Spengler, T. Über Die Bildung von Isochinolin-Derivaten Durch Einwirkung von Methylal Auf Phenyl-Äthylamin, Phenyl-Alanin Und Tyrosin. *Berichte der Dtsch. Chem. Gesellschaft* **1911**, *44*, 2030–2036.
- (41) Stöckigt, J.; Antonchick, A. P.; Wu, F.; Waldmann, H. The Pictet-Spengler Reaction in Nature and in Organic Chemistry. *Angew. Chem. Int. Ed.* **2011**, *50*, 8538–8564.

## Chapter 5. references

- (42) Comins, D. L.; Thakker, P. M.; Baevsky, M. F.; Badawi, M. M. Chiral Auxiliary Mediated Pictet-Spengler Reactions: Asymmetric Syntheses of (–)-Laudanosine, (+)-Glaucine and (–)-Xylopinine. *Tetrahedron* **1997**, *53*, 16327–16340.
- (43) Saito, A.; Numaguchi, J.; Hanzawa, Y. Pictet–Spengler Reactions Catalyzed by Brønsted Acid-Surfactant-Combined Catalyst in Water or Aqueous Media. *Tetrahedron Lett.* **2007**, *48*, 835–839.
- (44) Mons, E.; Wanner, M. J.; Ingemann, S.; van Maarseveen, J. H.; Hiemstra, H. Organocatalytic Enantioselective Pictet–Spengler Reactions for the Syntheses of 1-Substituted 1,2,3,4-Tetrahydroisoquinolines. *J. Org. Chem.* **2014**, *79*, 7380–7390.
- (45) Bonamore, A.; Rovardi, I.; Gasparrini, F.; Baiocco, P.; Barba, M.; Molinaro, C.; Botta, B.; Boffi, A.; Macone, A. An Enzymatic, Stereoselective Synthesis of (S)-Norcoclaurine. *Green Chem.* **2010**, *12*, 1623–1627.
- (46) Nishihachijo, M.; Hirai, Y.; Kawano, S.; Nishiyama, A.; Minami, H.; Katayama, T.; Yasohara, Y.; Sato, F.; Kumagai, H. Asymmetric Synthesis of Tetrahydroisoquinolines by Enzymatic Pictet–Spengler Reaction. *Biosci. Biotechnol. Biochem.* **2014**, *78*, 701–707.
- (47) Minami, H.; Kim, J.-S.; Ikezawa, N.; Takemura, T.; Katayama, T.; Kumagai, H.; Sato, F. Microbial Production of Plant Benzyloisoquinoline Alkaloids. *PNAS* **2008**, *105*, 7393–7398.
- (48) Nagubandi, S.; Fodor, G. The Mechanism of the Bischler-Napieralski Reaction. *Angew. Chem. Int. Ed.* **1972**, *11*, 919–920.
- (49) Wang, Z. Pomeranz-Fritsch Reaction. In *Comprehensive Organic Name Reactions and Reagents*; John Wiley & Sons, Inc.: Hoboken, NJ, USA, **2010**; 2256–2259.
- (50) Grajewska, A.; Rozwadowska, M. D. Diastereoselective Pomeranz–Fritsch–Bobbitt Synthesis of (S)-(–)-O-Methylbharatamine Using (S)-N-Tert-Butanesulfinimine as a Substrate. *Tetrahedron: Asymmetry* **2007**, *18*, 2910–2914.
- (51) Wenda, S.; Illner, S.; Mell, A.; Kragl, U. Industrial Biotechnology—the Future of Green Chemistry? *Green Chem.* **2011**, *13*, 3007–3047.
- (52) Sheldon, R. A. The E Factor: Fifteen Years on. *Green Chem.* **2007**, *9*, 1273.
- (53) Woodley, J. M. New Opportunities for Biocatalysis: Making Pharmaceutical Processes Greener. *Trends Biotechnol.* **2008**, *26*, 321–327.
- (54) Ma, S. K.; Gruber, J.; Davis, C.; Newman, L.; Gray, D.; Wang, A.; Grate, J.; Huisman, G. W.; Sheldon, R. A. A Green-by-Design Biocatalytic Process for Atorvastatin Intermediate. *Green Chem.* **2010**, *12*, 81–86.
- (55) Ress-Loschke, M.; Friedrich, T.; Hauer, B.; Mattes, R.; Engels, D. Method for Producing Chiral Carboxylic Acids from Nitriles with the Assistance of a Nitrilase or Microorganisms Which Contain a Gene for the Nitrilase. CA2347521 A1, **2000**.
- (56) Lancaster, M. Renewable Resources. In *Green Chemistry: An Introductory Text*; Lancaster, M., Ed.; The Royal Society of Chemistry, **2002**; pp 166–209.
- (57) Savile, C. K.; Janey, J. M.; Mundorff, E. C.; Moore, J. C.; Tam, S.; Jarvis, W. R.; Colbeck, J. C.; Krebber, A.; Fleitz, F. J.; Brands, J.; Devine, P. N.; Huisman, G. W.; Hughes, G. J. Biocatalytic Asymmetric Synthesis of Chiral Amines from Ketones Applied to Sitagliptin Manufacture. *Science* **2010**, *329*, 305–309.
- (58) Bornscheuer, U. T.; Huisman, G. W.; Kazlauskas, R. J.; Lutz, S.; Moore, J. C.; Robins, K. Engineering the Third Wave of Biocatalysis. *Nature* **2012**, *485*, 185–194.
- (59) Lorenz, P.; Schleper, C. Metagenome—a Challenging Source of Enzyme Discovery. *J. Mol. Catal. B: Enzym.* **2002**, *19–20*, 13–19.
- (60) Culligan, E. P.; Sleator, R. D.; Marchesi, J. R.; Hill, C. Metagenomics and Novel Gene Discovery. *Virulence* **2014**, *5*, 399–412.
- (61) Frommer, W. B.; Ninnemann, O. Heterologous Expression of Genes in Bacterial, Fungal, Animal, and Plant Cells. *Annu. Rev. Plant Physiol. Plant Mol. Biol.* **1995**, *46*, 419–444.

## Chapter 5. references

- (62) Ahmad, M.; Hirz, M.; Pichler, H.; Schwab, H. Protein Expression in *pichia Pastoris*: Recent Achievements and Perspectives for Heterologous Protein Production. *Appl. Microbiol. Biotechnol.* **2014**, *98*, 5301–5317.
- (63) *E. coli* Plasmid Vectors. In *Methods in Molecular Biology*; Casali, N., Preston, A., Eds.; Humana Press, **2003**; Vol. 235, pp 1–304.
- (64) Protein Purification Protocols. In *Methods in Molecular Biology*; Cutler, P., Ed.; Humana Press, **2004**.
- (65) Quax, T. E. F.; Claassens, N. J.; Söll, D.; Oost, J. Codon Bias as a Means to Fine-Tune Gene Expression. *Mol. Cell* **2015**, *59*, 149–161.
- (66) Bill, R. M. Playing Catch-up with *Escherichia coli*: Using Yeast to Increase Success Rates in Recombinant Protein Production Experiments. *Front. Microbiol.* **2014**, *5*, Article 85.
- (67) Romero, P. A.; Arnold, F. H. Exploring Protein Fitness Landscapes by Directed Evolution. *Nat. Rev. Mol. Cell Biol.* **2009**, *10*, 866–876.
- (68) Shafee, T. Evolvability of a Viral Protease: Experimental Evolution of Catalysis, Robustness and Specificity, University of Cambridge, **2013**.
- (69) Xiao, H.; Bao, Z.; Zhao, H. High Throughput Screening and Selection Methods for Directed Enzyme Evolution. *Ind. Eng. Chem. Res.* **2015**, *54*, 4011–4020.
- (70) Currin, A.; Swainston, N.; Day, P. J.; Kell, D. B. Synthetic Biology for the Directed Evolution of Protein Biocatalysts: Navigating Sequence Space Intelligently. *Chem. Soc. Rev.* **2015**, *44*, 1172–1239.
- (71) Melzer, S.; Sonnendecker, C.; Föllner, C.; Zimmermann, W. Stepwise Error-Prone PCR and DNA Shuffling Changed the pH Activity Range and Product Specificity of the Cyclodextrin Glucanotransferase from an Alkaliphilic *Bacillus Sp.* *FEBS Open Bio* **2015**, *5*, 528–534.
- (72) Raj, H.; Szymański, W.; de Villiers, J.; Rozeboom, H. J.; Veetil, V. P.; Reis, C. R.; de Villiers, M.; Dekker, F. J.; de Wildeman, S.; Quax, W. J.; Thunnissen, A.-M. W. H.; Feringa, B. L.; Janssen, D. B.; Poelarends, G. J. Engineering Methylaspartate Ammonia Lyase for the Asymmetric Synthesis of Unnatural Amino Acids. *Nat. Chem.* **2012**, *4*, 478–484.
- (73) Schuster, B.; Retey, J. The Mechanism of Action of Phenylalanine Ammonia-Lyase: The Role of Prosthetic Dehydroalanine. *Proc. Natl. Acad. Sci. USA* **1995**, *92*, 8433–8437.
- (74) Rowles, I.; Groenendaal, B.; Binay, B.; Malone, K. J.; Willies, S. C.; Turner, N. J. Engineering of Phenylalanine Ammonia Lyase from *Rhodotorula graminis* for the Enhanced Synthesis of Unnatural L-Amino Acids. *Tetrahedron* **2016**, *72*, 7343–7347.
- (75) de Lange, B.; Hyett, D. J.; Maas, P. J. D.; Mink, D.; van Assema, F. B. J.; Sereinig, N.; de Vries, A. H. M.; de Vries, J. G. Asymmetric Synthesis of (*S*)-2-Indolinecarboxylic Acid by Combining Biocatalysis and Homogeneous Catalysis. *ChemCatChem* **2011**, *3*, 289–292.
- (76) Abrahamson, M. J.; Vázquez-Figueroa, E.; Woodall, N. B.; Moore, J. C.; Bommaris, A. S. Development of an Amine Dehydrogenase for Synthesis of Chiral Amines. *Angew. Chem. Int. Ed.* **2012**, *51*, 3969–3972.
- (77) Ye, L. J.; Toh, H. H.; Yang, Y.; Adams, J. P.; Snajdrova, R.; Li, Z. Engineering of Amine Dehydrogenase for Asymmetric Reductive Amination of Ketone by Evolving *Rhodococcus* Phenylalanine Dehydrogenase. *ACS Catal.* **2015**, *5*, 1119–1122.
- (78) Oshima, T.; Tamiya, N. Mechanism of Transaminase Action. *Biochem. J.* **1961**, *78*, 116–119.
- (79) Park, E.-S.; Shin, J.-S.  $\omega$ -Transaminase from *Ochrobactrum anthropi* Is Devoid of Substrate and Product Inhibitions. *Appl. Environ. Microbiol.* **2013**, *79*, 4141–4144.
- (80) O'Reilly, E.; Iglesias, C.; Ghislieri, D.; Hopwood, J.; Galman, J. L.; Lloyd, R. C.; Turner, N. J. A Regio- and Stereoselective  $\omega$ -Transaminase/Monoamine Oxidase Cascade for the Synthesis of Chiral 2,5-Disubstituted Pyrrolidines. *Angew. Chem. Int. Ed.* **2014**, *53*, 2447–2450.
- (81) Simon, R. C.; Grischek, B.; Zepeck, F.; Steinreiber, A.; Belaj, F.; Kroutil, W. Regio- and Stereoselective Monoamination of Diketones without Protecting Groups. *Angew. Chem. Int. Ed.* **2012**, *51*, 6713–6716.

## Chapter 5. references

- (82) France, S. P.; Hussain, S.; Hill, A. M.; Hepworth, L. J.; Howard, R. M.; Mulholland, K. R.; Flitsch, S. L.; Turner, N. J. One-Pot Cascade Synthesis of Mono- and Disubstituted Piperidines and Pyrrolidines Using Carboxylic Acid Reductase (CAR),  $\omega$ -Transaminase ( $\omega$ -TA), and Imine Reductase (IRED) Biocatalysts. *ACS Catal.* **2016**, *6*, 3753–3759.
- (83) Wetzl, D.; Gand, M.; Ross, A.; Müller, H.; Matzel, P.; Hanlon, S. P.; Müller, M.; Wirz, B.; Höhne, M.; Iding, H. Asymmetric Reductive Amination of Ketones Catalyzed by Imine Reductases. *ChemCatChem* **2016**, *8*, 2023–2026.
- (84) Hussain, S.; Leipold, F.; Man, H.; Wells, E.; France, S. P.; Mulholland, K. R.; Grogan, G.; Turner, N. J. An (*R*)-Imine Reductase Biocatalyst for the Asymmetric Reduction of Cyclic Imines. *ChemCatChem* **2015**, *7*, 579–583.
- (85) Ghanem, A.; Aboul-Enein, H. Y. Application of Lipases in Kinetic Resolution of Racemates. *Chirality* **2005**, *17*, 1–15.
- (86) Nübling, C.; Dittrich, K.; Dully, C. Enzyme-Catalysed Racemic Cleavage of Primary Amines. US 6,465,223 B1, **2002**.
- (87) Stelzer, U.; Dreisbach, C. Process for the Preparation of Optically Active Amines. US 6,387,692 B1, **2002**.
- (88) Thalén, L. K.; Zhao, D.; Sortais, J.-B.; Paetzold, J.; Hoben, C.; Bäckvall, J.-E. A Chemoenzymatic Approach to Enantiomerically Pure Amines Using Dynamic Kinetic Resolution: Application to the Synthesis of Norsertaline. *Chem. Eur. J.* **2009**, *15*, 3403–3410.
- (89) Busto, E.; Simon, R. C.; Richter, N.; Kroutil, W. Enzymatic Synthesis of Chiral Amines Using  $\omega$ -Transaminases, Amine Oxidases, and the Berberine Bridge Enzyme. In *Green Biocatalysis*; John Wiley & Sons, Inc: Hoboken, NJ, **2016**; pp 17–57.
- (90) Wolvekamp, M. C. J.; de Bruin, R. W. F. Diamine Oxidase: An Overview of Historical, Biochemical and Functional Aspects. *Dig. Dis.* **1994**, *12*, 2–14.
- (91) Pollegioni, L.; Molla, G. New Biotech Applications from Evolved D-Amino Acid Oxidases. *Trends Biotechnol.* **2011**, *29*, 276–283.
- (92) Koetter, J. W. A.; Schulz, G. E. Crystal Structure of 6-Hydroxy-D-Nicotine Oxidase from *Arthrobacter nicotinovorans*. *J. Mol. Biol.* **2005**, *352*, 418–428.
- (93) Kopacz, M. M.; Fraaije, M. W. Turning a Monocovalent Flavoprotein into a Bicovalent Flavoprotein by Structure-Inspired Mutagenesis. *Bioorg. Med. Chem.* **2014**, *22*, 5621–5627.
- (94) Heath, R. S.; Pontini, M.; Bechi, B.; Turner, N. J. Development of an (*R*)-Selective Amine Oxidase with Broad Substrate Specificity and High Enantioselectivity. *ChemCatChem* **2014**, *6*, 996–1002.
- (95) *MAO - The Mother of All Amine Oxidases*, 1st ed.; Finberg, J., Youdim, M., Riederer, P., Tipton, K., Eds.; Springer-Verlag Wien GmbH, **1998**.
- (96) Shih, J. C.; Chen, K.; Ridd, M. J. Monoamine oxidase: From Genes to Behavior. *Annu. Rev. Neurosci.* **1999**, *22*, 197–217.
- (97) Schilling, B.; Lerch, K. Amine Oxidases from *Aspergillus niger*: Identification of a Novel Flavin-Dependent Enzyme. *Biochim. Biophys. Acta.* **1995**, *1243*, 529–537.
- (98) Schilling, B.; Lerch, K. Cloning, Sequencing and Heterologous Expression of the Monoamine Oxidase Gene from *Aspergillus niger*. *Mol. Gen. Genet.* **1995**, *247*, 430–438.
- (99) Erdem, S. S.; Karahan, Ö.; Yıldız, İ.; Yelekçi, K. A Computational Study on the Amine-Oxidation Mechanism of Monoamine Oxidase: Insight into the Polar Nucleophilic Mechanism. *Org. Biomol. Chem.* **2006**, *4*, 646–658.
- (100) Atkin, K. E.; Reiss, R.; Koehler, V.; Bailey, K. R.; Hart, S.; Turkenburg, J. P.; Turner, N. J.; Brzozowski, A. M.; Grogan, G. The Structure of Monoamine Oxidase from *Aspergillus Niger* Provides a Molecular Context for Improvements in Activity Obtained by Directed Evolution. *J. Mol. Biol.* **2008**, *384*, 1218–1231.
- (101) Sablin, S. O.; Yankovskaya, V.; Bernard, S.; Cronin, C. N.; Singer, T. P. Isolation and Characterization of an Evolutionary Precursor of Human Monoamine Oxidases A and B. *Eur. J. Biochem.* **1998**, *253*, 270–279.

## Chapter 5. references

- (102) Alexeeva, M.; Enright, A.; Dawson, M. J.; Mahmoudian, M.; Turner, N. J. Deracemization of  $\alpha$ -Methylbenzylamine Using an Enzyme Obtained by In Vitro Evolution. *Angew. Chem. Int. Ed.* **2002**, *41*, 3177–3180.
- (103) Carr, R.; Alexeeva, M.; Enright, A.; Eve, T. S. C.; Dawson, M. J.; Turner, N. J. Directed Evolution of an Amine Oxidase Possessing Both Broad Substrate Specificity and High Enantioselectivity. *Angew. Chem. Int. Ed.* **2003**, *42*, 4807–4810.
- (104) Carr, R.; Alexeeva, M.; Dawson, M. J.; Gotor-Fernández, V.; Humphrey, C. E.; Turner, N. J. Directed Evolution of an Amine Oxidase for the Preparative Deracemisation of Cyclic Secondary Amines. *ChemBioChem* **2005**, *6*, 637–639.
- (105) Dunsmore, C. J.; Carr, R.; Fleming, T.; Turner, N. J. A Chemo-Enzymatic Route to Enantiomerically Pure Cyclic Tertiary Amines. *J. Am. Chem. Soc.* **2006**, *128*, 2224–2225.
- (106) Foulkes, J. M.; Malone, K. J.; Coker, V. S.; Turner, N. J.; Lloyd, J. R. Engineering a Biometallic Whole Cell Catalyst for Enantioselective Deracemization Reactions. *ACS Catal.* **2011**, *1*, 1589–1594.
- (107) Chen, Z.; Ma, Y.; He, M.; Ren, H.; Zhou, S.; Lai, D.; Wang, Z.; Jiang, L. Semi-Rational Directed Evolution of Monoamine Oxidase for Kinetic Resolution of *rac*-Mexiletine. *Appl. Biochem. Biotechnol.* **2015**, *176*, 2267–2278.
- (108) Rowles, I.; Malone, K. J.; Etchells, L. L.; Willies, S. C.; Turner, N. J. Directed Evolution of the Enzyme Monoamine Oxidase (MAO-N): Highly Efficient Chemo-Enzymatic Deracemisation of the Alkaloid ( $\pm$ )-Crispine A. *ChemCatChem* **2012**, *4*, 1259–1261.
- (109) O'Reilly, E.; Iglesias, C.; Turner, N. J. Monoamine Oxidase- $\omega$ -Transaminase Cascade for the Deracemisation and Dealkylation of Amines. *ChemCatChem* **2014**, *6*, 992–995.
- (110) Köhler, V.; Wilson, Y. M.; Dürrenberger, M.; Ghislieri, D.; Churakova, E.; Quinto, T.; Knörr, L.; Häussinger, D.; Hollmann, F.; Turner, N. J.; Ward, T. R. Synthetic Cascades Are Enabled by Combining Biocatalysts with Artificial Metalloenzymes. *Nat. Chem.* **2013**, *5*, 93–99.
- (111) Bechi, B.; Herter, S.; McKenna, S.; Riley, C.; Leimkühler, S.; Turner, N. J.; Carnell, A. J. Catalytic Bio-chemo and Bio-bio Tandem Oxidation Reactions for Amide and Carboxylic Acid Synthesis. *Green Chem.* **2014**, *16*, 4524–4529.
- (112) Ghislieri, D.; Green, A. P.; Pontini, M.; Willies, S. C.; Rowles, I.; Frank, A.; Grogan, G.; Turner, N. J. Engineering an Enantioselective Amine Oxidase for the Synthesis of Pharmaceutical Building Blocks and Alkaloid Natural Products. *J. Am. Chem. Soc.* **2013**, *135*, 10863–10869.
- (113) Schrittwieser, J. H.; Groenendaal, B.; Resch, V.; Ghislieri, D.; Wallner, S.; Fischereeder, E.-M.; Fuchs, E.; Grischek, B.; Sattler, J. H.; Macheroux, P.; Turner, N. J.; Kroutil, W. Deracemization By Simultaneous Bio-Oxidative Kinetic Resolution and Stereo-inversion. *Angew. Chem. Int. Ed.* **2014**, *53*, 3731–3734.
- (114) Schrittwieser, J. H.; Groenendaal, B.; Willies, S. C.; Ghislieri, D.; Rowles, I.; Resch, V.; Sattler, J. H.; Fischereeder, E.-M.; Grischek, B.; Lienhart, W.-D.; Turner, N. J.; Kroutil, W. Deracemisation of Benzyloquinoline Alkaloids Employing Monoamine Oxidase Variants. *Catal. Sci. Technol.* **2014**, *4*, 3657–3664.
- (115) Kwok, J.; Turner, N. J. *Utilising Synthetic Biology to Navigate Fitness Landscapes Effectively for Improved Biocatalysts*; **2016**.
- (116) Novagen. pET System Manual. **1999**, 8th Edition.
- (117) Lezdey, J.; Kronis, K.; Lezdey, D. DNA for Expression of Alpha 1-Antitrypsin in Methylotrophic Yeast. US 20020164695 A1, **2002**.
- (118) Beaumont, D.; Waigh, R. D.; Sunbhanich, M.; Nott, M. W. Synthesis of 1-(Aminomethyl)-1,2,3,4-Tetrahydroisoquinolines and Their Actions at Adrenoceptors in Vivo and in Vitro. *J. Med. Chem.* **1983**, *26*, 507–515.

# ANNEX 1. CALIBRATION CURVES





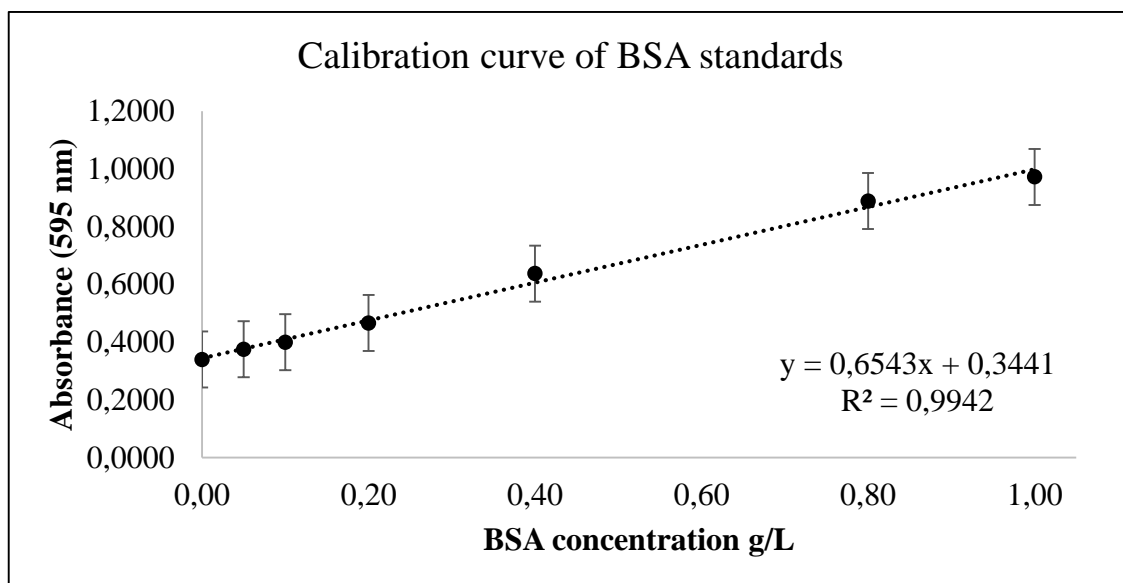


**Figure A1.1.** Calibration curve for the determination of protein concentration.

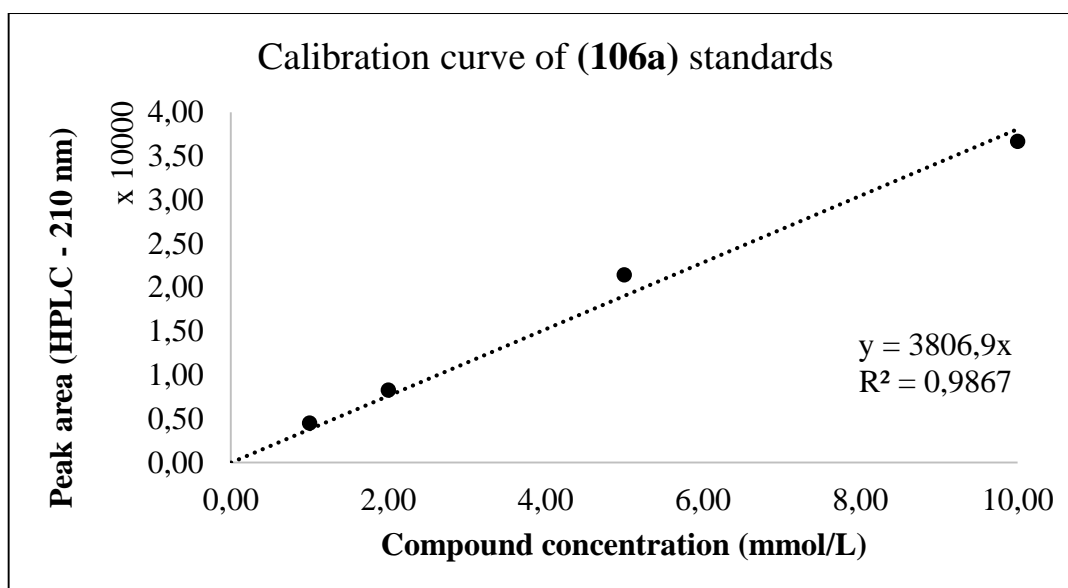


**Figure A1.2.** Calibration curve for the reverse-phase HPLC run of tetrahydroisoquinoline-1-carboxylic acid



## ANNEX 2. SPECIFIC ACTIVITY ASSAYS



**Table A2.1.** Specific activity of MAO-N variants with  $\alpha$ -MBA.

<b>MAO-N variant</b>	<b>Total protein in the assay (mg)</b>	<b>Specific activity (U/mg of protein)</b>	<b>Associated error (U/mg of protein)</b>
MAO-N D5	0,005	0,106	0,000
MAO-N D9	0,005	1,73	0,05
MAO-N D11	0,005	0,053	0,006
MAO-N D12 (A)	0,005	0,43	0,05
MAO-N D12 (B)	0,0013	0,68	0,02
MAO-N D12 (C)	0,0025	0,52	0,02
MAO-N D12 (D)	0,005	0,47	0,06
MAO-N D12 (E)	0,002	0,369	0,008
MAO-N D12 (F)	0,002	0,31	0,04
MAO-N D12 (G)	0,005	0,29	0,01
MAO-N D12 (H)	0,005	0,77	0,06

**Table A2.2.** Specific activity of MAO-N variants with THIQ.

<b>MAO-N variant</b>	<b>Total Protein in the assay (mg)</b>	<b>Specific activity (U/mg of protein)</b>	<b>Associated error (U/mg of protein)</b>
MAO-N D5	0,005	0,191	0,005
MAO-N D9	0,005	0,31	0,01
MAO-N D11	0,005	0,016	0,001
MAO-N D12 (A)	0,005	1,16	0,02
MAO-N D12 (B)	0,0013	1,66	0,01
MAO-N D12 (C)	0,0025	1,97	0,03
MAO-N D12 (D)	0,005	1,46	0,09
MAO-N D12 (E)	0,002	0,90	0,01
MAO-N D12 (F)	0,002	0,564	-
MAO-N D12 (G)	0,005	1,663	-
MAO-N D12 (H)	0,005	2,25	0,01

**Table A2.3.** Specific activity of MAO-N variants with 1-MTQ.

<b>MAO-N variant</b>	<b>Total Protein in the assay(mg)</b>	<b>Specific activity (U/mg of protein)</b>	<b>Associated error (U/mg of protein)</b>
MAO-N D5	0,005	0,007	0,000
MAO-N D9	0,0025	2,11	0,03
MAO-N D11	0,005	0,146	0,005
MAO-N D12 (A)	0,005	0,145	0,009
MAO-N D12 (B)	0,0013	0,044	0,001
MAO-N D12 (C)	0,0025	0,026	0,001
MAO-N D12 (D)	0,005	0,04	0,01
MAO-N D12 (E)	0,002	0,026	0,000
MAO-N D12 (G)	0,005	0,046	0,000
MAO-N D12 (H)	0,005	0,37	0,03

**Table A2.4.** Specific activity of MAO-N variants with 3-MTQ.

<b>MAO-N variant</b>	<b>Total Protein in the assay (mg)</b>	<b>Specific activity (U/mg of protein)</b>	<b>Associated error (U/mg of protein)</b>
MAO-N D5	0,005	-	-
MAO-N D9	0,0025	0,0054	0,0000
MAO-N D11	0,0025	0,0025	0,0000
MAO-N D12 (A)	0,005	0,012	0,001
MAO-N D12 (B)	0,0013	0,0061	0,0000
MAO-N D12 (C)	0,0025	0,0233	0,0009
MAO-N D12 (D)	0,005	0,0120	0,0007
MAO-N D12 (E)	0,002	-	-
MAO-N D12 (F)	0,002	0,0056	0,0000
MAO-N D12 (G)	0,005	0,026	0,002
MAO-N D12 (H)	0,005	0,031	0,001

**Table A2.5.** Specific activity of MAO-N variants with 4-MTQ.

<b>MAO-N variant</b>	<b>Total Protein in the assay(mg)</b>	<b>Specific activity (U/mg of protein)</b>	<b>Associated error (U/mg of protein)</b>
MAO-N D5	0,005	0,007	0,002
MAO-N D9	0,0025	0,0040	0,0001
MAO-N D11	0,0025	0,0019	0,0007
MAO-N D12 (A)	0,005	0,061	0,001
MAO-N D12 (B)	0,0013	0,088	0,009
MAO-N D12 (C)	0,0025	0,1084	-
MAO-N D12 (D)	0,005	0,0566	0,0009
MAO-N D12 (E)	0,002	0,04	0,01
MAO-N D12 (F)	0,002	0,015	0,003
MAO-N D12 (G)	0,005	0,098	0,001
MAO-N D12 (H)	0,005	0,1238	-

**Table A2.6.** Specific activity of MAO-N variants with 5-MTQ.

<b>MAO-N variant</b>	<b>Total Protein in the assay(mg)</b>	<b>Specific activity (U/mg of protein)</b>	<b>Associated error (U/mg of protein)</b>
MAO-N D5	0,005	0,25	0,04
MAO-N D9	0,0025	1,32	0,02
MAO-N D11	0,0025	0,0223	0,0009
MAO-N D12 (A)	0,005	1,20	0,05
MAO-N D12 (B)	0,0013	1,64	0,03
MAO-N D12 (C)	0,0025	1,24	0,09
MAO-N D12 (D)	0,005	1,74	0,09
MAO-N D12 (G)	0,005	1,31	0,03
MAO-N D12 (H)	0,005	2,04	0,06

**Table A2.7.** Specific activity of MAO-N variants with 6-MTQ.

<b>MAO-N variant</b>	<b>Total Protein in the assay(mg)</b>	<b>Specific activity (U/mg of protein)</b>	<b>Associated error (U/mg of protein)</b>
MAO-N D5	0,005	0,029	0,001
MAO-N D9	0,0025	0,72	0,02
MAO-N D11	0,0025	0,2619	0,0006
MAO-N D12 (A)	0,005	0,185	0,003
MAO-N D12 (B)	0,0013	0,258	0,003
MAO-N D12 (C)	0,0025	0,40	0,01
MAO-N D12 (D)	0,005	0,490	0,004
MAO-N D12 (G)	0,005	0,44	0,01
MAO-N D12 (H)	0,005	0,396	0,005

**Table A2.8.** Specific activity of MAO-N variants with 7-MTQ.

<b>MAO-N variant</b>	<b>Total Protein in the assay(mg)</b>	<b>Specific activity (U/mg of protein)</b>	<b>Associated error (U/mg of protein)</b>
MAO-N D5	0,005	-	-
MAO-N D9	0,005	-	-
MAO-N D11	0,005	-	-
MAO-N D12 (A)	0,005	0,0005	0,0001
MAO-N D12 (B)	0,0013	0,0002	0,0000
MAO-N D12 (C)	0,0025	0,0051	0,0002
MAO-N D12 (D)	0,005	0,0015	0,0001
MAO-N D12 (E)	0,002	-	-
MAO-N D12 (G)	0,005	0,0269	0,0003
MAO-N D12 (H)	0,005	0,0023	0,0004



**Table A2.9.** Specific activity of MAO-N variants with 8-MTQ.

MAO-N variant	Total Protein in the assay (mg)	Specific activity (U/mg of protein)	Associated error (U/mg of protein)
MAO-N D5	0,005	0,0303	0,0005
MAO-N D9	0,0025	1,915	0,017
MAO-N D11	0,0025	0,61	0,03
MAO-N D12 (A)	0,005	0,218	0,008
MAO-N D12 (B)	0,0013	0,2480	0,0008
MAO-N D12 (C)	0,0025	0,248	0,002
MAO-N D12 (D)	0,005	0,24	0,03
MAO-N D12 (G)	0,005	0,21	0,01
MAO-N D12 (H)	0,005	0,44	0,01

**Table A2.10.** Specific activity of MAO-N variants with DMTHIQ.

MAO-N variant	Total Protein in the assay (mg)	Specific activity (U/mg of protein)	Associated error (U/mg of protein)
MAO-N D5	0,005	-	-
MAO-N D9	0,0025	0,0038	0,0001
MAO-N D11	0,0025	0,0006	0,0002
MAO-N D12 (A)	0,005	0,0006	0,0002
MAO-N D12 (B)	0,0013	-	-
MAO-N D12 (C)	0,0025	0,0039	0,0003
MAO-N D12 (D)	0,005	0,0012	0,0004
MAO-N D12 (G)	0,005	0,0054	0,0002
MAO-N D12 (H)	0,005	0,0016	0,0002

**Table A2.11.** Specific activity of MAO-N variants with 1-M-DMTHIQ.

MAO-N variant	Total Protein in the assay (mg)	Specific activity (U/mg of protein)	Associated error (U/mg of protein)
MAO-N D5	0,005	-	-
MAO-N D9	0,005	0,0036	0,0004
MAO-N D11	0,005	0,0017	0,0001
MAO-N D12 (A)	0,005	0,0000	0,0004
MAO-N D12 (B)	0,0013	-	-
MAO-N D12 (C)	0,0025	0,0024	0,0008
MAO-N D12 (D)	0,005	-	-
MAO-N D12 (G)	0,005	-	-
MAO-N D12 (H)	0,005	0,0005	0,0002



## **ANNEX 3. RESPONSE FACTORS**



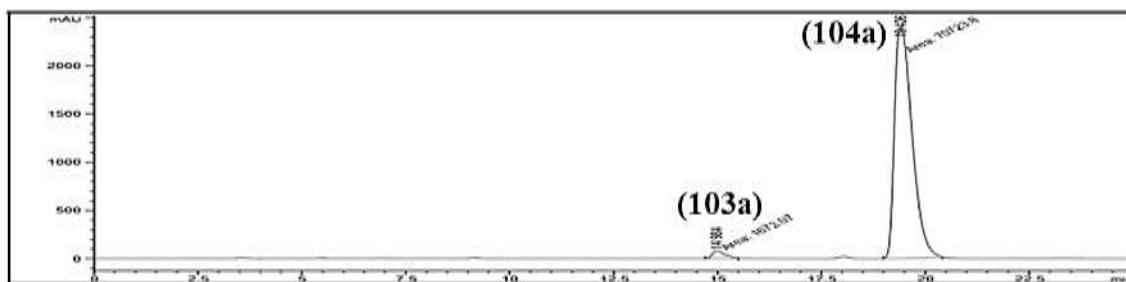


**Figure A3.1.** Normal phase HPLC trace (CHIRAPACK<sup>®</sup> IC<sup>™</sup> 250 mm x 4.6 mm, 5  $\mu$ m, eluent: hexane/isopropanol/diethylamine = 95/5/0.1, 1 mL/min, 254 nm) of a 2.5 mM equimolar solution of tetrahydroisoquinoline (**103a**) and 3,4-dihydroisoquinoline (**104a**).

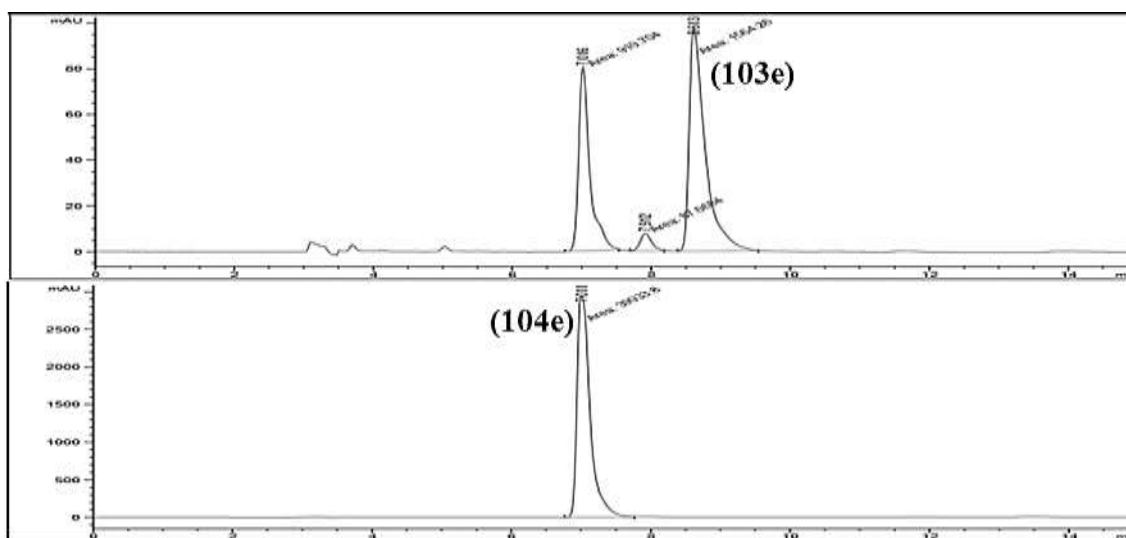


**Figure A3.2.** Normal phase HPLC trace (CHIRAPACK<sup>®</sup> OD-H 250 mm x 4.6 mm, 5  $\mu$ m, eluent: hexane/isopropanol/diethylamine = 90/10/0.1, 1 mL/min, 254 nm) of 5-MTQ (**103a**) (top) and 5-methyl-3,4-dihydroisoquinoline (**104e**) (bottom) 10 mM standards for determination of the response factor.

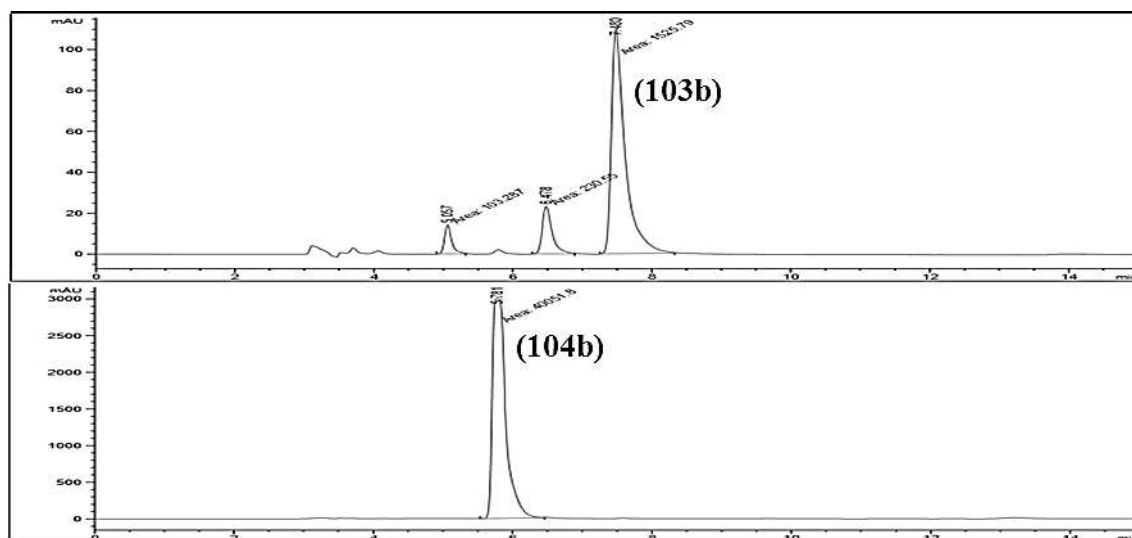


**Figure A3.3.** Normal phase HPLC trace (CHIRAPACK<sup>®</sup> OD-H 250 mm x 4.6 mm, 5  $\mu$ m, eluent: hexane/isopropanol/diethylamine = 90/10/0.1, 1 mL/min, 254 nm) of 6-MTQ (**103b**) (top) and 6-methyl-3,4-dihydroisoquinoline (**104b**) (bottom) 10 mM standards for determination of the response factor.

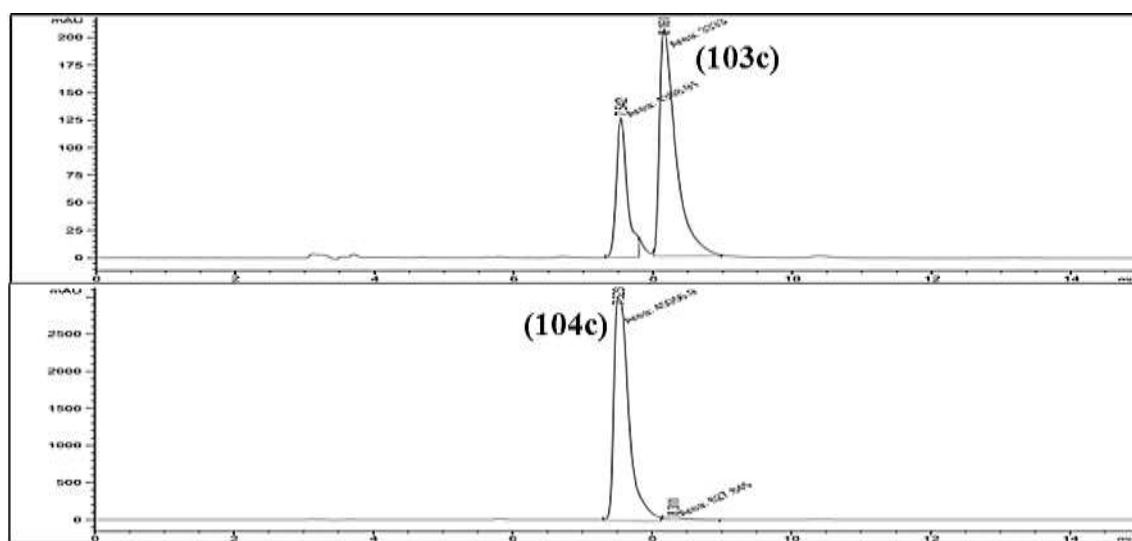


**Figure A3.4.** Normal phase HPLC trace (CHIRAPACK<sup>®</sup> OD-H 250 mm x 4.6 mm, 5  $\mu$ m, eluent: hexane/isopropanol/diethylamine = 90/10/0.1, 1 mL/min, 254 nm) of 8-MTQ (**103c**) (top) and 8-methyl-3,4-dihydroisoquinoline (**104c**) (bottom) 10 mM standards for determination of the response factor.

## ANNEX 4. NMR SPECTRA





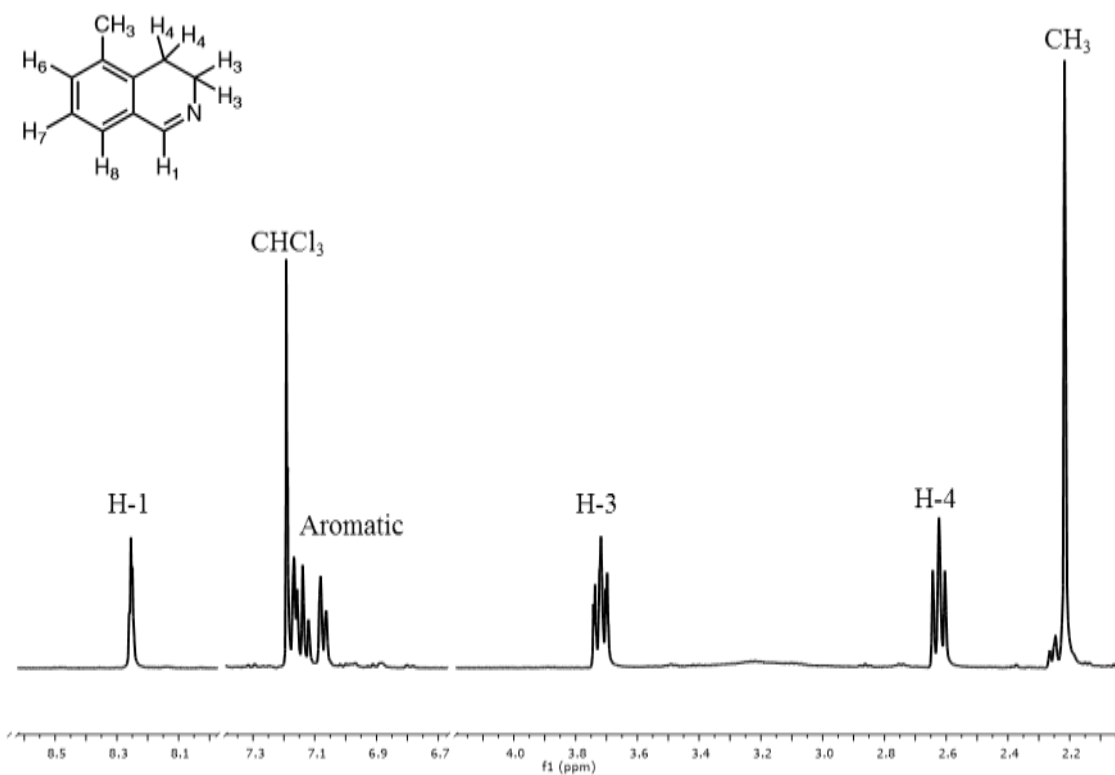


**Figure A4.1.** <sup>1</sup>H NMR spectrum of 5-methyl-3,4-dihydroisoquinoline

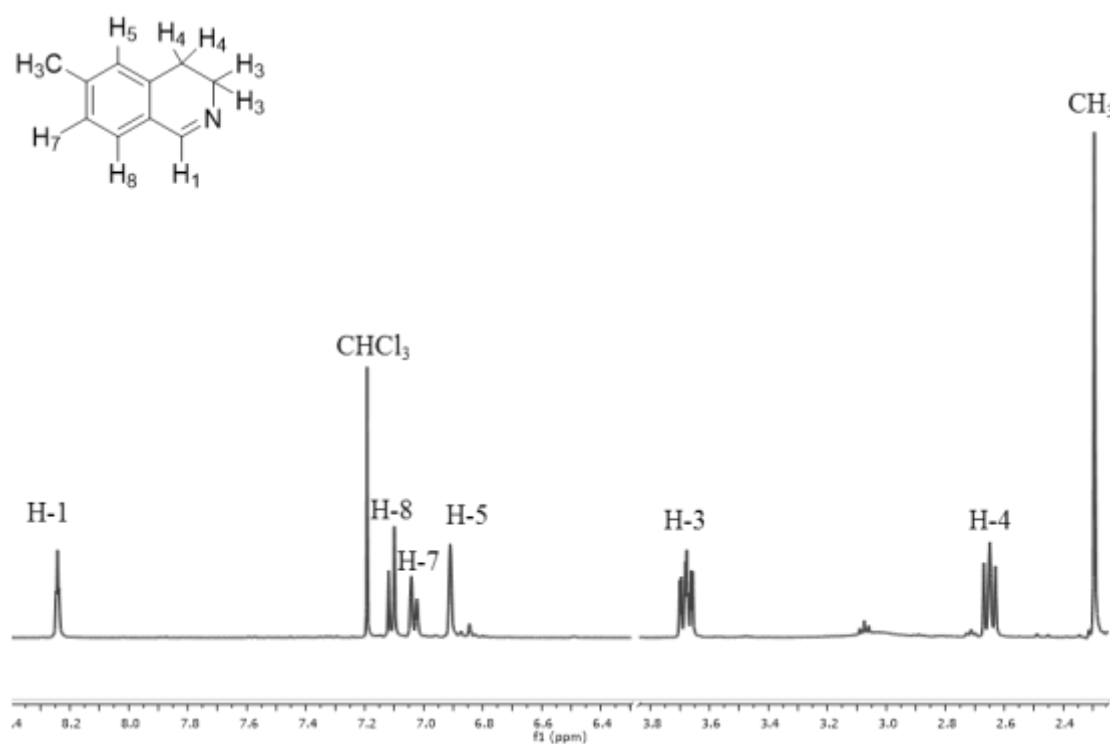


**Figure A4.2.** <sup>1</sup>H NMR spectrum of 6-methyl-3,4-dihydroisoquinoline

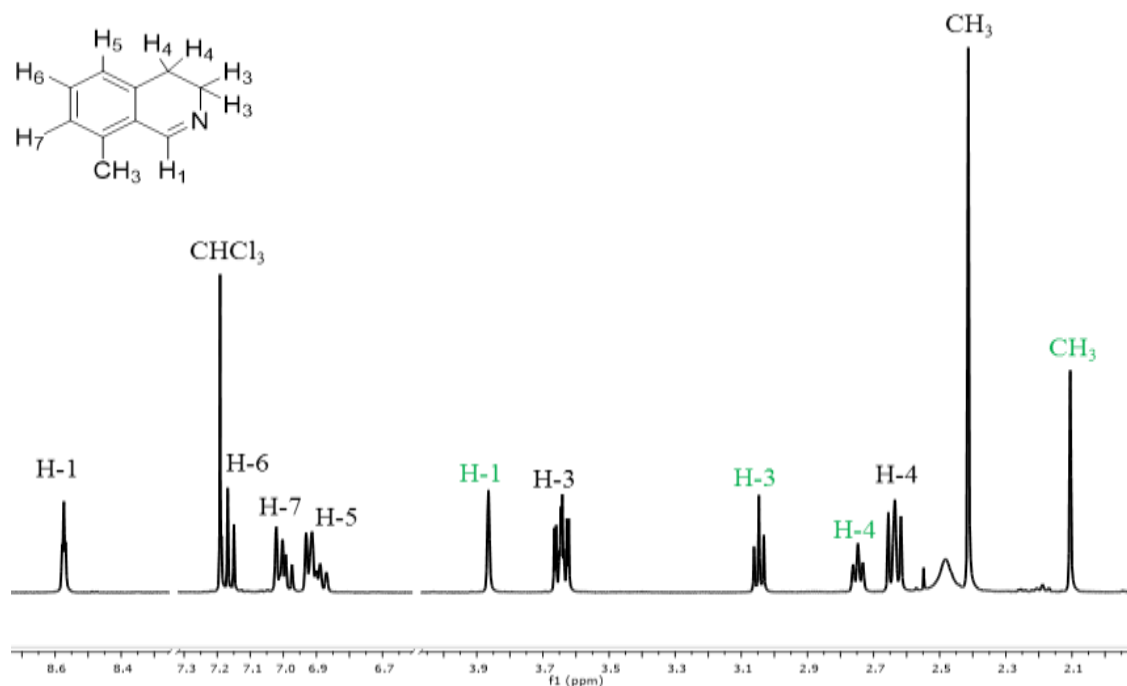


**Figure A4.3.**  $^1\text{H}$  NMR spectrum of 8-methyl-3,4-dihydroisoquinoline. The signals corresponding to its protons are identified in the figure in black. The markings in green identify the signals corresponding to an amine contamination due to only partial conversion. The remaining amine signals could not be unequivocally assigned.

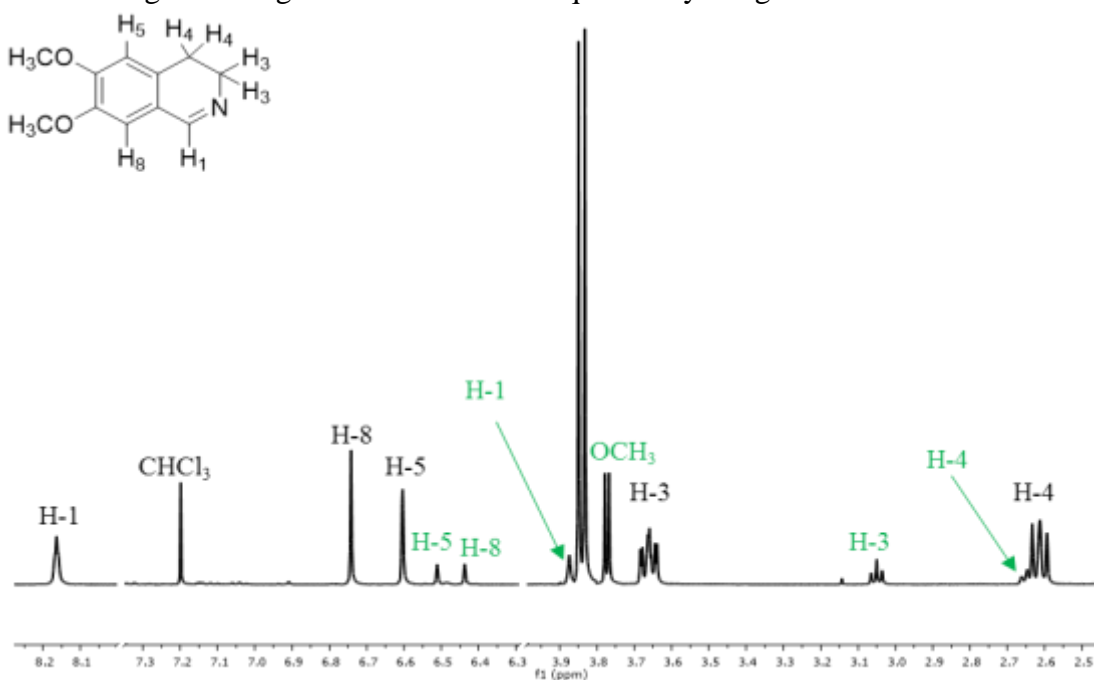


**Figure A4.4**  $^1\text{H}$  NMR spectrum of 6,7-dimethoxy-3,4-dihydroisoquinoline. The signals corresponding to its protons are identified in the figure in black. The markings in green identify the signals corresponding to an amine contamination due to only partial conversion.

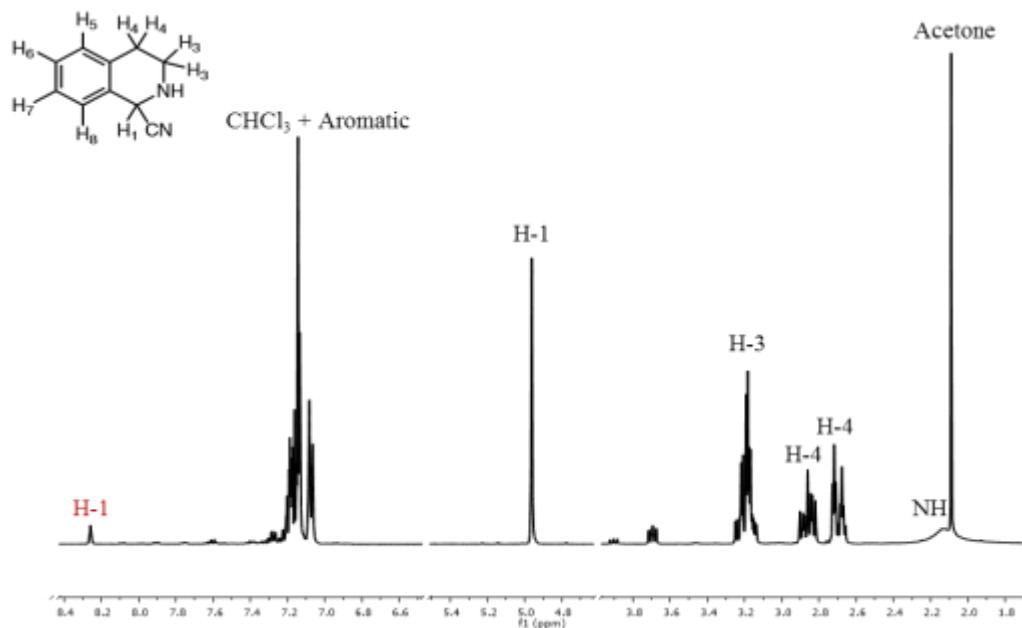


**Figure A4.5**  $^1\text{H}$  NMR of the product from the cyanation of 3,4-dihydroisoquinoline. The signals corresponding to the protons of 1-cyano-6-methyltetrahydroisoquinoline are identified in the figure in black. Also, the signal corresponding to the H-1 proton of its imine analogue is identified in red.

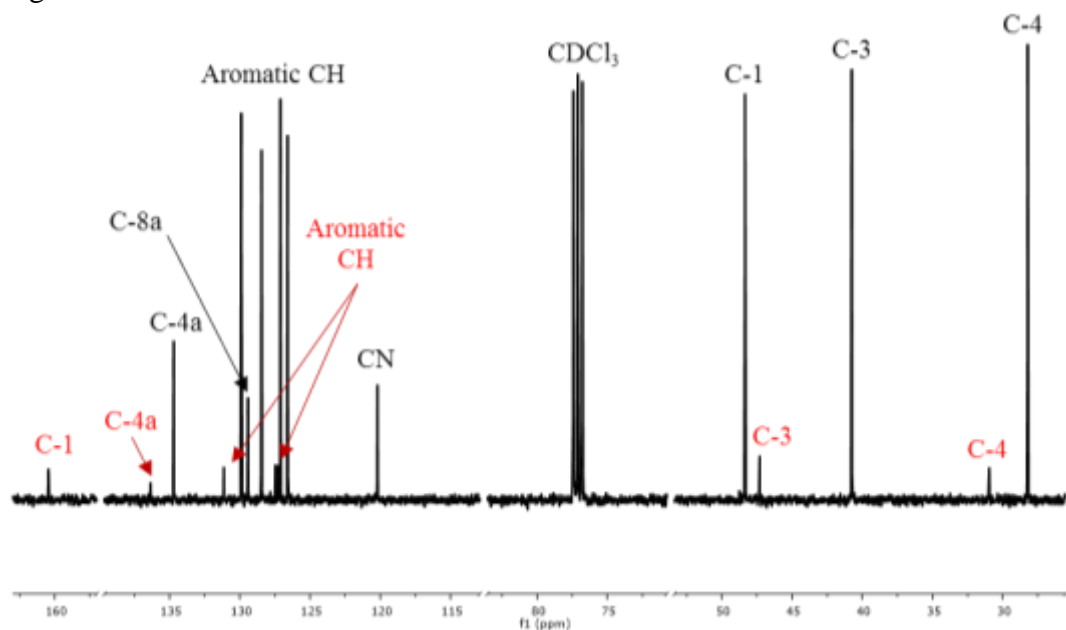


**Figure A4.6**  $^{13}\text{C}$  NMR of the product from the cyanation of 3,4-dihydroisoquinoline. The signals corresponding to the carbons of 1-cyanotetrahydroisoquinoline are identified in the figure in black. The markings identify the signals corresponding to the carbons of imine contamination - in red - due to only partial conversion. Remaining imine signals could not be unequivocally identified.

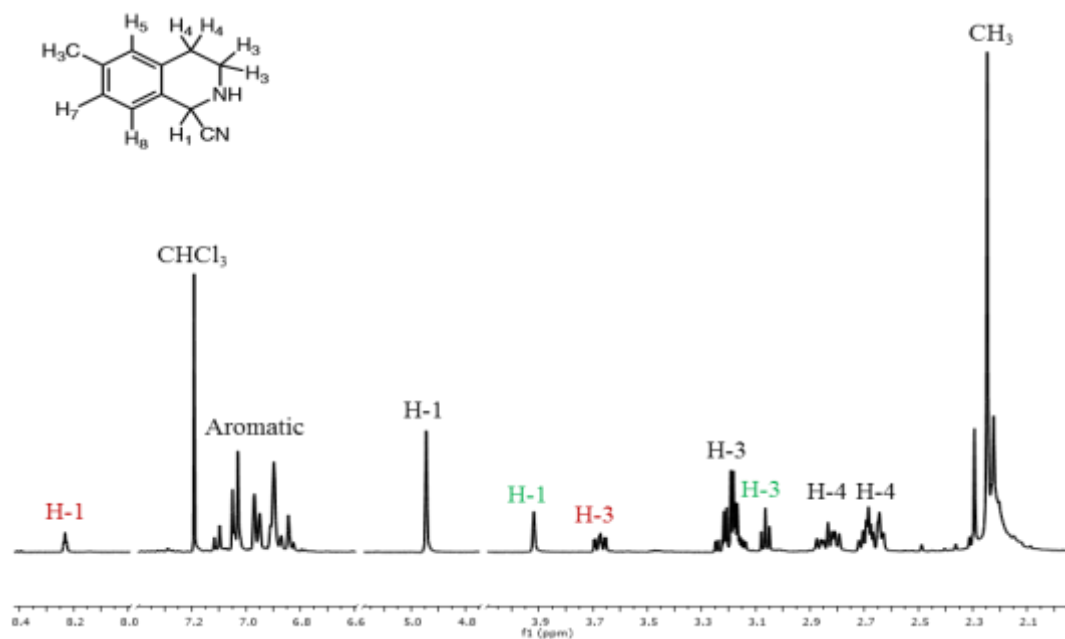


**Figure A4.7**  $^1\text{H}$  NMR of the product from the cyanation of 6-methyl-3,4-dihydroisoquinoline. The signals corresponding to the protons of 1-cyano-6-methyltetrahydroisoquinoline are identified in the figure in black. The markings identify the signals corresponding to the protons of both amine - in green - and imine - in red - contamination due to only partial conversion. Remaining amine and imine signals could not be unequivocally identified.

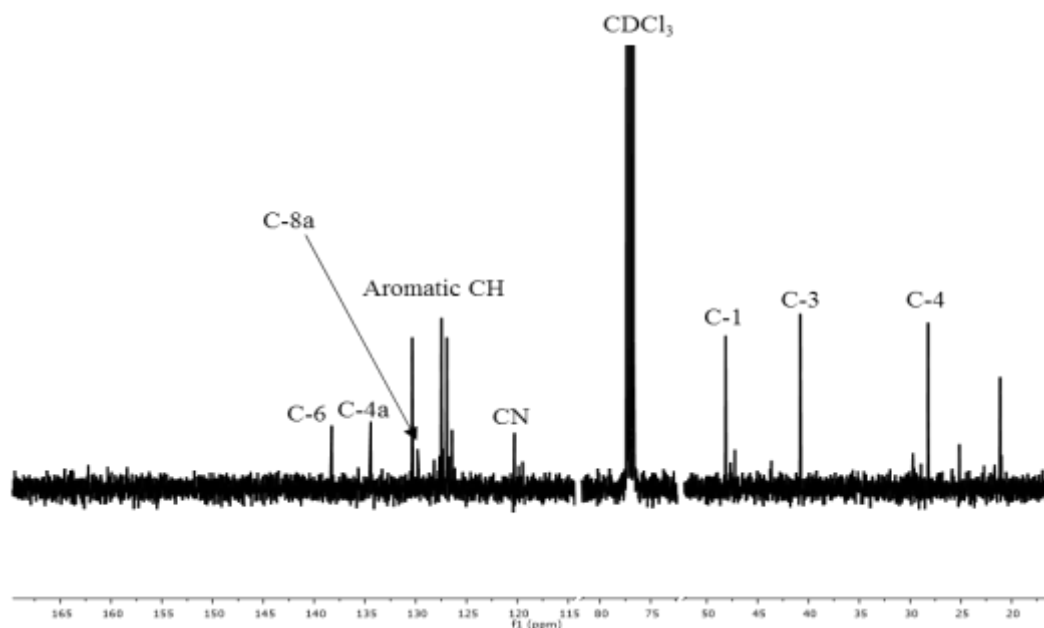


**Figure A4.8.**  $^{13}\text{C}$  NMR of the product from the cyanation of 6-methyl-3,4-dihydroisoquinoline. The signals corresponding to the carbons of 1-cyano-6-methyltetrahydroisoquinoline are identified in the figure in black. The signals corresponding to the carbons of the amine and imine contaminations could not be unequivocally identified.

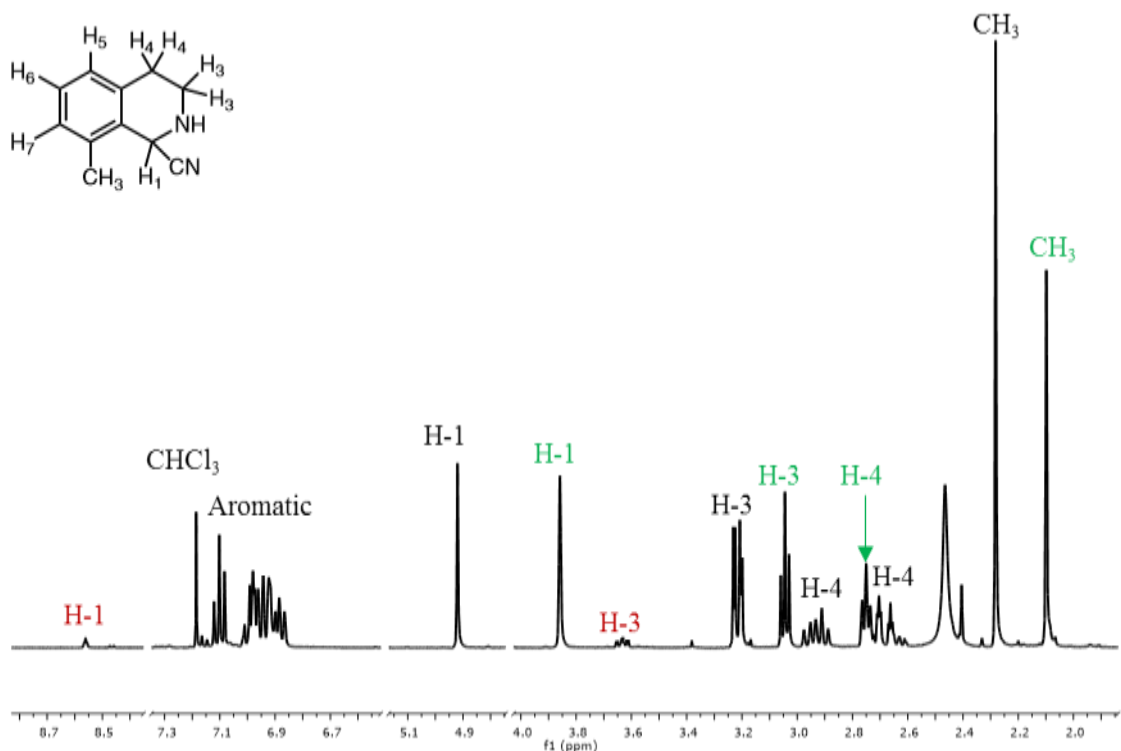


**Figure A4.9**  $^1\text{H}$  NMR of the product from the cyanation of 8-methyl-3,4-dihydroisoquinoline. The signals corresponding to the protons of 1-cyano-8-methyltetrahydroisoquinoline are identified in the figure in black. The markings identify the signals corresponding to the protons of both amine - in green - and imine - in red - contamination due to only partial conversion. Remaining amine and imine signals could not be unequivocally identified.

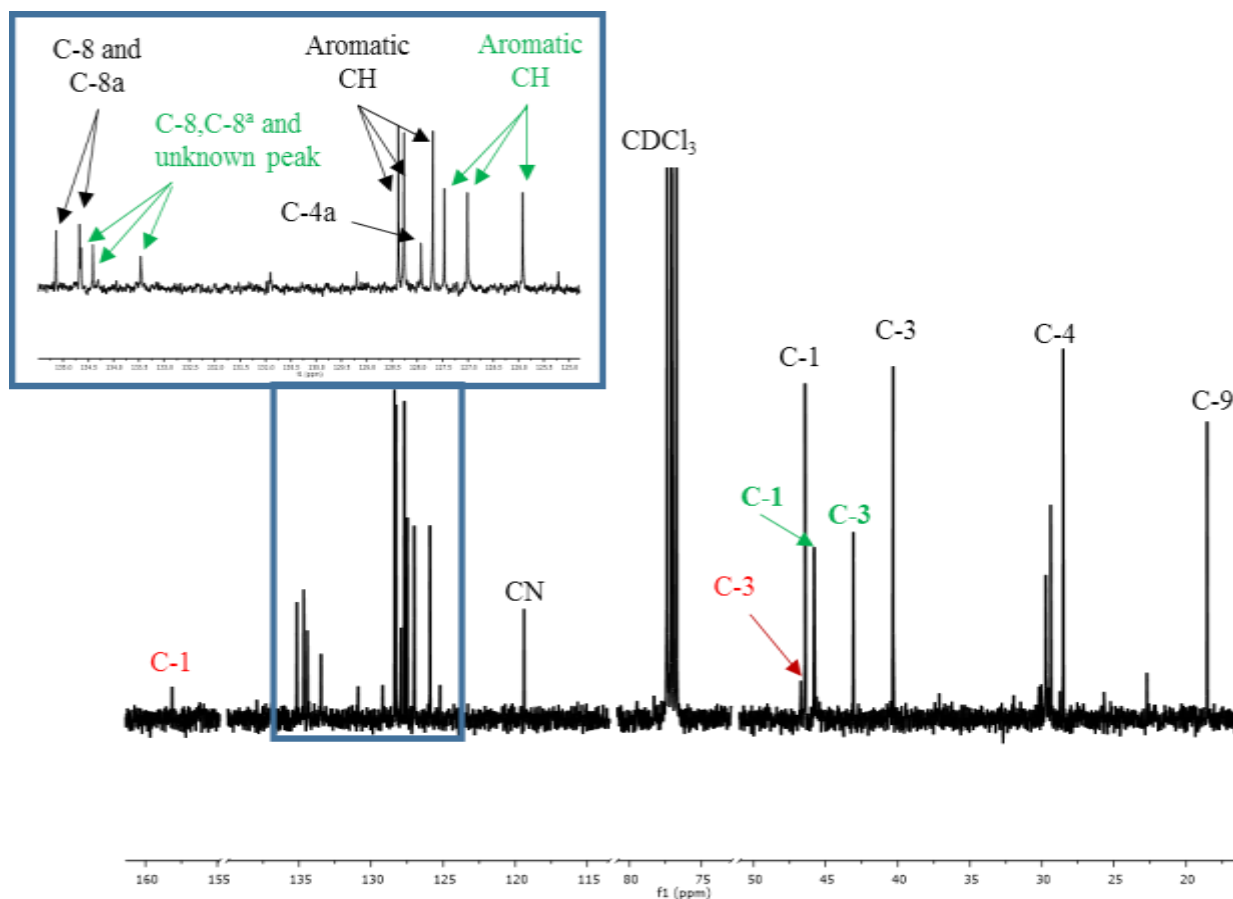


**Figure A4.10**  $^{13}\text{C}$  NMR of the product from the cyanation of 8-methyl-3,4-dihydroisoquinoline. The signals corresponding to the carbons of 1-cyano-8-methyltetrahydroisoquinoline are identified in the figure in black. The markings identify the signals corresponding to the carbons of both amine - in green - and imine - in red - contamination due to only partial conversion. Remaining amine and imine signals could not be unequivocally identified.

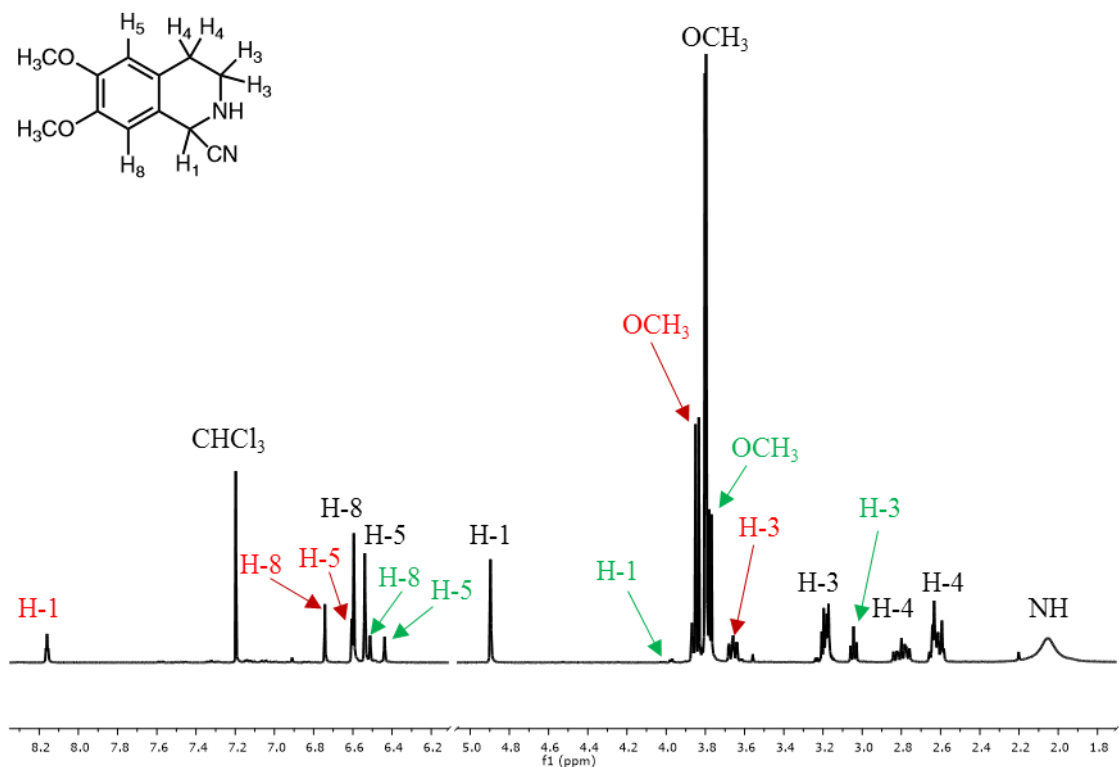


**Figure A4.11**  $^1\text{H}$  NMR of the product from the cyanation of 6,7-dimethoxy-3,4-dihydroisoquinoline. The signals corresponding to the protons of 1-cyano-6,7-dimethoxytetrahydroisoquinoline are identified in the figure in black. The markings identify the signals corresponding to the protons of both amine - in green - and imine - in red - contamination due to only partial conversion. Remaining amine and imine signals could not be unequivocally identified.

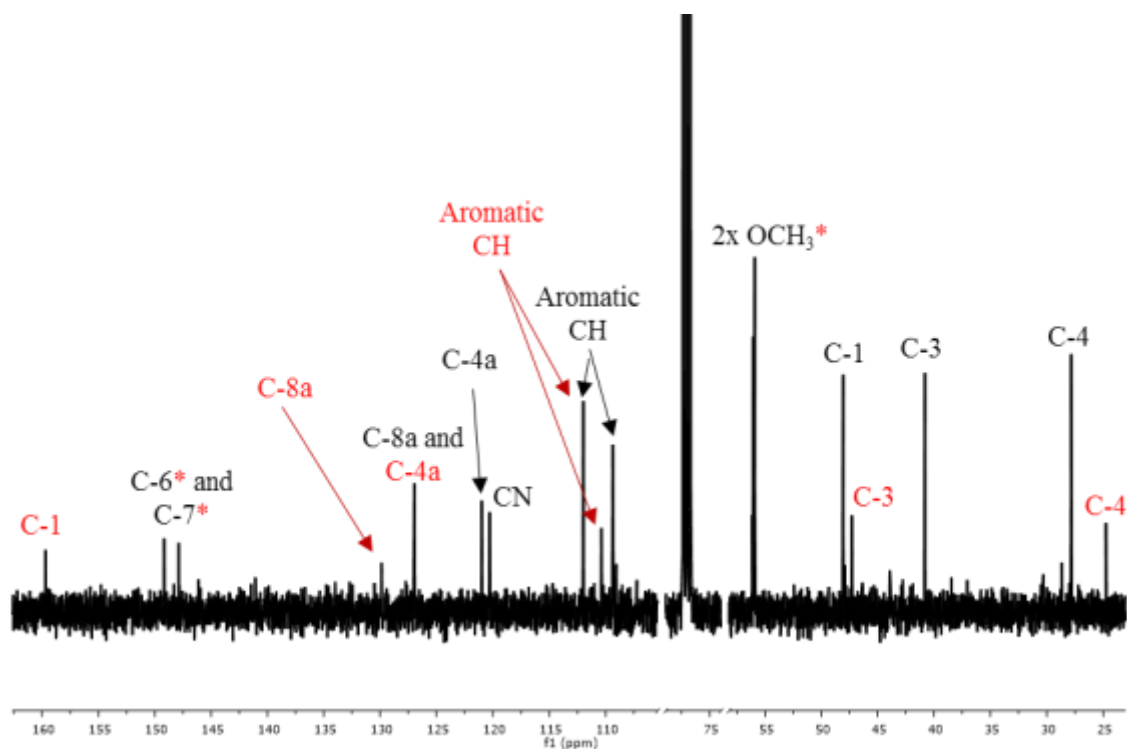


**Figure A4.12**  $^{13}\text{C}$  NMR of the product from the cyanation of 6,7-dimethoxy-3,4-dihydroisoquinoline. The signals corresponding to the carbons of 1-cyano-6,7-dimethoxytetrahydroisoquinoline are identified in the figure in black. The markings identify the signals corresponding to the carbons of imine contamination - in red - due to only partial conversion. Remaining imine signals could not be unequivocally identified.

\* Overlapping nitrile and imine signals.